CENTRO DE INVESTIGACIONES
EN OPTICA, A.C.

“GRAPHENE OXIDE-BASED BIOSENSING SYSTEMS FOR THE ANALYSIS OF PATHOGEN-RELATED ANALYTES”

Tesis que para obtener el grado de Doctora en Ciencias (Óptica)

Presenta: Mariana Denisse Avila Huerta

Director de Tesis: Dr. Eden Morales-Narváez

León · Guanajuato · México
Junio de 2023

To my Luna

Acknowledgments

I would like to acknowledge CONACYT for the financial support (Mexico, PhD scholarship, Grant No. 312271, and Grant No. 376135). Also acknowledge IDEA-GTO for financial support (Guanajuato, Mexico, Grants CMTEVAL-18-S01-03 and SICES/CONV/252/2019). Besides, I acknowledge Centro de Investigaciones en Óptica (CIO) for the infrastructure and resources provided for the realization of this PhD thesis.

I want to thank Dr. Eden Morales-Narváez, my mentor and thesis director for the last 6 years, for his mentoring, teachings, patience and dedication, who also encouraged me to participate in several projects that greatly enriched my experience and learning during all these years.

Otherwise, I would like to thank Dra. Valeria Piazza, Dr. Geminiano Ponce and Dr. Eduardo Coutiño for being part of my monitoring committee and always enriching my academic training with their comments and suggestions.

I want to thank to my OPTICA-SPIE student chapter work team, especially to my colleague and friend Dr. Karen Reyes, with whom I developed several soft skills and could work in beautiful science outreach projects. All this work allows me to develop myself holistically as a professional, as a scientist and personally.

And especially I want to thank and dedicated all these years of work to my family. To my mom and dad, who always support me and never doubt me, even when they don't understand me. To my sisters Cinthya and Karen and my brother Pablo, that always help me and herd me in the good and in the bad moments. To my nephew, Pablito, that during the last 3 years have been my light in the dark and my smile in every moment. To my husband, Andrés, that have support me and help me in this road, who doesn't let go of my hand, holds me when I need it most and makes me strong even when I don't believe in myself. And finally, to my daughter Luna, who has given me the last touch of motivation to successfully complete my doctoral work.

ABSTRACT

Biosensors are modern devices that can be employed in several contexts, such as health care, clinical diagnosis, food quality control, and environmental monitoring, among others. As a matter of fact, biosensors are convenient tools for infectious diseases diagnostics, because some of them meet the REASSURED (Real-time connectivity, Ease of specimen collection and environmental friendliness, Affordable, Specific, Sensitive, User-friendly, Rapid and robust, Equipment-free, and Delivered to the end-users) characteristics. Hence, biosensors represent as a powerful alternative to conventional diagnostic methods, such as microscopy, cell culture, immunoassays and nucleic-acid amplification. In this dissertation, a biosensing system targeting pathogen-related analytes was developed. The biosensing system comprises 96 microwell plates coated with graphene oxide, which performs as quencher of fluorescence from a specific immunoprobe. Such an immunoprobe is integrated by a fluorophore conjugated with a biorecognition element. The fluorescence of the immunoprobes that do not experiment immunoreactions (antibody-antigen) are deactivated by graphene oxide via non-radiative energy transfer, whereas those immunoprobes undergoing immunoreactions preserve its photoluminescence due to the distance and the low affinity between the immunocomplex and the graphene oxide-coated surface. This biosensing system was proven effective in the detection of (i) *E. coli*, to determine contamination in industrial food samples. (ii) Sialidase, to diagnose bacterial vaginosis and (iii) antibodies against SARS-CoV2 to determine COVID 19 seroconversion. The biosensing system was also proven useful with different matrixes (cauliflower extracts, vaginal swabs and human serum) to demonstrate that the overall approach is able to operate in real settings or real-world applications, proving to be highly sensitive, efficient, rapid and cost-effective, as well. Additionally, based on the same biosensing strategy, it was developed a paper-based disposable test for bacterial vaginosis detection. Our paper-based test is carried out within 20 minutes and the sample volume was 6 µL. Besides, it was tested with 14 vaginal swabs specimens to discriminate clinical samples of women with normal microbiota from those undergoing bacterial vaginosis. All in all, the development of this biosensing principle based on optically active nanomaterials, as well as all the potential applications, both as platform and disposable device, have significant impact in food industry for prevention of gastrointestinal diseases that may lead even to death due to the consumption of contaminated *E. coli* food, determination of COVID-19 seroconversion for clinical and health services purposes, and clinical diagnosis of Bacterial Vaginosis avoiding the consequences of misdiagnosis of this disease.

Table of contents

Table of figures and tables

SCIENTIFIC PRODUCTION

PUBLICATIONS

1. **Avila-Huerta, M. D.**; Leyva-Hidalgo, K.; Cortés-Sarabia, K.; Estrada-Moreno, A. K.; Vences-Velázquez, A.; Morales-Narváez, E. Disposable Device for Bacterial Vaginosis Detection. ACS Meas. Sci. Au 2023. https://doi.org/10.1021/acsmeasuresciau.3c00007.
2. **Avila-Huerta, M. D.**; Mancera-Zapata, D. L. Reach for the Stars─Inspiring Latin American Women in STEM. ACS Meas. Sci. Au 2022, 2 (6), 493–494. https://doi.org/10.1021/acsmeasuresciau.2c00060.
3. **Avila-Huerta, M. D.**; Ortiz-Riaño, E. J.; Mancera-Zapata, D. L.; Cortés-Sarabia, K.; Morales-Narváez, E. Facile Determination of COVID-19 Seroconversion via Nonradiative Energy Transfer. ACS Sens. 2021, 6 (6), 2136–2140. https://doi.org/10.1021/acssensors.1c00795.
4. Rodríguez-Nava, C.; Cortés-Sarabia, K.; **Avila-Huerta, M. D.**; Ortiz-Riaño, E. J.; Estrada-Moreno, A. K.; Alarcón-Romero, L. del C.; Mata-Ruíz, O.; Medina-Flores, Y.; Vences-Velázquez, A.; Morales-Narváez, E. Nanophotonic Sialidase Immunoassay for Bacterial Vaginosis Diagnosis. ACS Pharmacol. Transl. Sci. 2021, 4 (1), 365–371. https://doi.org/10.1021/acsptsci.0c00211.
5. **Avila-Huerta, M. D.**; Ortiz-Riaño, E. J.; Mancera-Zapata, D. L.; Morales-Narváez, E. Real-Time Photoluminescent Biosensing Based on Graphene Oxide-Coated Microplates: A Rapid Pathogen Detection Platform. Anal. Chem. 2020, 92 (17), 11511–11515. https://doi.org/10.1021/acs.analchem.0c02200.
6. Ortiz-Riaño, E. J.; **Avila-Huerta, M. D.**; Mancera-Zapata, D. L.; Morales-Narváez, E. Microwell Plates Coated with Graphene Oxide Enable Advantageous Real-Time Immunosensing Platform. Biosens. Bioelectron. 2020, 165, 112319. https://doi.org/10.1016/j.bios.2020.112319.

PROCEEDINGS

1. **Avila-Huerta MD**, Ortiz-Riaño EJ, Mancera-Zapata DL, Morales-Narváez E. Real-Time Pathogen Determination by Optical Biosensing Based on Graphene Oxide. Proceedings. 2020;60(1). doi:10.3390/IECB2020-07016
2. Ortiz-Riaño EJ, **Avila-Huerta MD**, Mancera-Zapata DL, Morales-Narváez E. Quenching of Fluorescence Caused by Graphene Oxide as an Immunosensing Platform in a Microwell Plate Format. Proceedings. 2020;60(1). doi:10.3390/IECB2020-07017

PARTICIPATION IN NATIONAL AND INTERNATIONAL CONGRESSES

- LatinXChem 2022 (November 2022)
- II Congreso de Ingeniería y Física Aplicadas a la Biomedicina (May 2022)
- SOMIXXXV y 1 Simposio Nacional De Biosensores (October 2021)
- The 25th International Conference on Miniaturized Systems for Chemistry and Life Sciences (October 2021)
- JASIS Conference International Conference Session, The Royal Society of Chemistry-Tokyo International Conference 2020 (December 2020)
- The 1st International Electronic Conference on Biosensors (November 2020)
- LatinXChem 2020 (September 2020)

AWARDS

- ✓ Best poster award in PhD category, II Congreso de Ingeniería y Física Aplicadas a la Biomedicina 2022
- ✓ Low- and Middle-Income Country (LMIC) Student/Young Researcher Award from the Chemical & Biological Microsystems Society (CBMS) 2021
- ✓ Best poster award at the JASIS Conference International Conference Session, The Royal Society of Chemistry- Tokyo International Conference 2020

COVER ART PUBLISHED

- ✓ ACS MEASURMENT SCIENCE (December 21, 2022)
- ✓ Analytical Chemistry (September 1, 2020)

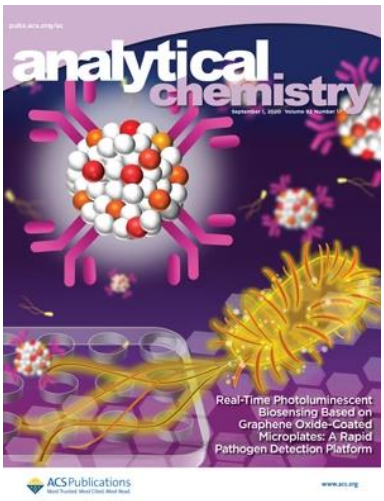

VOLUNTEERING

- ➢ Officer of the OPTICA student chapter (President 2020-2021)
- ➢ Officer of the SPIE student chapter (Secretary 2019)

CHAPTER 1. INTRODUCTION

The term "biosensor" was coined by Karl Camman in 1977[1], although an early approach of biosensor was introduced in 1962 to monitor blood gas levels during surgery by Clark and Lyons.[2] Biosensors are defined by the International Union of Pure and Applied Chemistry (IUPAC) as "a device that uses specific biochemical reactions mediated by isolated enzymes, immunosystems, tissues, organelles or whole cells to detect chemical compounds usually by electrical, thermal or optical signals".[3] Biosensors are characterized by their ease of use, high performance, low response time, and they overcome the human error. In the last years the REASSURED (Real-time connectivity, Ease of specimen collection and environmental friendliness, Affordable, Specific, Sensitive, User-friendly, Rapid and robust, Equipment-free, and Delivered to the end-users)[4] criteria in biosensors is imperative for future diagnostic systems, given the rapid progress in digital technology and mobile health. This would enable the diagnostic systems to provide real-time information for disease control strategies, enhance the effectiveness of healthcare systems, and ultimately lead to better patient outcomes.[4] Figure 1.1 illustrates the workflow generally performed in biosensors. Biosensors comprise a biorecognition element that recognize the analyte and a transducer system that converts the bio-recognition event into a measurable signal.[5] These important elements will be detailed later. In recent years the field of biosensors has been revolutionized by the integration of nanotechnology. Due to its stunning properties, nanomaterials in the field of biosensing can offer excellent characteristics including a large surface-to-volume ratio, manifestation of biological transduction and signaling mechanisms, and electro-chemical/photonic properties.[6] Hereupon some nanomaterials and its influence in biosensors will be described. In the following section basic concepts employed or developed in this thesis are briefly introduced.

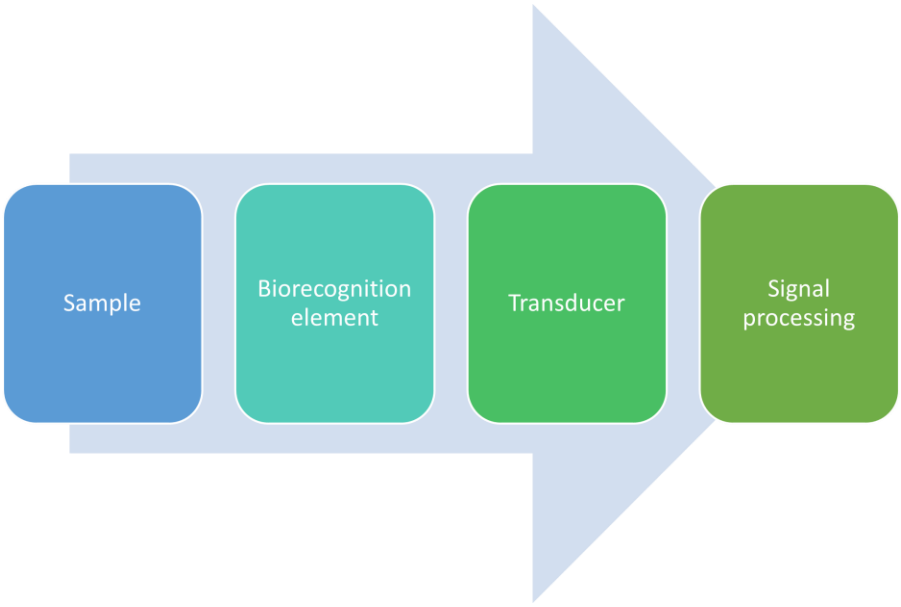

***Figure 1.1**. Biosensing process*

A. Basic concepts

1. Biorecognition element

Biorecognition element is the part of the biosensor which interacts with the target analyte. Specificity and selectivity of biosensors depend directly on the biorecognition element, because it is in charge of the capture of the target analyte. Analyte can be defined as the interest component of the analyzed sample, or the bio-chemical species that are targeted to measure/detect.[1,6]

There are several biological elements that can be used, but the most common biorecognition elements used in biosensors are:

- Antibodies
  Antibodies are proteins that provide immunity and are generated by immune system cells in response to the presence of antigens, such as pathogenic bacteria or viruses. These proteins consist of Y-shaped molecules that selectively attach to an antigen, which may also serve as an analyte in biosensing, owing to their geometric compatibility as a lock-and-key combination.[7]

- Aptamers
  Aptamers are oligonucleotides acid that bind to a specific target molecule. Aptamers are usually created by selecting them from a large random sequence pool.[8]

- Enzymes
  An enzyme is a molecule composed of one or more amino acid chains that acts as a catalyst in living organisms, regulating the rate at which chemical reactions proceed without itself being altered in the process. The amino acid sequence determines the characteristic folding patterns of the protein structure, which is essential to enzyme specificity.

- Nucleic acids
  Nucleic acids are polynucleotide chains in which ribonucleotides and deoxyribonucleotides are the monomeric units. The nucleic acids structures involve nitrogenous bases which only interact with its complementary base, this characteristic allow to use nucleic acids as biorecognition element of target genes.[9]

2. Transduction mechanisms

A transducer converts one form of energy to another. In biosensors, transducer converts the biorecognition event into a measurable signal. Typically, biosensors employ optical, electrochemical transduction mechanisms.[1,3,10]

- Optical biosensors
  Optical biosensors detect biological or chemical responses and report it as change in any optical signals change, including but not limited to absorption, fluorescence, refractive index, polarization, amplitude, phase, etc. Optical biosensors exploit the interaction of the optical field with a biorecognition element following an optical detection technique such as

evanescent-wave-based fluorescence, surface-enhanced Raman spectroscopy, reflectometric interference spectroscopy, colorimetric detection, optical coherence tomography, surface plasmon resonance, slot waveguides, fluorescence optical sensors and metamaterials.[1,10]

- Electrochemical biosensors
  Electrochemical biosensors combine the sensitivity of electroanalytical methods with the inherent bioselectivity of the biological component. The biological component in the sensor recognizes its analyte resulting in a catalytic or binding event that ultimately produces an electrical signal monitored by a transducer that is proportional to analyte concentration.[11]

3. Nanotechnology

Nanotechnology is the technology implemented at the nanoscale in the real world. Nanotechnology includes the control and restructuring of matter at the atomic and molecular levels in sizes below 100 nm, these materials are known as nanomaterials and exhibit dramatic changes in properties. Biosensors integrates with nanomaterials are called nano-biosensors; biosensors have a wide range of bioanalytical applications in fields such as bio-imaging, diagnostics, drug administration and treatment.[6,12,13]

Nanomaterials

Mechanical, chemical, structural and electrical properties of nanomaterials used biosensors help to overcome challenges based on the sensitivity and detection limit of devices. Nanomaterials are promising candidates due to the possibility to immobilize an enhanced quantity of bioreceptor units at reduced volumes and even to act itself as transduction element.[1,12,13] Nanomaterials include structures such as metal nanoparticles, semiconductor quantum dots, polymer nanoparticles, carbon nanotubes, graphene among others.[14] Below is described some of the main nanomaterials used in this research work.

a) Quantum Dots (QD)

QDs are semiconductor nanocrystals with unique optical and electrical properties which have a diameter between 2 and 10 nm. The composition of Quantum Dots (QDs) comprises of a core composed atoms of group II-VI such as Cadmium Selenide (CdSe) or group III-V atoms from the periodic table such as Indium Phosphide. Additionally, a semiconductor shell is incorporated to encapsulate the core, commonly Zinc Sulfide (ZnS), to enhance the optical properties, stability, and reduce cytotoxicity. Furthermore, an organic coating is applied to convert the nanoparticle into a hydrophilic compound to facilitate conjugation with biomolecules. QDs emit different wavelengths of visible light, depending on the size of the QD.[15]

b) Graphene oxide

Graphene is a flat array one atom thick of sp^2-bonded carbon atoms ordered in a two-dimensional hexagonal lattice. Graphene oxide (GO) has a similar atomic structure but possesses oxygen-containing functional groups (See Figure 1.2). Since GO exhibit innovative mechanical, electrical, thermal and optical properties; besides, GO displays advantageous characteristics to be used in biosensing platforms owing to the easy conjugation with biomolecules due to its heterogeneous chemical and electronic structure. Due to its electronic properties graphene is a highly efficient

quencher of fluorophores capabilities. GO can be proposed as a universal highly efficient long-range quencher. [16,17]

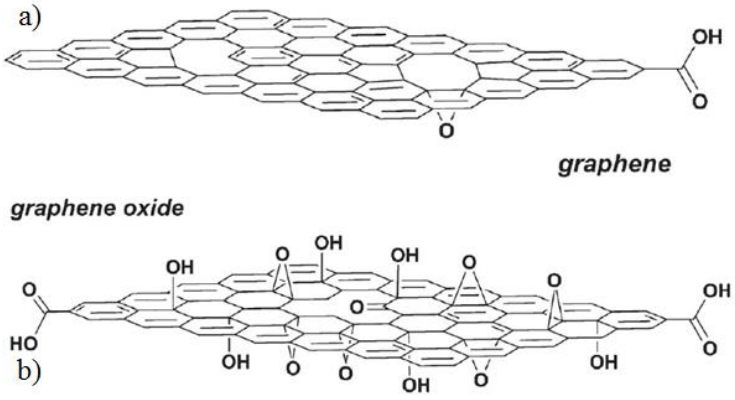

Figure 1.2. *Graphene and Graphene Oxide structure. Adapted with permission.[17] Copyright 2010, Wiley-VCH.*

4. FRET

"Föster (or fluorescence) resonance energy transfer (FRET) is a phenomenon in which photo excitation energy is transferred from a donor fluorophore to an acceptor molecule."[16,18] The efficiency of the process depends on (i) the distance between donor and acceptor, (ii) the spectral characteristics of the donor and acceptor and their relative orientation. Optimal coupling of the transient electromagnetic fields can be achieved when they are in a collinear arrangement while parallel arrangement of the transition dipoles reduces the FRET efficiency and perpendicular orientation avoids FRET. Distances around 2-6 nm can be measured in a typical FRET phenomenon, but using GO as acceptor the fluorescence quenching can be observable at distances up to 30 nm; that is, this 2D material can enhance the efficiency of the phenomenon.[16]

5. Infectious diseases

Infectious diseases are commonly caused by pathogenic microorganisms such as viruses, bacteria, parasites and fungi. Compared with other health threats, infectious diseases can be exponentially spread all over the world rapidly causing significant morbidity and mortality and threatening the general public health and, potentially, the economy. Diagnosis is a key tool to hold back infectious diseases spread, to order an appropriated and effective medical treatment and to improve global health. [19–21] Usually, these health conditions are diagnosed through a variety of laboratory-based tests including microscopy, cell culture, immunoassays (ELISA) and nucleic-acid amplification (PCR), although these conventional methods are useful and effective, are time-consuming and require centralized laboratories, skilled personnel and bulky equipment.[20,22]

6. Cell culture

Cell culture are laboratory methods that facilitate the proliferation of eukaryotic or prokaryotic cells in physiological conditions. Its origin can be found in the early 20th century when it was employed to study tissue growth and maturation, virus biology and vaccine development, the role of genes in disease and health, and the use of large-scale hybrid cell lines to generate biopharmaceuticals. Cell culture methods are time consuming whereby the method is rapidly losing its place and its relative significance in the diagnosis of human diseases because of the need of an immediate and accurate

clinical diagnostic for early and effective intervention. Besides, cell culture required expertise and trained technologists as well as sophisticated equipment.[23,24]

7. ELISA

Enzyme-linked immunosorbent assay (ELISA), is the most reliable and accurate type of immunoassay, known as the golden standard of immunoassays. This immunological test is highly sensitive and is primarily used to detect and quantify a range of substances, including antigens, antibodies, hormones, glycoproteins, and proteins. The detection of these products is accomplished by complexing antibodies and antigens to produce a measurable result. Typically, these immunoassays are performed in 96-well polystyrene plates coated to bind protein very strongly. ELISA testing involves a variety of components such as primary and/or secondary detection antibodies, analyte/antigen, coating antibody/antigen, buffer, wash, and substrate/chromogen, depending on the type of ELISA being performed. Besides, ELISA require several steps such as coating, blocking, detection and final read. There are four major types of ELISA: 1) Direct, 2) Indirect, 3) Sandwich, and 4) Competitive. [25]

8. PCR

PCR is the most well-developed molecular technique up to now. PCR is a laboratory technique that utilizes enzymes to amplify short regions of DNA invitro. This process requires prior knowledge of some portions of the target DNA sequence, which are then used to design specific oligonucleotide primers that will bind to the target sequence.[26]

B. Biosensing technology proposal.

1. Biosensing system based on 96 microwell plate targeting pathogen-related analyte.

As a potential alternative for conventional detection methods, in our research group we have proposed a biosensing platform targeting pathogen-related analytes, that comprises 96 microwells coated with GO and require a bioprobe that is a biorecognition element conjugated with a fluorophore. Based on FRET, the fluorescence of the immunoprobes that do not experiment immunoreactions are deactivated by graphene oxide via non-radiative energy transfer, whereas those immunoprobes undergoing immunoreactions preserve its photoluminescence due to the distance and the low affinity between the immunocomplex and the graphene oxide-coated surface. The biosensing platform have been tested with analytes such as (i) *E. coli* to determine contamination in industrial food sample[27], (ii) Sialidase to diagnose bacterial vaginosis[22] and (iii) COVID-19 antibodies to determine COVID-19 seroconversion.[28] This biosensing platform has been demonstrated to be successful with real samples, which supports its potential applications in real-world. In the next chapters this technology will be described in detail, explaining methodology, outcomes and discussing it.

2. Disposable biosensor for Bacterial Vaginosis diagnosis.

Disposable biosensors are affordable and easy-to-use devices for a single measurement, which are now integrated into our daily life, for example, in pregnancy or fertility tests and wearable blood glucometers.[29] Microfluidic paper-based analytical devices (µPADs) have a wide range of applications as disposable biosensors. These devices are promising tools for medical diagnostics and environmental monitoring and can be used at the point-of care (POC).[30,31] We report a novel microfluidic paper-based analytical device for Bacterial Vaginosis (BV) diagnosis. Sialidase, a biomarker overexpressed in BV, was detected by exploiting a biosensing mechanism explained

previously, via no radiative energy transfer. Immunoprobes that do not experience immunoreactions lose their fluorescence due to graphene oxide quenching capabilities. On the other hand, immunoprobes that undergo immunoreactions maintain their photoluminescence because of the distance and low affinity between the immunocomplex and the surface coated with graphene oxide. Our paper-based test was typically carried out within 20 minutes and the sample volume was 6 µL. Besides, it was tested with 14 vaginal swabs specimens to discriminate clinical samples of women with normal microbiota from those undergoing BV. Our disposable device empowers a new tool to prevent the consequences of asymptomatic or misdiagnosed BV. Chapter 4 details the operation of the device as well as the results and the correspondent discussion.

CHAPTER 2. Real-Time Photoluminescent Biosensing Based on Graphene Oxide-Coated Microplates: A Rapid Pathogen Detection Platform

Pathogenic bacterial outbreak is a major threat to safety and human health and the environment. In response to this safety issue, is presented a suitable single-step, wash-free, and real-time bacterial detection platform operating with a single antibody to detect *Escherichia coli* (*E. coli*) and prevent bacterial contamination. This biosensing technology get advantage of the quenching capabilities of the graphene oxide (GO), using a 96 microwell plate coated with GO and photoluminescent bioprobes. Because of the quenching capabilities of the GO, using nonradiative energy transfer, microwell coated with graphene oxide can deactivate the photoluminescence of the bioprobes that are not experimenting immunoreactions via antibody-analyte affinity. Otherwise, when the bioprobes are experimenting immunoreactions, they preserve their photoluminescence because of the distance and the low affinity between the immunocomplex bioprobe-analyte and microwells coated with GO. The biosensig platform calibrated with *E. coli* samples exhibiting concentrations between 0 and 10^6 CFU mL^{-1} obtained a limit of detection of ~ 2 CFU mL^{-1} with an optimal time response of 30 minutes. Then, the biosensing platform was tested with industrial food samples obtained from "La Próxima Estación", a Mexican company devoted to produce frozen fruits and vegetables. In this chapter, the development of the biosensing technology targeting *E. coli* will be described in detail, as well as the followed methods and the outcomes.

A. Introduction

Pathogenic bacterial outbreaks are responsible for the highest numbers of hospitalization and deaths compared to those of viral or chemical origin. Due to it, bacterial contamination represents a major concern to safety and human health and environment. Additionally, this problem continues growing because of bacterial antibiotic is evolving, and this issue may become more deadly than cancer-related diseases, unless specific actions are taken. One of these actions might be the development and use of efficient methods of bacterial detection. Hence, timely detection of bacteria is crucial in environmental monitoring, food quality assessment, and clinical diagnostic testing.[27]

Although the conventional techniques employed for pathogenic bacterial detection are highly effective and consistent, they frequently require highly specialized technical skills, high-cost, cumbersome procedures, and time consuming (up to 72h). These techniques for pathogenic bacteria detection includes culture- based methods (microbiological plating, microscopic visualization, biochemical tests), and other biomolecular methods such as enzyme-linked immunosorbent assay (ELISA) and polymerase chain reaction (PCR). Under this context, the use of nanomaterials for the development of detection alternatives continues increasing. Some of these nanomaterials exhibit exceptional optical properties, that can be used for the development of optical biosensing platforms. Literature highlights optically active nanoparticles, carbon-based materials, and metal−organic frameworks as innovative platforms facilitating fast, highly sensitive, and selective biosensing targeting bacteria. In addition, the application of nanotechnology in biosensing for the identification of pathogenic-related analytes may be suitable adapted to high-throughput formats for single-step assays.[27]

Based on this background, we propose a biosensing platform based on graphene oxide (GO) quenching capabilities and the use of a photoluminescent bioprobe (PBP), which comprises quantum

dots (QD) nanocrystals conjugated with antibodies anti-*E. coli*. The use of QD nanocrystals in biosensing, have been proven advantageous due to their highly efficient fluorescence, size-tunable Gaussian emission spectrum, excellent stability against photobleaching, large Stokes shift, and minimal background signal. The platform proposed for the biosensing technology is a 96 microwell plates coated with GO in the microwell surface. These 96 microwell plates are widely used for clinical diagnostics and allow for the analysis of several samples at the same time, giving the high-throughput characteristic to the proposed biosensing platform. As a single-step biosensing system via no radiative energy transfer, which is a spectral and distance-dependent phenomenon, microwells coated with GO deactivate the photoluminescence of those PBP that do not experiment immunoreactions via antibody-analyte affinity. Nevertheless, those PBP that experiment immunoreactions preserve their photoluminescence due to the distance and low affinity between the complex (PBP-analyte) and the GO-coated microwell. The biosensing concept of the highly sensitive and selective bacterial detection platform is illustrated in Figure 2.1.[27]

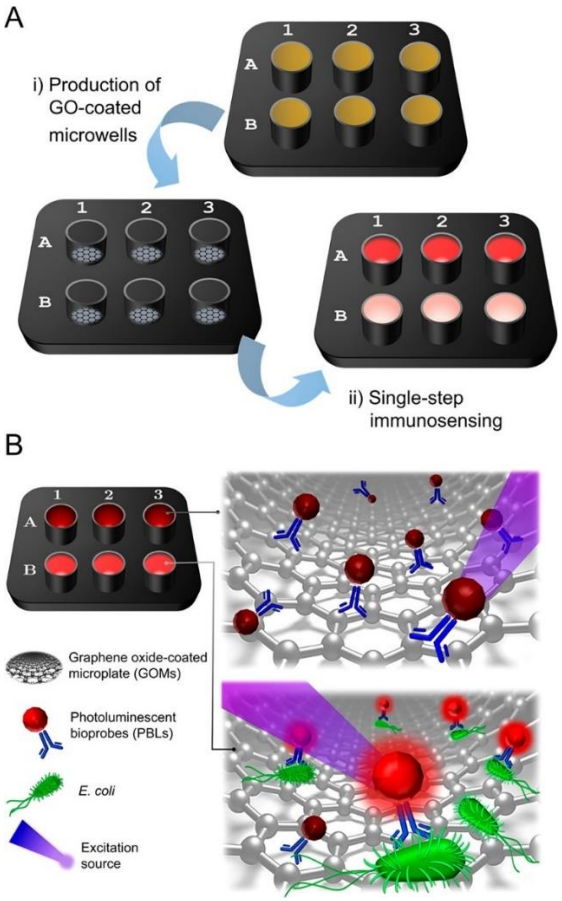

Figure 2.1. A. *Schematic representation of the general procedure to coat microwell plates with GO. (i) microplates decorated with GO via hydrophilic interactions. (ii) Microplates coated with GO, a ready-to-use bacterial detection platform.* ***B.*** *Operational principle of the proposed single-step, wash-free, and real-time bacterial detection platform. Using nonradiative energy transfer, microwell coated with GO can deactivate the photoluminescence of the bioprobes that are not experimenting immunoreactions via antibody-analyte affinity. Otherwise, when bioprobes are experimenting immunoreactions, they preserve their photoluminescence because of the distance and the low affinity between the immunocomplex bioprobe-analyte and microwells coated with GO. Adapted with permission.[27] Copyright 2020, ACS.*

B. Experimental Methods

Reagents and equipment

All the reagents were selected, purchased and carefully handled according to the data sheets provided by the suppliers. Table 2-1 summarizes the supplier and specifications of each reagent.

***Table 2-1**. Reagent suppliers and specifications*

Reagent	Supplier	Specifications
Monolayer GO aqueous suspension	Angstron Materials	lateral size ∼500 nm, carbon/oxygen ratio ∼1
Sterilized culture-treated 96-well black plates	Costar	bottom and lid of polystyrene
Bovine serum albumin (BSA)	Sigma- Aldrich	-
Tween 20	Sigma- Aldrich	-
Phosphate-buffered saline (PBS) tablets	Sigma- Aldrich	-
Biotinylated polyclonal anti-Escherichia coli antibody	Abcam	ab68451, exhibit ∼4− 8 molecules of biotin per antibody molecule
Streptavidin quantum dot 655	Life Technologies	QDs have ∼5−10 molecules of streptavidin per nanocrystal.
bacterial strains	Obtained and treated following previously reported methods	-
Milli-Q system	Millipore	>18.2 MΩcm^{-1}

The photoluminescence measurements were performed using a Cytation5 multimode reader (BioTek).

Buffers

Buffers are solutions that contain a mixture of a weak acid and its conjugated base to maintain pH, which prevents biomolecules changes and avoid ionic changes.[32]

Phosphate Buffered Saline (PBS) was used to perform dilutions of different reagents such as the sample and bioprobe dilutions. Besides, PBS is used as the blank or control sample. PBS is a water-based salt solution containing disodium hydrogen phosphate, sodium chloride and, in some formulations, potassium chloride and potassium dihydrogen phosphate. It is prepared with 200 mL of ultrapure water and one PBS tablet from Sigma-Aldrich. Immunobuffer is used to promote Ab-QD conjugation or immunolabeling, this buffer facilitates interaction between biotinylated antibodies and streptavidin-QD.[33–35] It is prepared using PBS supplemented with 0.5% Tween 20 (v/v) and 1% Bovine Serum Albumin (BSA) (w/v). This buffer needs storage at 4-8°C.

Production of GO coated microwells.

According to the supplier, the microplates employed have functional groups at the bottom of each microwell which give to the surface hydrophilic properties. Since GO also have oxygen functional groups, that is hydrophilic domains, these microplates can be decorated with GO via hydrophilic

interactions using different concentrations of GO aqueous suspensions (from 1100 to 1600 μgmL^{-1}). Each microwell was incubated overnight with 100 μL or GO suspension and then washed at least three times using ultrapure water to remove the GO overage that was not attached to the microwell surface. After the washing stage, the microplate is ready to be used for single step bacterial biodetection, or to be stored at room temperature being stable in terms of quenching capabilities at least for two weeks.

In optimal conditions the microwell coatings were prepared with GO concentrated at 1200 μg mL^{-1}.

PBP conjugation

Photoluminescent bioprobe (PBP) comprises quantum dots (QDs) nanocrystals conjugated with antibodies anti-*E. coli*. This conjugation was performed by mixing 100μL of streptavidin-QDs concentrated at 9 nM with 100μL of biotinylated anti-*E. coli* concentrated at 72 μg mL^{-1}. The mix was diluted in immunobuffer during 45 min of mixing at 650 rpm. Then it was diluated again, this time in PBS to reach the optimized concentration, [QD]= 0.1125 nM and [Ab] = 0.90 μg mL$^{-1.}$

Binding of biotin with streptavidin is one of the strongest noncovalent biological interactions in nature. The high affinity between this pair is a result from many factors such as the formation of multiple hydrogen bonds and van der Waals interactions. [36,37]

Single step biosensing targeting E. coli.

Inside each microwell, it is possible to analyze one sample by adding 100 μL of the sample and 100 μL of the PBP. For each sample, three parallel experiments were performed to evaluate the concerning precision. The readout of the photoluminescence was realized using Cytation5, a multimodal reader that includes filter- and monochromator-based fluorescence detection, luminescence, and UV-Vis absorbance detection by Biotek, photoluminescence readout was taken every five minutes for 120 minutes (excitation wavelength: 365nm, emission wavelength 660± 20nm). Limit of detection was computed as the read of the mean of the blank samples plus three times its standard deviation, interpolating then this value in the respective calibration curve equation. In optimized conditions, PBP is concentrated at [QD]= 0.0562 nM and [Ab] = 0.45 μg mL^{-1} in microwell where "Ab" represents the employed antibody anti-*E. coli*.

Specificity

To demonstrate the specificity of the bacterial detection platform, we designed and performed an experiment using a Salmonella typhimurium strain as an interference model. Although the specificity of the employed antibody is guaranteed by the manufacturer, we tested the bacterial detection platform targeting *E. coli* with different concentrations of this nontarget bacteria (*S. Thyphi*.), ranging from 5 to 10^6 CFU mL^{-1}. We also analyzed other samples containing (i) a relatively low concentration of *E. coli* (10^3 CFU mL^{-1}) and a relatively high concentration of *Salmonella* (10^5 CFU mL^{-1}) and (ii) relatively high concentrations of both strains (both concentrated at 10^5 CFU mL^{-1} in the same sample).

Preparation of Industrial Samples

Industrial samples of cauliflower were analyzed to demonstrate that the biosensing technology is useful to detect bacteria in real food matrix. These cauliflower samples were provided by "La próxima estación S.P.R.deR.L.", a Mexican company dedicated to process frozen fruits and vegetables. Prior to analysis with the proposed bacterial biosensing platform, the samples were analyzed using 3M Petrifilm *E.coli*/ Coliform Count (EC) Plates via culture-based method. These samples were prepared

using a relationship 1/10 (w/v) in PBS and were processed in a sterile plastic bag and homogenized using a Stomacher. After this process, the samples were diluted using a relationship of 1/40 to be analyzed via the proposed technology. Statistical comparison of positive and negative samples was performed via two-way analysis of variance.

C. Results and discussions

Both, bioreagents and nanomaterials are required to be systematically optimized, taking in consideration the best performance of the biosensing system quenching of fluorescence ratio (I_f/I_0) and the concentration of the reagents.

For the microwell plates coated with graphene oxide, is important to optimize the GO concentration to determine which concentration exhibits the best performance in terms of quenching of fluorescence ratio. Quenching fluorescence ratio is defined as I_f/I_0, where I_f is the photoluminescence intensity of PBP at time f (generally from 5 to 120 min), and I_0 is the photoluminescence intensity of PBP at time 0. Quenching fluorescence ratio can be interrogated in real-time, this is extraordinary in label-based optical biosensing because real-time interrogation is usually an advantage of label-free optical biosensors. As mentioned in the experimental methods, microwells were coated with GO with different concentrations ranging from 1100 to 1600 µg mL^{-1}. QDs were diluted at 0.1 nM to evaluate such a quenching ratio. Figure 2.2 shows the trend in the quenching ratio according to the evaluated GO concentration, the lower I_f/I_0 ratio was observed using GO at 1100 µg mL^{-1}, whereas the highest quenching ratio was observed using GO at 1200–1400 µg mL^{-1}. Microwells coated with GO at 1600 µg mL^{-1} exhibited a less effective quenching phenomenon when compared with that obtained with GO at 1200–1400 µg mL^{-1} in terms of the I_f/I_0 ratio, we explain this saturation behavior given mass-transport limitations, thereby microwells prepared with GO at 1600 µg mL^{-1} saturated such a decoration process.

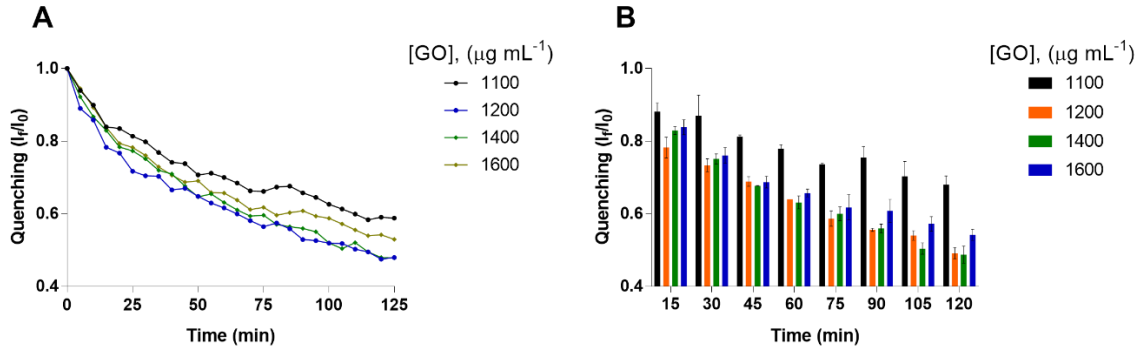

Figure 2.2. *Microplates coated with GO at different concentrations and their QDs quenching capabilities in terms of the I_f/I_0 ratio.* ***A.*** *Real-time interrogation.* ***B.*** *Performance of the studied photoluminescence quenching across different times. The error bars represent the standard deviation of three parallel experiments. QDs were used at [QD] = 0.1 nM. Adapted with permission.*[27] *Copyright 2020, ACS.*

To confirm the optimum concentration of GO to obtain the highest photoluminescence quenching ratio, we performed an assay using [QD]=0.1nM and [Ab]=1.25 µg mL^{-1}. PBP mixed with Samples of *E. coli* at different concentration ranging from 0 to 10^6 CFU mL^{-1} and microwells coated with GO at several concentrations (1100 to 1400 µg mL^{-1}). Figure 2.3 shows that microwells coated with GO at 1200 µg mL^{-1} gives I_f/I_0 values proportional to the analyte concentration, proving that the proposed

biosensing system is technically feasible. Based on this outcome, GO at 1200 µg mL^{-1} was chosen as optimal.

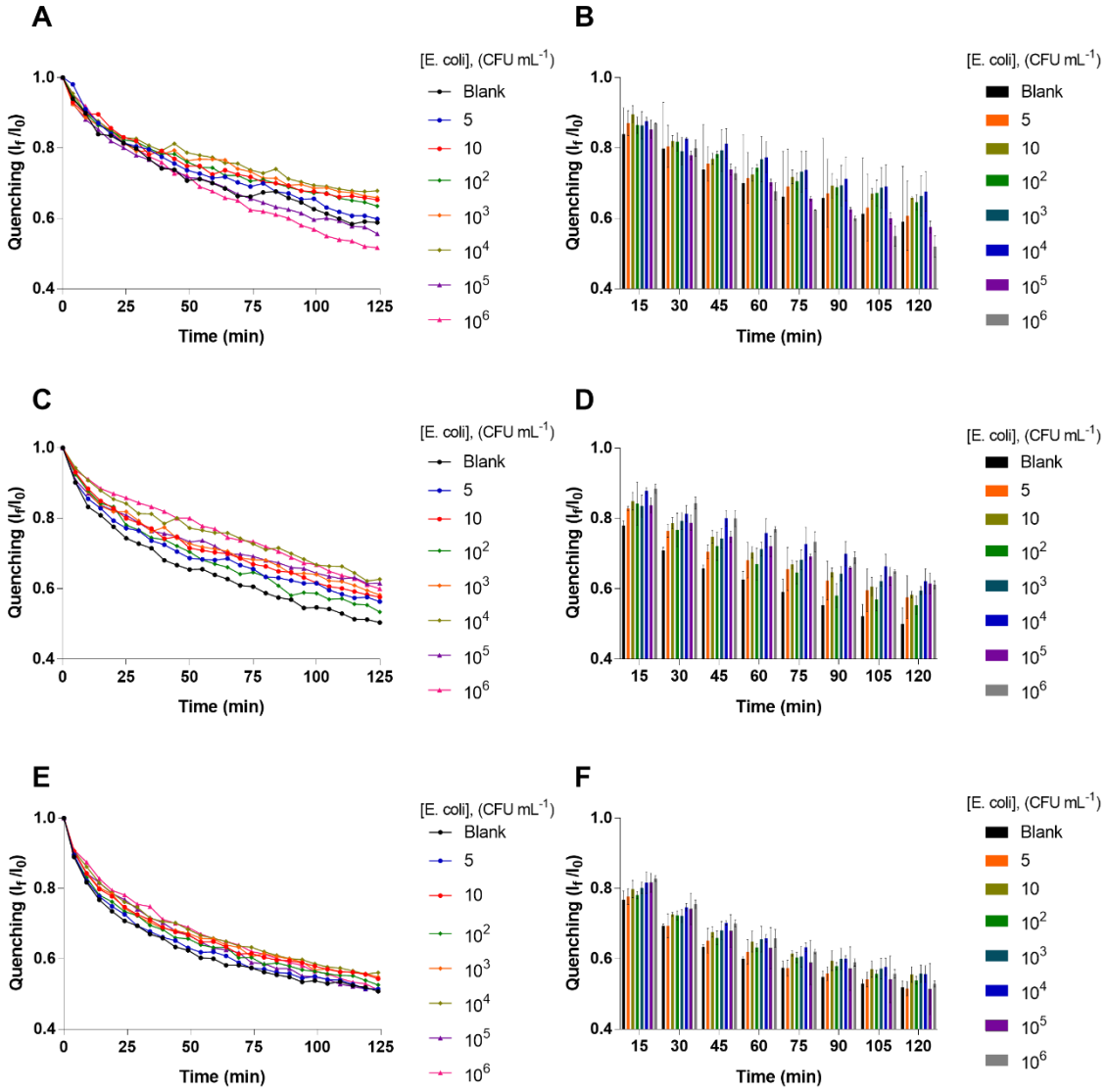

Figure 2.3. *Real-time performance of the proposed bacterial detection platform GO at different concentrations.* ***A-B****. Microwells coated with GO at 1100 µg* mL^{-1} *as bacterial detection platform.* ***C-D****. Microwells coated with GO at 1200 µg* mL^{-1} *as bacterial detection platform.* ***E-F****. Microwells coated with GO at 1400 µg* mL^{-1} *as bacterial detection platform. The error bars represent the standard deviation of three parallel experiments. PBP concentrated at [QD] = 0.1 nM and [Ab] = 1.25µg* mL^{-1}*. Adapted with permission.*[27] *Copyright 2020, ACS.*

To optimize the concentration of PBP in term of sensitivity and variability and reach the most efficient behavior of the biosensing system, we used [QD] = 0.1125 nM and different concentrations of antibodies anti-*E. coli* (Ab) such as 1.5, 1.25, and 0.9 µg mL^{-1}, respectively. The results obtained using these different concentrations of PBP are shown in Figure 2. 4. PBP with a final concentration of QDs-antibody at 0.1125 nM and 0.9 µg mL^{-1}, respectively, were observed to offer the best

analytical performance in terms of both sensitivity and coefficient of variation (CV). In those experiments performed with QDs-antibody conjugates at 0.1125 nM and 0.9 µg mL^{-1}, respectively, the CVs range from 0.39 to 12.43%, which according to the literature, this level of precision is acceptable for immunoassays[38], see Table 2-2.

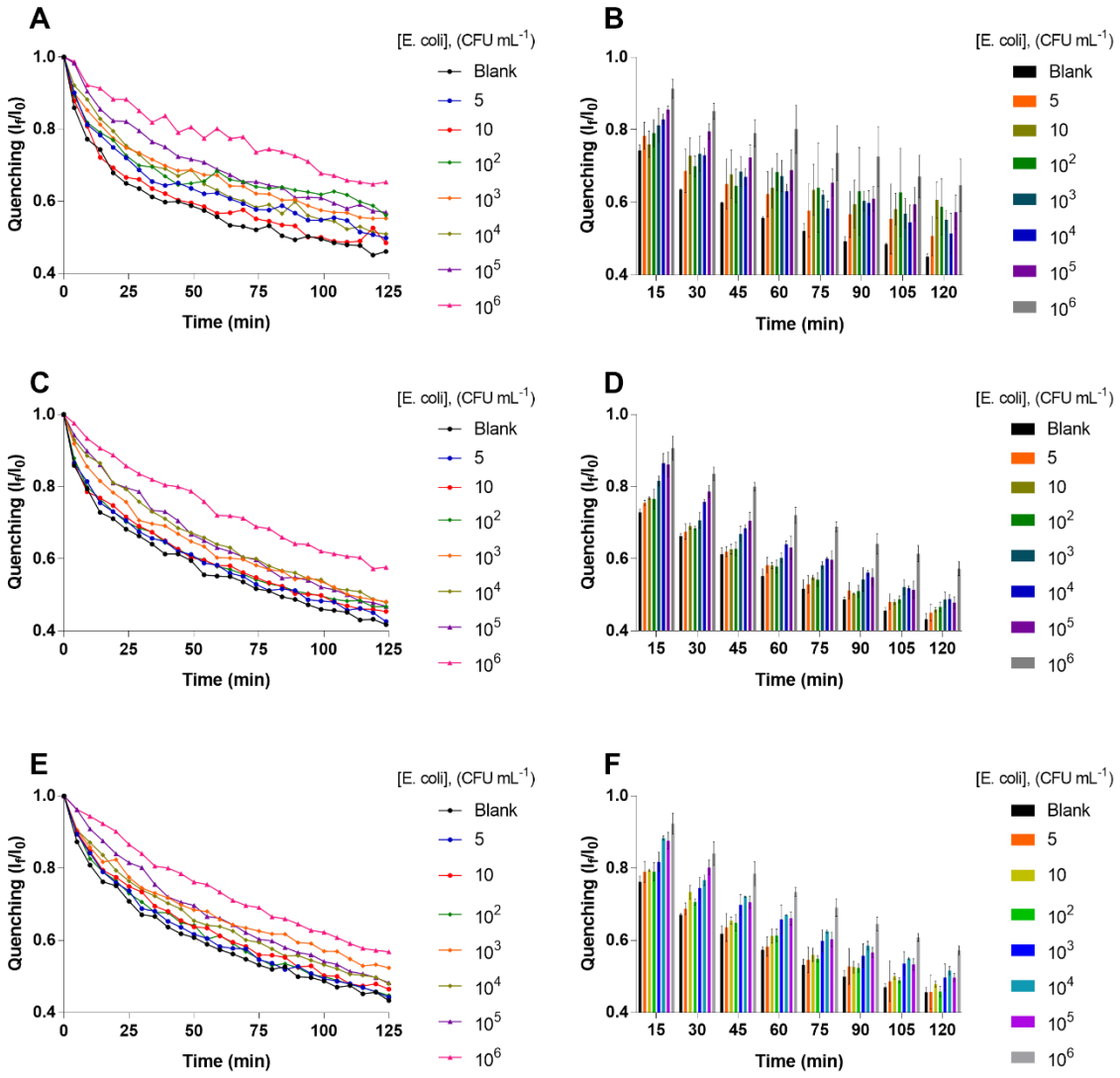

Figure 2.4. *Real-time performance of the proposed bacterial detection platform using PBP at different concentrations.* ***A-B.*** *PBP prepared with [QD] = 0.1125 nM and [Ab] = 1.25µg mL^{-1}.* ***C-D.*** *PBP prepared with [QD] = 0.1125 nM and [Ab] = 1.5 µg mL^{-1}.* ***E-F.*** *PBP prepared with [QD] = 0.1125 nM and [Ab] = 0.90 µg mL^{-1}. Microplate coated with GO at 1200 µg mL^{-1}. The error bars represent the standard deviation of three parallel experiments. Adapted with permission.[27] Copyright 2020, ACS.*

Table 2-2. *CVs of the optimized biosensing system using E. coli as model analyte. PBP prepared with [QD] = 0.1125 nM and [Ab] = 0.90 µg mL^{-1}. Adapted with permission.[27] Copyright 2020, ACS.*

[*E. coli*] (CFU mL^{-1})	**CV (15 min)**	**CV (30 min)**	**CV (45 min)**	**CV (60 min)**	**CV (75 min)**	**CV (90 min)**	**CV (105 min)**	**CV (120 min)**
0	2.12%	0.49%	3.53%	1.45%	3.02%	3.21%	2.07%	2.98%
5	3.66%	2.31%	6.03%	4.62%	6.43%	9.34%	11.56%	10.15%
10	0.39%	2.57%	1.45%	3.11%	3.35%	3.21%	1.59%	1.66%
10^2	3.26%	1.22%	3.55%	2.80%	1.65%	2.29%	1.48%	3.00%
10^3	3.34%	3.93%	4.04%	5.99%	8.23%	11.39%	11.05%	12.43%
10^4	9.63%	6.43%	8.69%	8.67%	8.88%	8.67%	9.26%	6.48%
10^5	2.67%	2.54%	2.40%	2.72%	3.26%	2.48%	2.98%	2.25%
10^6	3.15%	3.85%	4.22%	1.75%	3.44%	2.89%	1.74%	2.12%

Figure 2.5 summarizes the results of the proposed technology operating in optimal conditions. The bacterial detection platform was noted to exhibit a modulated sensitivity within the first 45 min of analysis, reaching its best performance at 30 min, and at the same time the limit of detection accounted for 2 CFU mL^{-1}, which is competitive when compared with that of other recently developed bacterial detection platforms (i.e., ranging from 1 to 1000 CFU mL^{-1}).[39–41]

With these results in mind, we decided to prove the selectivity of the bacterial detection platform through the assay detailed in experimental methods section. Figure 2.5A-B shows that the samples containing only *Salmonella* in any concentration behave as blank samples in terms of I_f/I_0. Hence, *Salmonella* is not generating any cross interference.

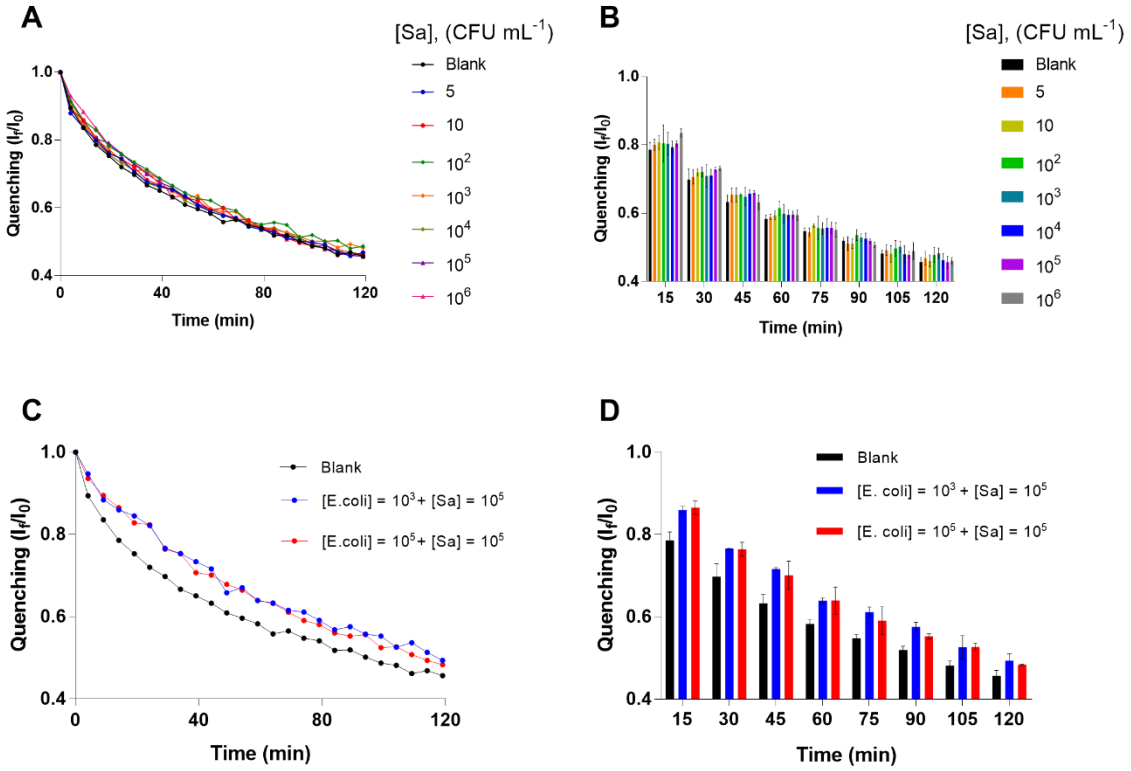

Figure 2.5. *Selectivity of the proposed bacterial detection platform operating in optimal conditions.* ***A-B****. Real-time performance of the biosensing system with different concentrations of Salmonella as a potential interference.* ***C-D****. Real-time performance of the analysis of samples containing E. coli and Salmonella at different concentrations. Blank samples were also included as a reference. PBP prepared with [QD] = 0.1125 nM and [Ab] = 0.90 µg mL*$^{-1}$*. Using GO at 1200 µg mL*$^{-1}$*. The error bars represent the standard deviation of three parallel experiments. Adapted with permission.*[27] *Copyright 2020, ACS.*

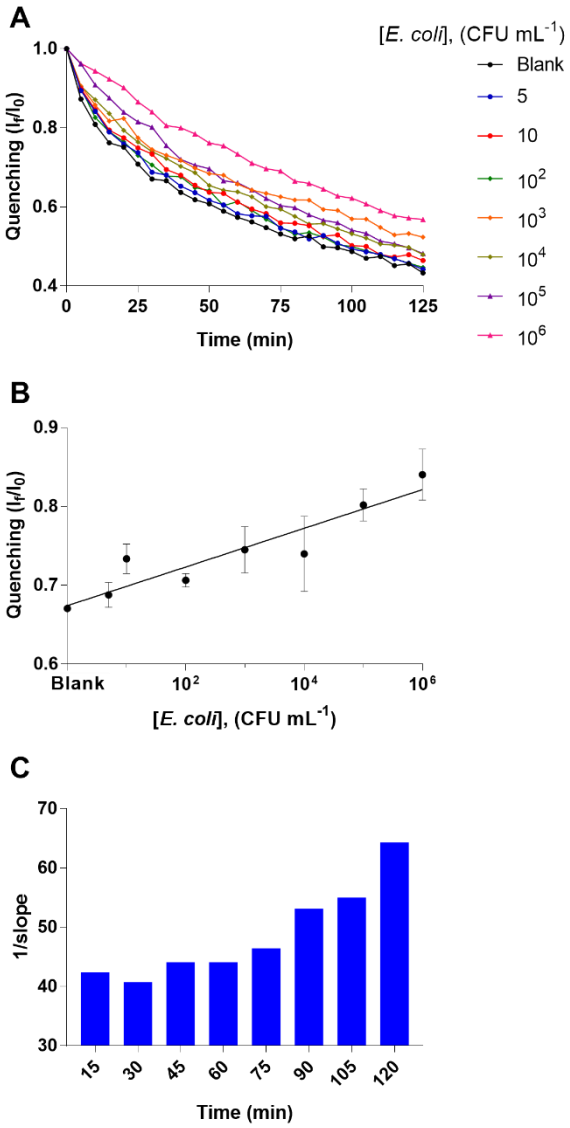

Figure 2.6. *Bacterial detection platform operating in optimal conditions. PLBs were prepared with [QD] = 0.1125 nM and [Ab] = 0.90 µg mL^{-1}. Microplates coated with GO at 1200 µg mL^{-1}.* ***A.*** *Real-time quenching profile of different E. coli concentrations.* ***B.*** *The calibration curve resulting at 30 min of the assay. The error bars represent the standard deviation of three parallel experiments.* ***C.*** *Evolution of the sensitivity of the assay in terms of 1/slope values (The lower 1/slope the higher sensitivity). Adapted with permission.*[27] *Copyright 2020, ACS.*

To prove that the proposed biosensing technology is useful beyond the controlled conditions of the laboratory, as a proof-of-concept, we analyzed industrial samples of cauliflower using the developed bacterial detection platform. As mentioned in the experimental methods section, all the cauliflower samples were provided and previously classified via culture-based methods as negative or positive for *E. coli* by "La próxima estación". We used four negative and four positive samples, which were classified as positive and negative using the proposed bacterial detection technology, Figure 2.7 shows the classification of the samples at different times. I_f/I_0 ratio from negative samples is equivalent to I_f/I_0 from blank sample. Staring from this classification, we performed a statistical analysis where the resultant I_f/I_0 values of the two groups of samples were reported to be statistically

different, reaching the lower P value ~30 min of the assay (P = 0.004), see Figure 2.8 and Table 2-3. P value was obtained by means of an unpaired T-student test. The employed confidence interval was 95 %, thereby, the threshold related to the respective statistical significance of the P value is < 0.05.

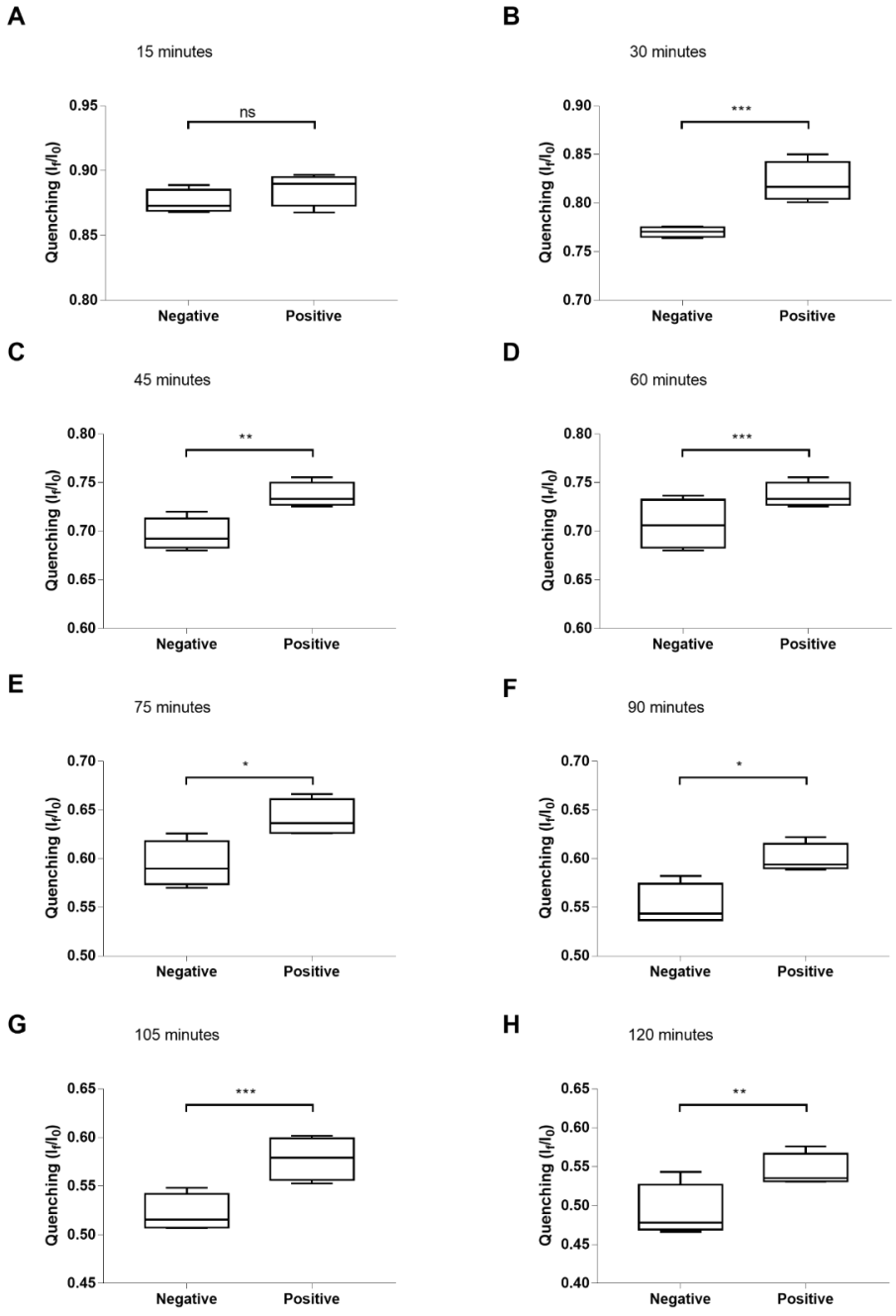

Figure 2.7. *Statistical analysis of the analytical behavior of the proposed bacterial platform operating with industrial samples of cauliflower in terms of the resulting I_f/I_0 ratio. Performance at 15 (**A**), 30 (**B**), 45 (**C**), 60 (**D**), 75 (**E**), 90 (**F**), 105 (**G**) and 120 (**H**) minutes. The box plots show the median, 25th and 75th percentiles and the extreme values of the respective distribution of I_f/I_0 values. Adapted with permission.*[27] *Copyright 2020, ACS.*

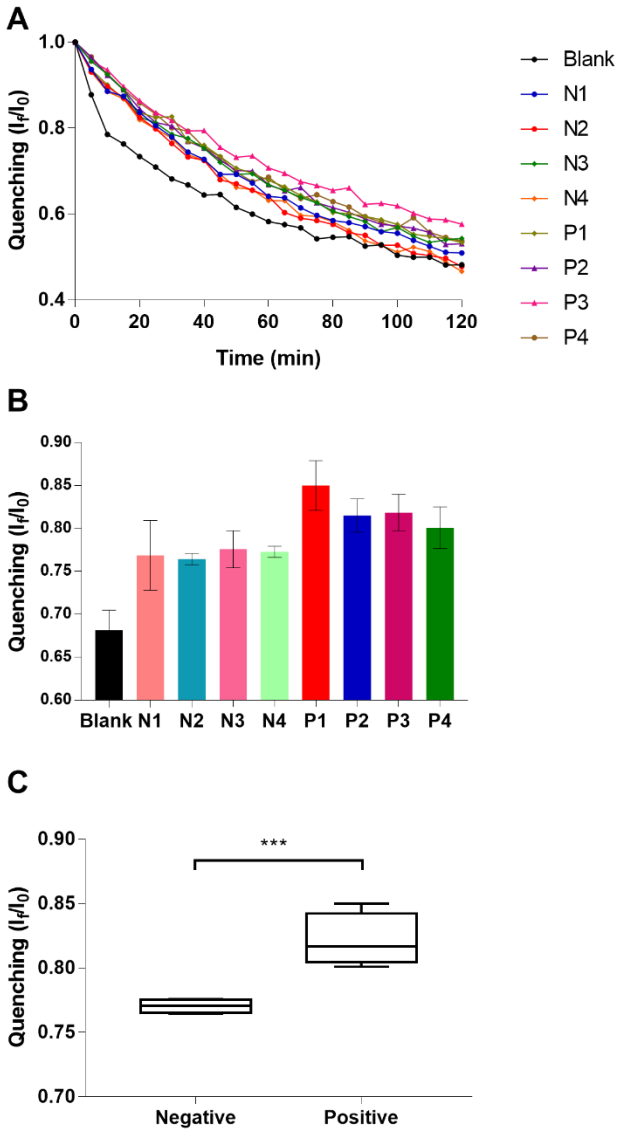

Figure 2.8. *Analysis of industrial samples of cauliflower via the proposed bacterial platform—a proof of concept. The samples were previously classified as negatives or positives via a culture-based method (four negative, Ni, and four positive samples, Pi, respectively).* ***A****. Real-time quenching profile of the analyzed samples.* ***B****. Analytical performance of the studied technology with real samples at 30 min. The error bars represent the standard deviation of three parallel experiments.* ***C****. Distribution of the respective I_f/I_0 values at 30 min of the assay. The box plots show the median, 25th, and 75th percentiles and the extreme values of the respective distribution. Adapted with permission.*[27] *Copyright 2020, ACS.*

Table 2-3. *Two-way analysis of variance of the analytical behavior of the proposed bacterial platform operating with industrial negative and positive samples of cauliflower in terms of the resulting I_f/I_0 ratios.*

Time (min)	% of total variation	P value	Significant
15	4.478	0.4253	ns
30	58.74	0.0004	***
45	42.67	0.0022	**
60	25.72	0.0004	***
75	34.16	0.0112	*
90	35.75	0.0127	*
105	41.71	0.0044	**
120	31.32	0.0096	**

In this context, the proposed technology is potentially useful in high-throughput analysis of industrial samples of food.

All in all, this chapter discussed a conceptually innovative and advantageous bacterial detection platform based on GO quenching capabilities. This bacterial detection platform was demonstrated to have several technological advantages such as avoiding the need of secondary antibodies; it is single step and wash free which provides a fast response and avoids cumbersome procedures; it uses a high throughput format with high sensitivity (around 2 CFU mL^{-1}); it is cost-effective compared with the culture-based method used in the food industry ($2.50 USD), the cost per test is around $0.44 USD at laboratory scale (see Table 2-4). Besides, it is a transformative platform as GO is able to quench different fluorophores, and other pathogens can be detected by simply changing the involved antibody.

Table 2-4. *Cost estimation*

Material	**Total volume**	**Concentration**	**Cost**	**Volume per assay**	**Used concentration**	**Cost per assay**
Microwell plate	96 wells	N/A	$5.00	3 wells	N/A	$0.17
GO	1000 mL	5000 µg mL^{-1}	$195.00	72 µL	1200 µg mL^{-1}	$0.02
Anti- *E. coli* (Ab)	500 µL	4000 µg mL^{-1}	$630.00	0.07 µL	0.9 µg mL^{-1}	$0.09
QD	200 µL	1 µM	$690.00	0.034 µL	0.1125 nM	$0.12
PBS	100 tablets	N/A	$130.00	N/A	N/A	$0.01
BSA	25 g	N/A	$930.00	N/A	N/A	$0.03
Tween 20	100 mL	N/A	$40.00	N/A	N/A	$0.01
					TOTAL	$0.44

CHAPTER 3. Facile Determination of COVID-19 Seroconversion via Nonradiative Energy Transfer

During the COVID-19 pandemic, serological testing became paramount, since these tests are a significant tool to identify citizens with potential immunity, specific regions with herd immunity as well as monitoring immunity after vaccination. The development of fast, cost-effective and effective serological and clinical diagnostics tools is a major necessity to face pandemic scenarios. Hence, we proposed a high-throughput, fast, cost-effective, and straightforward technology aimed at the interrogation of COVID-19 seroconversion. Such a technology is mainly composed of a SARS-CoV-2 spike receptor binding domain (RBD) recombinant protein as recognition element labeled with FITC. As a result, it is obtained a FITC-RBD bioprobe (F-RBD) intended to detect COVID-19 antibodies. The aim of the F-RBD probe in the assay for COVID-19 seroconversion is to deactivate or preserve its fluorescence via nonradiative energy transfer. The nonradiative energy transfer occurs due to the presence of graphene oxide (GO) coated surface. Under this feature, the analysis of a sample clean of COVID-19 antibodies will deactivate the fluorescence in the bioprobe. On the contrary, a sample containing COVID-19 antibodies will preserve the fluorescence in the bioprobe. The reported COVID-19 seroconversion test offers optimum results within 42 minutes with a cost of less than 0.5 USD per test at laboratory scale. The technology was demonstrated to be useful for COVID-19 antibodies detection in clinal samples: 34 human serum samples were analyzed via the seroconversion assay described in this Chapter. These samples were successfully differentiated between positive and negative requiring only 1 µL of serum sample.

A. Introduction

SARS-CoV-2

During the last three years the world has lived a catastrophic scenario: the COVID-19 pandemic. In December 2019, an outbreak of pneumonia of unknown origin was reported in Wuhan, China. The study and analysis of respiratory human samples, led to the isolation of a novel respiratory virus and its genome analysis showed a novel coronavirus related to SARS-CoV, named severe acute respiratory syndrome coronavirus 2 (SARS-CoV-2). The global spread of SARS-CoV-2 and the thousands of deaths caused by coronavirus disease (COVID-19) led the World Health Organization (WHO) to declare a pandemic on 12 March 2020.[42,43] Experts agree that testing along with the risk management and the healthcare system is a pivotal response in all outbreaks and leads to lower mortality rates. In this context, biosensors are powerful tools for effective assessment of clinical progress and to provide alertness on severity or critical trends of infection.[42]

It is possible to detect SARS-CoV-2-related infections throughout several biomolecules, which are shown in Figure 3.1. “Novel coronavirus exhibits spike proteins which are immunogenic; hence, the immune system is able to produce immunoglobulins to trigger an immune response against the pathogen.”[42] Immunoglobulin M (IgM) antibodies are produced during the first days of infection, between 4 and 10 days, and the immunoglobulin G (IgG) response is produced later (around 2 weeks).[42]

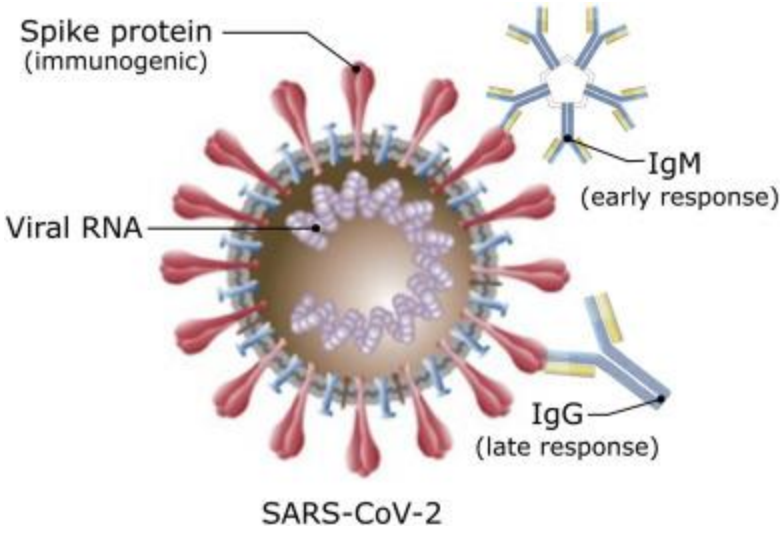

Figure 3.1. *Schematic representation illustrating the structure of SARS-CoV-2 and related targeting sites (biomolecules). Adapted with permission.*[42] *Copyright 2020, Elsevier.*

The SARS-CoV-2 spike glycoprotein is a type I membrane protein (Figure 1a), which forms a trimer, anchored to the viral membrane by its transmembrane segment. The structure of the Spike protein includes receptor-binding domain (RBD) which is the site binding with the ACE 2 from the host (infected cell). [44,45] Due to this, the RBD from SARS-CoV-2 is commonly used for the development of serological tests.

Determination of COVID-19 seroconversion

A serological test can be defined as a laboratory test that checks for the presence of antibodies or other substances in a blood sample. Antibodies are proteins made by the immune system in response to a foreign substance or microorganism, such as a virus. Serology tests look for certain antibodies to see whether a person has been exposed to or infected with an infectious agent.[46] Specifically, determination of COVID-19 seroconversion, in a pandemic scenario, can be useful (i) for the detection of past infection, (ii) in convalescent plasma donation processes, (iii) for the evaluation of protection against later viral exposure and/or for contact tracing roles, (iv) for vaccine selection and prioritization, and (v) in future application to identify COVID-19 medical sequelae. Generally, a COVID-19 serological test determines an immune response against the spike (S) protein of SARS-CoV-2.[28]

Currently, there exist commercially accessible bioassays targeting COVID-19 antibodies, whose results can range from 10 min (Xiamen AmonMed Biotechnology) to 45 min (Cepheid Xpert Xpress). Their formats, requiring at least two bioreagents with capture and detection purposes, include colloidal gold/lateral flow immunoassays and fluorescence immunoassays (Goldsite diagnostics kit). Nevertheless, it would be a progress to add high-throughput, fast, cost-effective, and straightforward technologies to facilitate and enhance the efficiency of COVID-19 seroconversion bioassays. With the intention of adding these interesting characteristics to the COVID-19 seroconversion bioassays, we put forward fluorescein-tagged SARS-CoV-2 spike receptor-binding domain recombinant protein (F-RBD) to operate as a bioprobe for COVID-19 antibody (anti-RBD) biodetection. F-RBD bioprobe emits a strong fluorescence upon anti-RBD detection; meanwhile, F-RBD (donnor) fluorescence is deactivated by graphene oxide (GO)-decorated surfaces (acceptor) when COVID-19 antibodies are absent in the sample due to nonradiative energy transfer. The proposed bioassay technology is illustrated in the Figure 3.2. The determination of COVID-19 seroconversion is carried out in a 96-

microwell plate platform. The bioassay can be interrogated in real time and offers a high-throughput and standard format widely employed in diagnostics.[28]

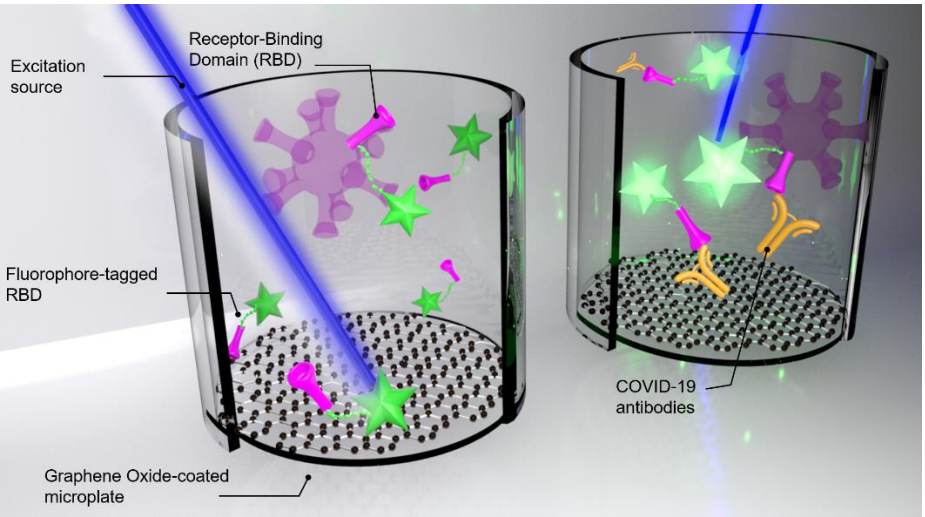

Figure 3.2. *Operational principle of the proposed bioassay for the determination of COVID-19 seroconversion. Fluorescein tagged SARS-CoV-2 spike receptor-binding domain recombinant protein (F-RBD) is proposed as a bioprobe to determine the presence of COVID-19 antibodies. F-RBD emits a strong fluorescence upon COVID-19 antibody detection, meanwhile F-RBD fluorescence is deactivated by graphene oxide-decorated surfaces, via nonradiative energy transfer, when COVID-19 antibodies are absent in the sample. Adapted with permission.[28] Copyright 2021, ACS.*

B. Experimental methods

Reagents and equipment

All the reagents were selected, purchased and carefully handled according to the data sheets provided by the suppliers. Table 3-1 summarized the supplier and specification of each reagent used.

Table 3-1. *Reagent suppliers and specifications*

Reagent	Supplier	Specifications
Monolayer GO aqueous suspension	Global graphene group	lateral size ~500 nm, carbon/oxygen ratio ~1
Sterilized culture-treated 96-well black plates	Costar	bottom and lid of polystyrene
Phosphate-buffered saline (PBS) tablets	Sigma- Aldrich	-
FITC Conjugation Kit (Fast)-Lightning-Link	Abcam	ab188285
SARS-CoV-2 Spike RBD Recombinant Protein	SinoBiological	Cat: 40592-VNAH
SARS-CoV-2 Spike RBD Antibody	SinoBiological	Cat: 40592-T62
Milli-Q system	Millipore	>18.2 MΩcm^{-1}

The photoluminescence experiments were performed using a Cytation5 multimode reader (BioTek).

Decoration of Polystyrene Surfaces with GO

96 microwell plates were used as platform to carry out the bioassay to determine COVID-19 seroconversion. The surface of each microwell is decorated with graphene oxide (GO). In each microwell, 100 μL of GO concentrated at 1200 μg mL^{-1} was introduce and gently shaken overnight at 650 rpm. After that, 3 washing steps were executed to eliminate the GO that did not adhere onto the microwell surface. The optimal concentration of GO to be incubated within the microplate should be carefully studied. [27,47] As explained in the previous chapter, the supplier of the microplates informed that microplates have functional groups at the bottom of each microwell which provide the surface with hydrophilic properties. Since GO also have oxygen functional groups, that is hydrophilic domains, these microplates can be decorated with GO via hydrophilic interactions. After this process the microwell surface is ready to perform the serological bioassay.

Production of bioprobe F-RBD

The bioprobe (F-RBD) required for the serological bioassay comprises fluorescein (FITC) conjugated with SARS-CoV-2 Spike RBD Recombinant Protein (RBD). RBD was obtained lyophilized from the supplier, reconstitution was performed with 100 μL of ultrapure water. The employed FITC conjugation kit allows for the covalent labeling of proteins with FITC by targeting amine groups. Following the instructions of the supplier, to conjugation of FITC with RBD, it was necessary to add 10 μL of the respective modifier reagent in 100 μL of RBD and it was gently mixed. Then, the mix was added in the respective FITC vial, and the solution was mixed using a pipette. After that, the vial was incubated for 15 min in the dark at room temperature. Finally, 10 μL of the corresponding quencher reagent was gently mixed in the conjugation vial. After the mix was incubated for 5 min, F-RBD was ready to be employed as a photoluminescent probe.

Detection of COVID-19 antibodies

To perform the determination of COVID-19 antibodies (anti-RBD), 100 μL of the sample and 100 μL of the bioprobe (F-RBD) were added in each GO decorated microwell. These solutions were prepared using PBS. Three parallel assays were performed to estimate the precision of each measurement. Blank samples were very important not only to monitor the overall behavior of the bioassay but also to build the calibration curve, which was crucial to obtain the limit of detection, which was estimated by interpolating the mean of the blank plus 1.645 times the standard deviation of the blank plus 1.645 times the standard deviation of the lowest concentration measured in the corresponding calibration curve. The fluorescence intensity related to the immunoassay was recorded via a kinetic analysis. Fluorescence intensity readout was taken every 90 seconds for 50 minutes. The probe, F-RBD, was excited at 485 ± 10 nm, and its photoluminescence was recorded with an emission centered at 528 ± 10 nm.

Human serum samples

Clinical samples were collected by our colleagues at Universidad Autońoma de Guerrero (Guerrero, Mexico). All subjects signed an informed consent based on the Helsinki declaration (2013). Samples

of pre-Covid-19 human sera were collected in 2014 and stored at −20 °C. Moreover, samples of human sera were collected from subjects who had a positive COVID-19 PCR test (at least 30 days prior to serum extraction). To avoid risks of infection, the samples were deactivated according to the literature.[48]
In the analysis of the clinical samples 1 μL of the respective serum sample was diluted in 1999 μL of PBS. Then, using PBS, a second dilution at different levels was performed for each serum sample ranging from 1/8875 to 1/12500. For the analysis of the respective dilution, 100 μL of the dilution was added in a microwell decorated with GO and mixed with 100 μL of F-RBD, following the procedure described above.

Statistical Analysis of sera sample testing

A collection of 34 clinical samples were analyzed, 28 samples of pre-COVID-19 human sera and 6 COVID-19 human sera samples from patients previously diagnosed by PCR test. All the box plots presented in this study exhibit the median and the extreme values of the corresponding distribution. The P values were derived from an unpaired Student t-test. The confidence interval used for the analysis was 95%, resulting in a threshold associated with the statistical significance of the P value of <0.05.

C. Results and discussions

Notice that in the proposed serological test, it is important to optimize the F-RBD and GO concentrations. The importance of optimizing these two concentrations relies on their roles; F-RBD as donor and GO coating as acceptor, both in the nonradiative process. The quenching ratio I_f/I_0 is an indicator that can be used to determine the behavior of the biosensing system; where I_f represents the intensity of the fluorescence of F-RBD at time f, and I_0 the intensity of the fluorescence of F-RBD at time 0. Hence, an I_f/I_0 close to 1 indicates a weak quenching phenomenon, whereas an I_f/I_0 close to 0 suggests a strong quenching phenomenon. Based on previous research, using FITC as donor in nonradiative energy transfer,[47] we incubate the bioprobe F-RBD at 60 ng mL^{-1} in microwells decorated with different concentrations of GO (800, 1000, 1200, 1400 and 1600 μg mL^{-1}) during 120 minutes. Figure III.3 shows the behavior obtained with each concentration of the bioprobe, using surfaces decorated with different concentrations of GO. In this series of experiments, a concentration of GO at 1200 μg mL^{-1} was found to be the minimum concentration of GO with the maximum quenching capabilities in a kinetic analysis performed across 120 min (see Figure 3.3A). Besides, surfaces decorated with GO at 1200 μg mL^{-1} offered less variability, this can be observed in the error bars depicted in Figure 3.3B-D. Hence, GO concentrated at 1200 μg mL^{-1} was chosen as an optimal concertation for this approach.
Then, we explored the behavior of the bioprobe F-RBD mixed with blank samples and anti-RBD samples at several concentrations ranging from 0.1 to 400 ng mL^{-1}, interacting with GO decorated surface for 50 minutes. Figure 3.4 shows the behavior obtained from these interactions. It can be observed that anti-RBD samples exhibited a minimum quenching of F-RBD, whereas the blank sample induced a maximum quenching of F-RBD. Based on this experiment we confirmed that F-RBD was useful as a photoluminescent probe to detect COVID-19 antibodies when they are incubated in GO-decorated surfaces. We explain this behavior starting from the fact that the interaction F-RBD/Anti-RBD interferes between FITC (donor) and GO-decorated surface (acceptor), preventing the nonradiative energy transfer. When there is no interaction F-RBD/Anti-RBD, fluorescence intensity from F-RBD is quenched by GO-decorated surface.

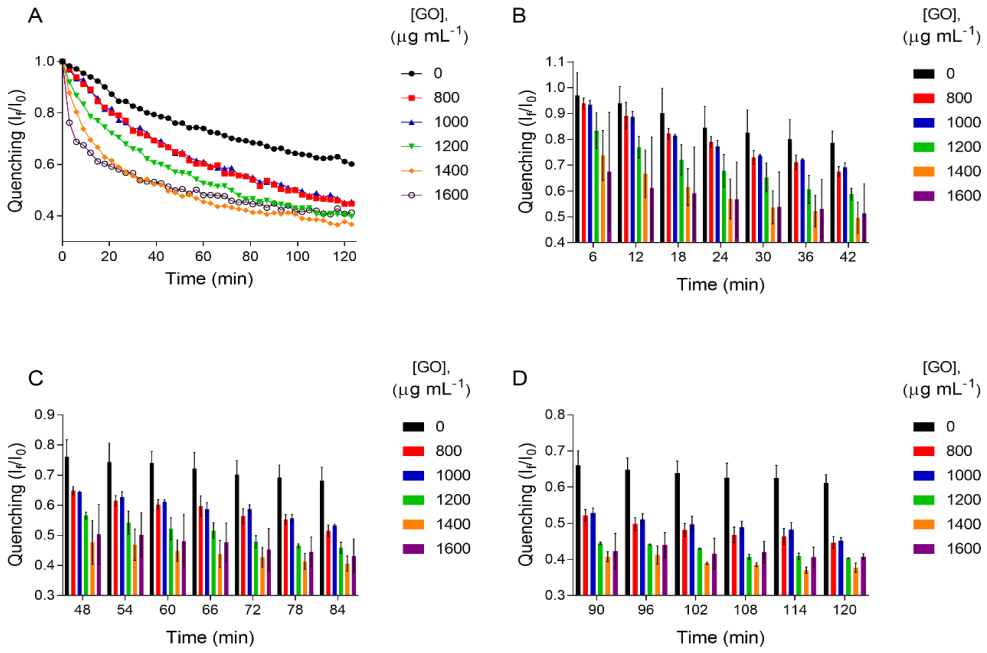

Figure 3.3. *Nonradiative energy transfer occurring between F-RBD (donor) and GO (acceptor). F-RBD concentrated at 60 ng mL^{-1} incubated in microwells decorated with different concentrations of GO.* ***A****. Kinetic analysis during 120 min.* ***B-D****. Bar charts displaying the fluorescence quenching phenomenon at specific times and its variability (depicted by the corresponding error bars). The error bars represent de standard deviation of three parallel experiments. Adapted with permission.*[28] *Copyright 2021, ACS.*

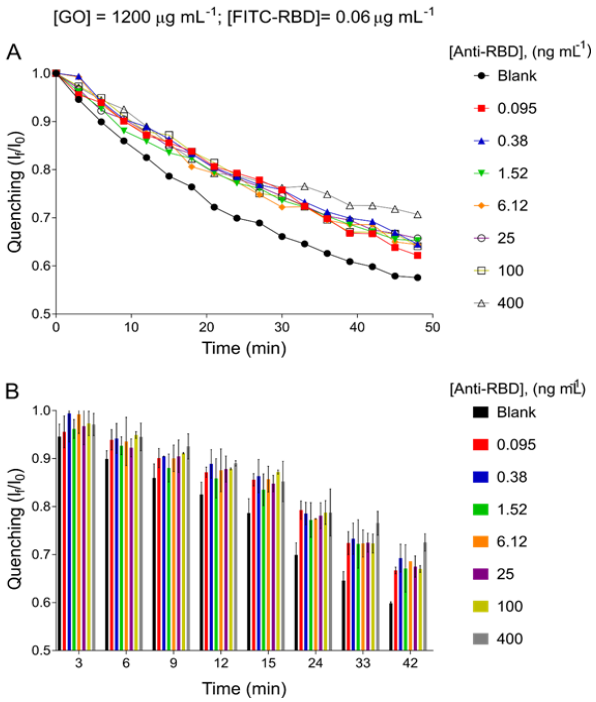

Figure 3.4. *Analytical behavior of F-RBD incubated in GO-decorated surfaces at 1200 μg mL^{-1}, when mixed with blank samples and different concentrations of antibody against SARS-CoV-2 Spike RBD (Anti-RBD).* ***A.*** *Kinetic analysis.* ***B.*** *Quenching of F-RBD at specific times. The error bars represent de standard deviation of three parallel experiments. Adapted with permission.[28] Copyright 2021, ACS.*

Although the bioprobe F-RBD was proven useful for the serological bioassay, the explored range of anti-RBD (0.1 to 400 ng mL^{-1}) triggered similar I_f/I_0 levels across the explored time, suggesting a saturated analytical performance. From these results, we decided to restrict the analytical range of anti-RBD from 0.0039 to 0.5 ng mL^{-1}. Figure 3.5 depicts the corresponding analytical performance where we observe that the sensitivity of the assay evolves across time, we evaluated the bioassay in terms of the inverse of slope of the calibration curve obtained for each time of observation, and its respective limit of detection. From the data obtained, the best sensitivity of the assay is achieved around 42 min within the proposed analysis, where the inverse slope is minimum ~48, and the estimated LOD is around 3 pg mL^{-1}. Table 3-2 shows a summary of all the data obtained and used for the evaluation of each response time.

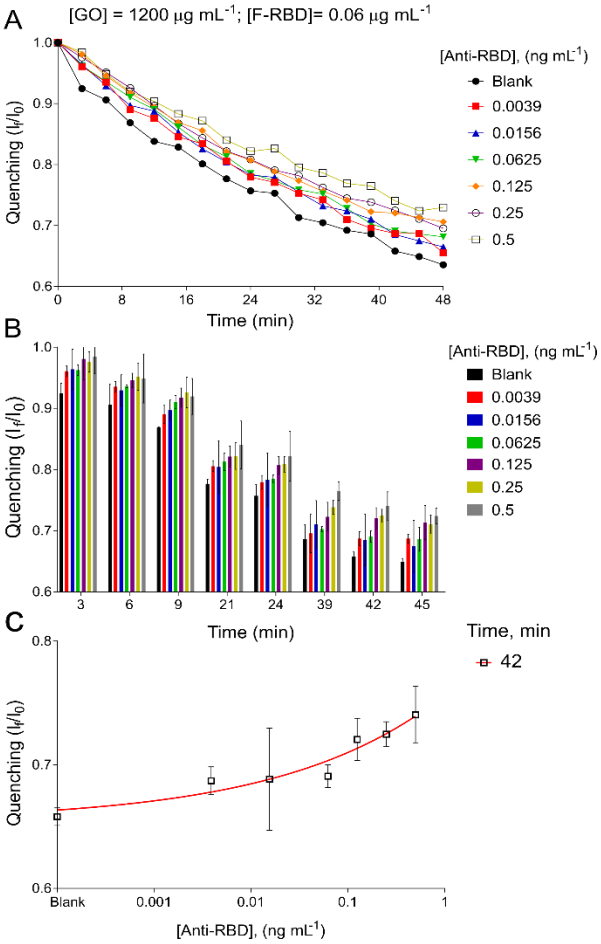

Figure 3.5. *Experimental outcomes of the analytical performance of the biosensing platform targeting different levels of Anti-RBD (standard samples in PBS).* ***A.*** *Real-time analysis in terms of I_f/I_0 ratio.* ***B.*** *Bar chart showing the analytical behavior of the assay at specific times.* ***C.*** *Calibration curve built with data obtained at 42 minutes of the assay. The error bars represent the standard deviation of three parallel experiments. Adapted with permission.*[28] *Copyright 2021, ACS.*

Table 3-2. *Analytical data and coefficient of variation (CV) of the explored biosensing system with optimized reagent concentrations. Adapted with permission.[28] Copyright 2021, ACS.*

Time	**3**	**6**	**9**	**12**	**15**	**24**	**33**	**42**	**45**	**48**
1/slope	66.73	87.03	64.65	59.55	73.63	61.68	53.26	48.45	53.37	42.84
LOD (ng mL^{-1})	0.095	-	1.7x10^{-4}	0.161	2.66	0.46	7.56x10^{-4}	2.22x10^{-3}	1x10^{-3}	4.17x10^{-3}
[Anti-RBD] (ng mL^{-1})	**C.V %**									
Blank	1.759	3.746	0.081	2.36	2.304	2.428	0.702	1.074	0.871	1.446
0.0039	0.944	0.896	1.655	0.649	1.661	1.372	1.518	1.64	1.049	4.912
0.0156	3.394	2.735	1.835	2.769	4.874	5.609	6.677	6.174	6.229	5.975
0.0625	0.895	0.213	1.153	1.625	0.987	0.795	0.406	1.337	2.845	0.808
0.125	3.47	1.234	1.703	1.737	2.32	1.748	3.025	2.381	3.909	2.42
0.25	1.685	2.306	2.718	1.122	2.629	1.566	3.37	1.395	2.05	1.223
0.5	2.854	4.211	3.186	4.581	2.372	4.99	2.028	3.11	1.811	4.229

Enzyme-linked immunoabsorbent assay (ELISA) is consider as gold standard when it comes to immunoassays. ELISA usually offer limits of detection on the order of pg to ng mL^{-1}.[49] In general, the limit of detection of our proposed technology not only is comparable with the commercially available gold standard test, but surpasses other immunoassays targeting COVID-19 antibodies reported by FITC, which offer limits of detection of tens (25-43) of ng mL^{-1}.[50]

For each analyzed sample, we performed three parallel experiments to investigate the intra-assay variability in terms of coefficient of variation (CV) which accounted from 0.8 to 6.7%, see Table 3-2.

We also evaluated the inter-assay variability in terms of CV, using three different GO decorated microplates and executing the experiment three times in the same conditions, the results show that the respective variability (CV) ranged from 2.9 to 6.8% (see Table 3-3). According to the literature, our serological bioassay offers a variability that meets the criteria recommended for clinical analyses, that is, a variability below 15%.[38] We are convinced that the proposed technology is cost effective, after the estimation of cost of each reagent taking in consideration the cost of importation of some reagents in our region, the cost of each test (considering 3 parallel assays) accounts for 0.47 USD, at laboratory scale, see Table 3-4.

Table 3-3. *Evaluation of the inter-assay precision of the proposed technology. Adapted with permission.[28] Copyright 2021, ACS.*

[Anti-RBD] **(ng mL^{-1})**	**Mean** **(I_f/I_0)**	**SD**	**CV %**
blank	0.676	0.031	4.62
0.015	0.715	0.021	2.939
0.031	0.717	0.046	6.48
0.062	0.731	0.043	5.94
0.125	0.713	0.048	6.794
0.25	0.7	0.036	5.11
0.5	0.73	0.026	3.628
1	0.737	0.044	5.99

Table 3-4. Cost estimation

	Stock quantity	*Stock concentration*	*Cost*	*Volume per test*	*Required concentration*	*Cost per test*
Plate	96 wells	N/A	$ 4.7	3 wells	N/A	$ 0.15
Graphene oxide	1000 mL	5000 µg mL^{-1}	$ 200.00	79.2 µL	1200 µg mL^{-1}	$ 0.015
PBS	100 tablets	N/A	$ 117.49	1/192 tablet	N/A	$ 0.0058
FITC (conjugation kit)	3 kits	N/A	$ 571.73	N/A	N/A	N/A
RBD	100 µg	N/A	$ 650.86	N/A	N/A	N/A
F-RBD	120 µL	833.33 µg mL^{-1}	$ 841.44	0.043 µL	0.12 µg mL^{-1}	$ 0.3
		Total per test				$ 0.47

After the optimization and evaluation of the serological test, we set out to test the performance of the proposed bioassay using clinical samples of human serum to demonstrate the relevance and potential real application of the generated technology. As mentioned above, two groups of samples were used for the study, one group includes serum samples collected in 2014 (pre-COVID-19) an the other comprises sera collected from COVID-19 subjects (positive by PCR). Based on the limit of detection offered by our technology and the minimum dilution utilized in commercially available ELISA kits targeting COVID-19 antibodies (~1/6400)[51], we carried out some experiments to determine the optimum serum dilution for our assay. According to the methods explained in experimental methods section, we mixed 100 µL of the probe with 100 µL of the respective serum sample at different dilution factors. We analyzed, 4 pre-COVID-19 samples and 2 samples from COVID-19 subjects at dilution factors of 1/8875, 1/9000, 1/10000, 1/11000, 1/11250, 1/11500 and 1/12500, with the intention to compare the mean I_f/I_0 ratio obtained from each group and determine the respective statistical significance, it should be remembered that we expect to I_f/I_0 ratio from pre-COVID-19 samples be equivalent to I_f/I_0 ratio blank samples. We estimated the P value associated to each dilution factor throughout an analysis of 48 minutes, interrogating the performance of the assay in real-time every 3 minutes, see Figures A1-A7 in Appendix I. In this series of experiments, the lower P values were found at a dilution factor of 1/11500, specifically accounting for 0.0021 at 42 min of the assay. To confirm the outcomes, we decided to increase the number of pre-COVID-19 samples to 14 serum samples, and to continue using 2 samples from COVID-19, to be analyzed at dilution factors of 1/11875, 1/12000, 1/12125, 1/12200 and 1/12250. In this new series of experiments, the lower P values were found at a dilution factor of 1/12200, specifically accounting for <0.0001 at 15 min and other times of the assay (18, 21 and 24 min), see Figure A8-A12 in the Appendix I. After this dilution exploration, we decided to analyze the whole sera collection, analyzing 28 pre-COVID-19 samples and 6 samples from COVID-19 patients at dilution factors of 1/12125 and 1/12200, for 50 min. The lower P value was found at a dilution factor of 1/12200, <0.0001 (see Table A-1 and A-2 in Appendix I), at 12 min of the analysis (see Figures A13-A14 in Appendix I), these outcomes are in good agreement with previous series of experiments and the data obtained at optimum conditions regarding the analytical sensitivity. Figure III.6 shows the box plot corresponding to the analysis of the whole sera collection using a dilution factor of 1/12200 at 42 minutes. The serum samples were successfully differentiated without data overlapping between the resulting I_f/I_0 values of the two groups and considering an I_f/I_0 ratio around 0.767 as a threshold to determine a positive or negative result of the

test, no false negative/positive results were determined. Such a threshold was established through the average resulting from the higher I_f/I_0 value of the group of pre-COVID-19 samples and the lower I_f/I_0 value of the group of samples from COVID-19 subjects.

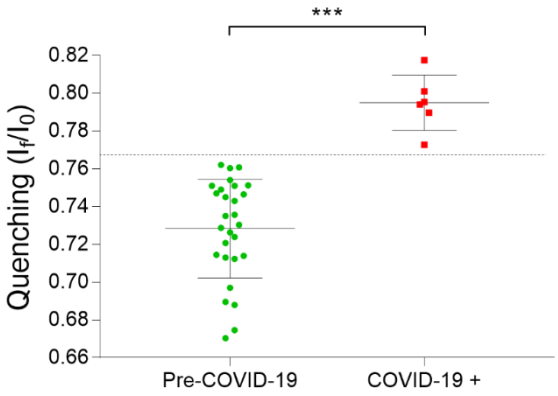

Figure 3.6. *Box plot of sera sample collection analysis in optimal conditions at 42 min of the assay. Dilution factor: 1/12200. 28 pre-COVID-19 samples and 6 samples from COVID-19 subjects were assayed. The box plots display the median and the extreme values of the respective distribution. The employed confidence interval was 95 %. Adapted with permission.[28] Copyright 2021, ACS.*

The proposed technology was demonstrated to be a potential tool for clinical diagnosis offering a qualitative result, reporting immunoglobulins binding to F-RBD; however, it is important to discuss the limitations of this development, as quantitative detection of levels of COVID-19 antibodies in serum samples is restricted. For example, all the serum samples from COVID-19 subjects yielded I_f/I_0 values exceeding the dynamic range of the optimized calibration curve, we think that this behavior with clinical samples is due to the presence of different immunoglobulins (A, E, M) in COVID-19 positive samples, whereas the calibration curve was performed using exclusively immunoglobulin G (Anti-RBD), this could result in different interactions that may interfere in the proposed non-radiative energy transfer-based biosensing mechanism. Besides, using serum samples involves the manipulation of a complex matrix, in which we can find diglycerides, triglycerides, phospholipids, fatty acids, steroids and steroid derivatives among other components,[52]these molecules may also interfere and does not allow to interpolate I_f/I_0 values from serum samples within I_f/I_0 values resulting from the analysis of standard samples for quantitative purposes. For further investigation a partnership with a clinical institution would be necessary to perform an advanced and reliable clinical evaluation of the proposed test.

All in all, this chapter reported the use of the SARS-CoV-2 Spike RBD recombinant protein (RBD) labeled with FITC as photoluminescent biorecognition probe targeting COVID-19 antibodies (anti-RBD) when incubated in GO-coated surfaces. Avoiding the employment of two bioreagents with capture and detection purposes, blocking and washing steps, we are offering a qualitative approach to determine COVID-19 seroconversion in a high-throughput, fast (42 min) and cost-effective (0.47 USD per test, at laboratory scale) that was demonstrated efficient for the facile determination of COVID-19 seroconversion. Finally, it is worth noting that the proposed test can be transferred to on-site applications using miniaturized technologies involving microfluidics and/or paper-based analytical devices.

CHAPTER 4. Disposable Device for Bacterial Vaginosis Detection

Clinical testing devices at the point of care have become necessity goods, intended to prevent the spread of several infectious diseases. Bacterial vaginosis (BV) is an infectious disease that commonly affects reproductive-age women and predisposes the infection of sexually transmitted diseases. For women infected with BV is usual to present an asymptomatic infection case, which can lead to several complications such as pelvic inflammatory conditions, postpartum endometritis and preterm labor and it is hard to diagnose because the conventional methods of BV diagnosis involve microscope analysis of vaginal swab samples, it thus requires highly trained personnel. As a potential alternative, a novel microfluidic paper-based analytical device for BV diagnosis is proposed. Sialidase is an enzyme overexpressed in BV patients, that is why detection of sialidase can promote the timely diagnosis of BV. The sialidase overexpression can be detected by exploiting an immunosensing mechanism previously pioneered by our team. As was detailed in Chapter 2 and Chapter 3, this technology employs a graphene oxide-coated surface as quencher of fluorescence. The fluorescence of the immunoprobes that do not experiment immunoreactions (antibody-antigen) is deactivated by graphene oxide via non-radiative energy transfer, whereas those immunoprobes undergoing immunoreactions preserve their photoluminescence due to the distance and the low affinity between the immunocomplex and the graphene oxide-coated surface. Our paper-based device offers results withing 20 minutes, using only 6 µL of the sample to analyze. To remark the relevance of the developed device, the approach was tested with 14 vaginal swabs specimens to discriminate clinical samples of women with normal microbiota from those undergoing BV. Our device potentially can become in an important tool to diagnose and prevent BV consequences.

A. Introduction

Microfluidic paper-based analytical devices

Microfluidic paper-based analytical devices (µPADs), as a promising analytical platform, have gain significant interest for the scientific community in the last decade. µPADs present several advantages in comparison with traditional microfluidic systems, such as easy fabrication, economical cost, ability to drive and manipulate flow without equipment, capability of storing reagents for various applications, minimal sample requirement and good sensitivity, selectivity and accuracy.[30,53] µPADs are very useful for point of care devices or health care devices applied in several fields such as diagnostics, biological, food safety, environmental, electrochemical among others. [54]

Historically, paper-based microfluidics were introduced to the scientific world by Whitesides' group at Harvard University, they presented the first device comprised of a protein-glucose assay patterned by lithography method in paper. But previously, in 1949, Muller and Clegg reported the fabrication of a paraffin-patterned paper, which is considered as the first-time to fabricate fluidic channels on paper and the first paper-based assay. In the following years, the evolution of µPADs that utilized various kinds of papers substrates, nowadays these substrates functionalized with various molecular probes like nanomaterials, biomolecules and several other range of probes like spin-crossover particles, quantum dots, metamaterials and aptamers to develop a broad range of µPADs.[54]

Talking about fabrication methods, several technologies and methods have been reported for the effective fabrication of μPADs. Fabrications methods of μPADs can be categorized into two: (i) 2-D shaping/cutting of paper and (ii) pattern drawing of hydrophilic/hydrophobic barriers on paper. Some of the traditional fabrication methods are laser cutting, photolithography, polydimethyl-siloxane (PDMS) stamping and printing, plasma treatment, vapor phase deposition, screen printing, ink-jet printing and wax dipping/printing.[54] Wax-based fabrication technique is a low-cost method which uses non-toxic hydrophobization pattern reagents. These methods give some advantages such as rapid fabrication, suitable for mass production, high resolution, inexpensive reagent.[54] Wax-printed μPADs require two steps, printing wax on a paper and heat to melt the wax and impregnate the substrate to form the hydrophobic barriers, see Figure 4.1.

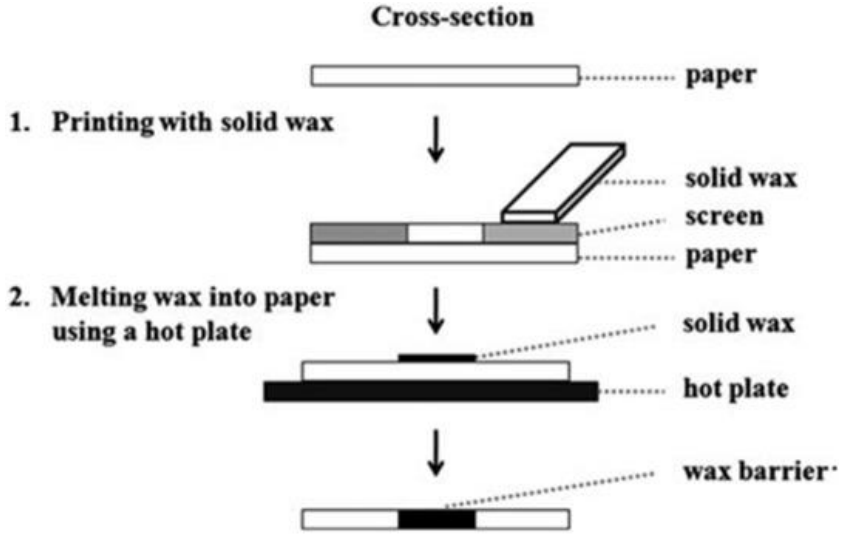

Figure 4.1. *Schematic representation of the process of the fabrication for wax screen-printing method. Adapted with permission.[55] Copyright 2011, Elsevier.*

Disposable Device for Bacterial Vaginosis Diagnosis

In our daily live we use disposable biosensors, for example, in pregnancy or fertility tests and wearable blood glucometers. Disposable biosensors are affordable and easy-to-use devices for a single measurement.[29] As mentioned above, microfluidic paper-based biosensors might be excellent for a wide range of applications as disposable biosensors and can be used at the point of care (POC). μPADS are easy to manufacture and low-cost, the use of printing techniques eliminates the need of complex microfluidic components such as pumps and valves. [31,56] In general, μPADS have been used as biosensors to determine different analytes using optical and electrochemical transduction systems; for example, glucose, uric acid, antibody IgG, cancer biomarkers, Hepatitis C virus, Zika viral gene markers, *E. coli*, etc. [57–62]

A usual affection of reproductive-age-women is bacterial vaginosis (BV) which is an infectious disease provoked by an alteration in vaginal microbiota. Generally, the symptoms of BV include moderate white-grayish vaginal secretion after sexual intercourse, fishy odor, vaginal discharge, and in some cases dysuria and dyspareunia. However, this infectious disease can be presented in an asymptomatic fashion and this condition may eventually lead to negative consequences in reproductive health, such as postpartum endometritis, pelvic inflammatory disease and predisposition to sexually transmitted diseases, including those caused by *Chlamydia trachomatis*, *Neisseria gonorrhea*, human papillomavirus and human immunodeficiency virus.[22,63,64] Typically, health

professionals used an evaluation of Amsel[65] or Nugent [66] criteria to diagnose BV infection. However, patients might be misdiagnosed because of the lack of specialized analytical diagnostic tools or the strict application of the diagnostic criteria of the respective clinical indicator tests (white or grayish vaginal discharge, vaginal pH > 3.5, amine production, and the presence of clue cells).[22,64] A diverse community of anaerobic bacteria are involved in the alteration of microbiota, such as *Prevotella*, *Bacteroides*, *Mobiluncus* and *Gardnerella*, all of them produce hydrolytic enzymes such as sialidase. Hence, sialidase is a suitable biomarker for BV determination.[22,64] A very common technique for detection of sialidase in vaginal swabs is based on the enzymatic hydrolysis of methoxyphenyl acetyl muramic acid via sialidase, in this way initiating the formation of methoxyphenol, which is then measured. Usually, in this technique, methoxyphenol concentrations greater than 5.1 nM are considered as BV positive. As far as we know, only one commercially available test targeting sialidase exists, which is called OSOM BVBLUE (Sekisui Diagnostics, Burlington, MA).[67] Nevertheless, this test offers a multistep qualitative colorimetric result for the determination of SLD, which eventually leads to different levels of specificity and sensitivity.[22] In this context, our collaborative team from Universidad Autónoma de Guerrero, engineered a monoclonal antibody that recognizes sialidase with high specificity.[68]

As a potential tool to improve the diagnosis of this infectious disease, we proposed the development of a wax-printed µPAD to detect sialidase as BV biomarker, even in clinical samples. As detailed in chapter III and IV, our research group has developed a high throughput biosensing system that consist of photoluminescent bioprobes and 96 microwell plates modified with graphene oxide (GO), taking advantage of the capabilities of GO to quench fluorescence efficiently.[17,22,27] Using non-radiative energy transfer, GO-coated microwells deactivate the fluorescence of the bioprobes that are not establishing immunoreactions, as the distance between the bioprobes and GO allows for the dipole-dipole interaction.[69] Whereas, fluorescent biorecognition probes showing immunoreactions preserve their photoluminescence because of the distance and the low affinity between the immunocomplex (biorecognition probe - analyte) and the GO-coated surface.[22,70–72] The distance between the FITC (from bioprobe) and the GO coated surface can be computed as the size of anti-sialidase plus the size of sialidase, that is 8.4 nm from an average antibody plus 4 nm from sialidase, that is 12.4 nm.[73,74] We are taking advantage of this wash-free technology to develop a disposable device for sialidase determination.[75]

Other tests for BV diagnosis are based on catalytic reactions,[22] however, to the best of our knowledge, our approach represents the first paper-based immunoassay for BV diagnosis. The proposed device comprises a wax pattern printed onto a nitrocellulose membrane. The strip displays a Y-shaped pattern, including 3 zones of interest: i) the entrance, where the probe and the sample are drop-casted; ii) the control zone, that do not contain GO, where the biorecognition probe, composed by a monoclonal anti-sialidase monoclonal antibody conjugated with FITC fluorophore (FAS). FAS will preserve its conventional fluorescence because there is nothing in C area that modifies the fluorescence of the biorecognition probe, and iii) the test zone, which is the area coated with a GO film. Following the biosensing technology discussed in previous Chapters, the GO film from the test zone deactivates the fluorescence of those FAS that are not experimenting immunoreactions, whereas those FAS experimenting immunoreactions preserve their photoluminescence. Hence, the photoluminescence exhibited in the test zone by FAS is proportional to the analyte concentration, as illustrated in Figure 4.2.[75]

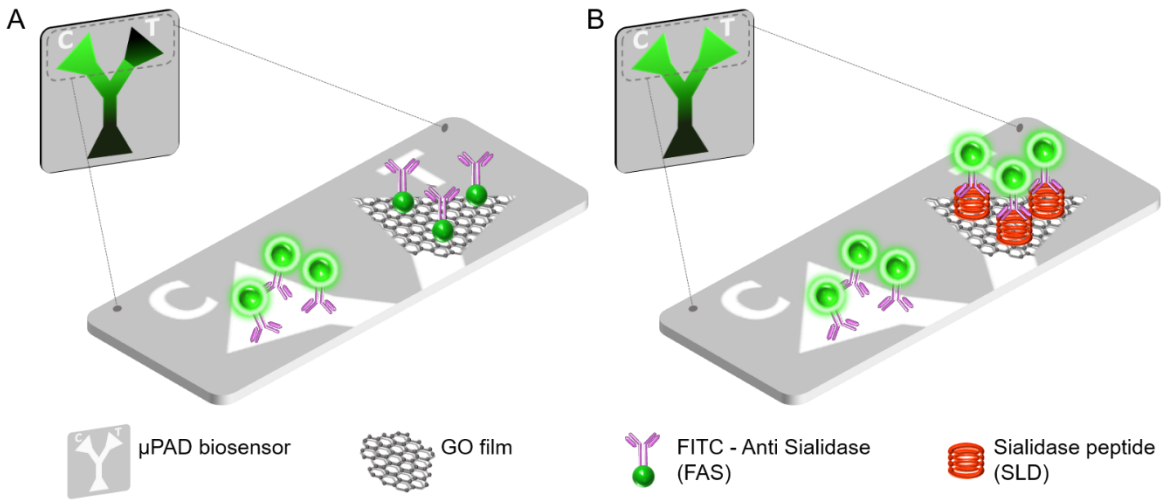

Figure 4.2. *Schematic representation of the disposable device for BV diagnosis and its biosensing mechanism. In the control area (C), FAS preserves its fluorescent intensity, due to the lack of a reagent (such as GO) that can modify FAS fluorescence emission state.* ***A.*** *In the absence of immunoreactions in the assay, fluorescence intensity of FAS is quenched in the test zone (T) by the GO film via non-radiative energy transfer.* ***B.*** *When FAS experiments immunoreactions in the assay, the fluorescent intensity of FAS is preserved according to the analyte concentration, because of the distance between FITC and GO (>20 nm) and the low affinity between the immunocomplex and the GO film. Published under Creative Commons (CC by 4.0).*[75] *https://creativecommons.org/licenses/by/4.0/legalcode*

B. Experimental methods

Materials and equipment

All the materials and equipment used for this research were selected, purchased and carefully handled according to the data sheets provided by the suppliers. Table 4-1 summarizes the supplier and specification of each employed material.

Fabrication of the paper-based biosensor

The proposed paper-based biosensor is easy to fabricate. The printing process of the wax pattern onto the proposed paper-based device only requires two steps: (i) print the wax pattern onto the nitrocellulose membrane; (ii) heat the device using a hot plate at 150°C for 90 seconds (in order to form the required hydrophobic barriers). Once the device reaches the room temperature, this is ready to use. Due to the absorbent capabilities of nitrocellulose,[76] it is relatively effortless to coat this substrate with graphene oxide (GO). GO was diluted using ultrapure water supplemented with Tween 20 at 0.05% to coat the substrate with GO. Deposition of GO was carried out by drop casting the GO suspension (concentrated at 500 μg mL^{-1}) only onto the test zone, and heating the device at 45°C to speed up the water evaporation in which the GO was suspended. Up to 3 GO deposition (5 μL of GO, each deposition) steps were implemented and evaluated. Between each stage of GO deposition, it is necessary to wait for the device to dry (4 minutes) and drop cast then the GO suspension once again. After GO gets completely dried, the device is ready to perform the sialidase test.[75]

Table 4-1. *Material and equipment: suppliers and specifications*

Material	Supplier	Specifications
Nitrocellulose membrane	Sartorius	1UN18ER100025NT
Aqueous suspension of single layer GO	Global Graphene Group	S1319112702 lateral size around 50 nm C/O ratio ~1
Tween 20	Sigma-Aldrich	P9416-100ML
Phosphate buffer saline (PBS) tablets	Sigma-Aldrich	P4417-100TAB
FITC Conjugation Kit Fast-Lightning-Link	abcam	ab188285
Anti-sialidase monoclonal Antibody	-	Produced by our colleagues at the Universidad Autónoma de Guerrero
Sialidase peptide	-	produced by our team at the Universidad Autónoma de Guerrero
Printer ColorQube 8085	Xerox	-
Hot plate StableTemp	Cole-parmer	-
Cytation 5 multimodal reader	Biotek	-

Image analysis

ImageJ (version 1.53t, 24 August 2022) was used to analyze all the images. Figure 4.3 illustrate the areas of interest: i) control zone covered by the sample, ii) test zone covered by the sample and iii) clear nitrocellulose, as a background section.

The quenching of fluorescence ratio (Q) was calculated according to Equation 1:

$$Q = \frac{I_T - I_R}{I_{C-I_R}} \quad \text{(Equation 1)}$$

where I_T is the average pixel intensity in the test area, I_C is the average pixel intensity in the control area and I_R is the average pixel intensity of the background (nitrocellulose).[75]

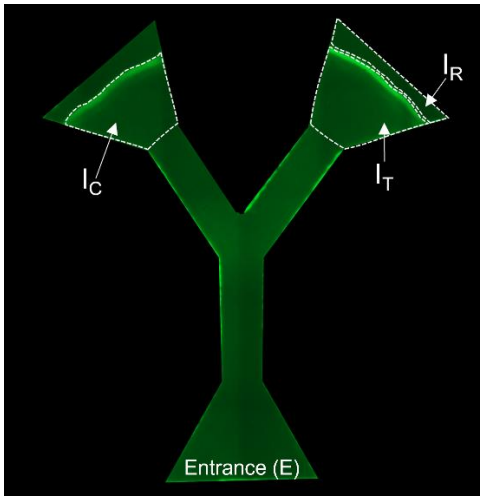

Figure 4.3. *Model depicting the employed image analysis method. I_C: Average intensity of the pixels in the control area. I_T: Average intensity of the pixels in the test area. I_R: Average intensity of the pixels in the background area. Published under Creative Commons (CC by 4.0).*[75] *https://creativecommons.org/licenses/by/4.0/legalcode.*

Sialidase determination

FITC conjugated with anti-Sialidase (FAS) and the sample to be analyzed were mixed and incubated in a microtube during 10 min using a 1:1 relationship. The final concentration of FAS was 80 µg mL^{-1}. 6µL of this mix was then added to the entrance of the device to reach the control and test zones. After 20 min, the respective image was recorded using a Cytation 5 imager from Biotek (excitation wavelength: 469/35 nm, emission filter: 525/39 nm). Eventually, the resultant images were analyzed using the method explained in the previous section and the respective fluorescence quenching ratio was calculated using Equation 1. All the samples were tested by triplicate to evaluate the resulting precision.[75]

Vaginal swab sample preparation and analysis

Vaginal swab samples were collected by "Servicio de Diagnóstico Integral en la detección Oportuna del Cáncer Cérvico Uterino" at Universidad Autónoma de Guerrero (Chilpancingo, Guerrero, Mexico). Signed consent was obtained from those women who participated in this research. The samples used in this research were previously analyzed by Amsel and Nugent criteria to compare our results with such standard diagnostic methods. To determine the optimal dilution factor to analyze real samples, two vaginal swab samples were tested, one of them from the normal microbiota (NM) group and the other one from BV group. Both samples were diluted in PBST (PBS supplemented with Tween 20 at 0.5% v/v) in a dilution factor range from 1:4 to 1:48 to determine which dilution factor offered the most significant difference in terms of statistic parameters (P value) between both group of samples. The optimization of such a dilution factor was performed using the photoluminescent quenching ratio (Q) of the resulting tests. In the Appendix II, Figure B1 shows the graph correspondent to this analysis and Table B-1 in Appendix II, summarizes the resultant P value of the t-test to estimate the statistical difference between the analyzed samples. 1:32 dilution factor exhibited the smallest P value (P = 0. 0141), which corresponds to the most significant difference between the NM and the BV group. To estimate the sialidase concentration of each analyzed sample, it was computed the interpolation of the corresponding *Q* value in the resulting calibration curve and multiplying by a factor of 32 (given the optimal dilution factor previously mentioned).[75]

Importantly, given the filtration capabilities of paper-based devices,[77] the vaginal swabs specimens were not centrifuged prior to analysis via the proposed disposable device.[75]

C. Results

Design and fluidic performance of the disposable device

There are several parameters to consider in the design of the hydrophobic patterns of the proposed paper-based device, including the width and length of the channels, morphology of the circuit and its specific regions of interest (entrance, control and test zone), as well as the volume required to fill the circuit without fluid leakage. To determine the appropriate width channel, several multichannel designs were used. Each multichannel device consisted of five different width channels connected to a circular zone emerging from the center of another circular area. The widths of the channels that were explored were 0.6, 0.8, 1, 1.3, 1.5, 2, 2.5 and 3 mm, and the diameter of the circular areas were 2 and 6 mm, respectively. These couple of multichannel devices were tested using a volume of 10 µL of anthocyanin-dyed water to follow the flow of the sample throughout the microfluidic circuit. In both devices, it was observed that the liquid samples could not flow until the final area in the thinner channels (0.6 and 1 mm, respectively). In the wider channels with those circles of 6mm, the sample could not fill the whole area. However, in those channels between 1.3 and 1.5 mm connected to the 2 mm diameter circular area, the sample covered the interest area completely, but some outflows were observed. Given this microfluidic performance in the multichannel devices, we decided to use a channel width of 1.6 mm (slightly wider than the 1.5 mm tested) and circular areas with a diameter of around 3 mm to avoid outflows. Full details on the behavior of the sample flow in the discussed multichannel devices are included in Figure 4.4.[75]

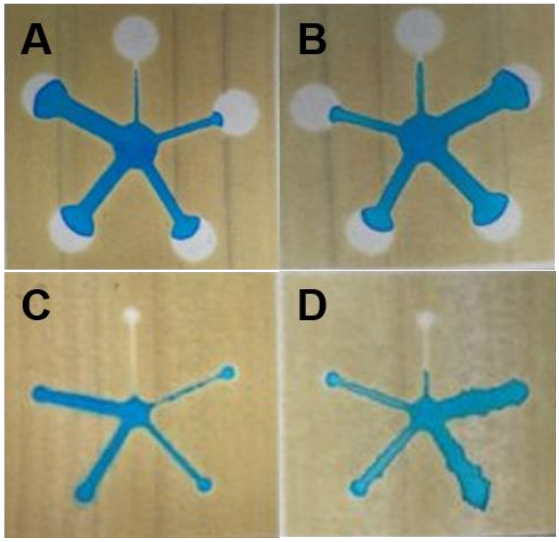

Figure 4.4. *Optimization of the channel width.* ***A****. Front side of the device. Channel width assessment, from 1 to 3 mm (1, 1.5, 2, 2.5,3 mm).* ***B****. Back side of the device. Channel width evaluation, from 1 to 3 mm.* ***C****. Front side of the device. Channel width optimization, from 1 to 1.5 mm (0.6, 0.8, 1, 1.3, 1.5 mm).* ***D****. Back side of the device. Channel width evaluation, from 1 to 1.5 mm. Published under Creative Commons (CC by 4.0).*[75] *https://creativecommons.org/licenses/by/4.0/legalcode.*

Using the aforementioned channel width of 1.6 mm we design a first approach of our paper-based device design, which is shown in Figure 4.5, where the entrance, control, and test zones exhibit a

circular shape. From this design, some modifications were made to improve the flow of the sample throughout the microfluidic circuit and to avoid fluid outflows. Since the liquid sample contains the target analyte of the disposable biosensor, it is very important to reach the control and test zones of the circuit, but at the same time liquid leakage should be avoided. To promote fluid coverage in a larger area of the circuit, the surface tension of the employed liquid was modified by using PBST (PBS supplemented with Tween 20) to dilute the bioprobe (FAS). The concentration of Tween 20 was optimized by evaluating the area of the circuit covered by the fluid, particularly the explored concentrations ranged from 0.1 to 0.5% (v/v). Figure 4.6 shows the flow of the sample using FAS diluted in PBS supplemented with different concentrations of Tween 20. From this behavior we can conclude that FAS diluted in PBS supplemented with Tween 20 at 0.5% (v/v) covered the largest area.[75]

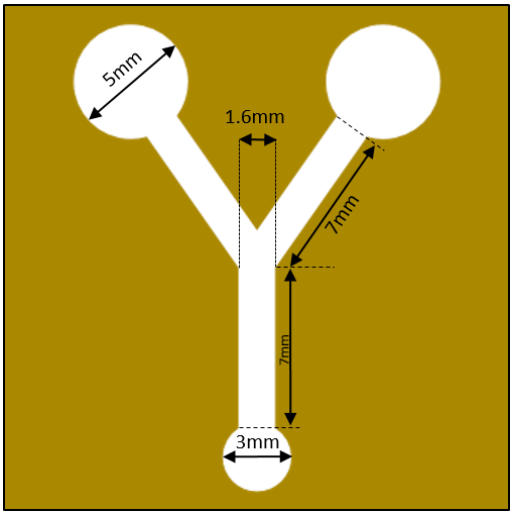

Figure 4.5. *First approach of the design of the disposable device. Published under Creative Commons (CC by 4.0).[75] https://creativecommons.org/licenses/by/4.0/legalcode.*

Some other changes of the aforementioned parameters were modified to achieve an optimal microfluidic design, all these modifications are summarized in Table 4-2 with its corresponding micrographs presented in Figure 4.7. After this process, a disposable device with an optimal fluidic performance was achieved (without outflows and the largest area covered in the circuit), which is shown in Figure 4.8. The dimensions and specifications of the optimal design are the length of the trunk/branches of the Y shape was 4 mm, the width of the channels was 1.6 mm and the shape of the entrance, control and test zones was a trapeze with a long base of 5 mm.[75]

Table 4-2. Optimization of the design of the microfluidic circuit.

#	Entrance geometry	Entrance width	Trunk width	Trunk length	Branches width	Branches length	Control/Test geometry	Control/Test width	Volume (µL)	Outflow	Covered area
A	circle	5	1.6	7	1.6	7	circle	4	5	NO	65.18%
B	trapeze	5	1	4	1	4	circle	4	6	YES	85.35%
C	trapeze	5	1.2	4	1.2	4	circle	4	6	YES	75.86%
D	trapeze	5	1.6	4	1.6	4	circle	4	6	YES	65.81%
E	trapeze	5	1.2	4	1.2	4	trapeze	5	6	YES	76.60%
F	trapeze	5	1.4	4	1.4	4	trapeze	5	6	YES	79.99%
G	**trapeze**	**5**	**1.6**	**4**	**1.6**	**4**	**trapeze**	**5**	**6**	**NO**	**75.22%**
H	trapeze	5	1.6	4	1.6	4	trapeze	5	7	YES	84.04%

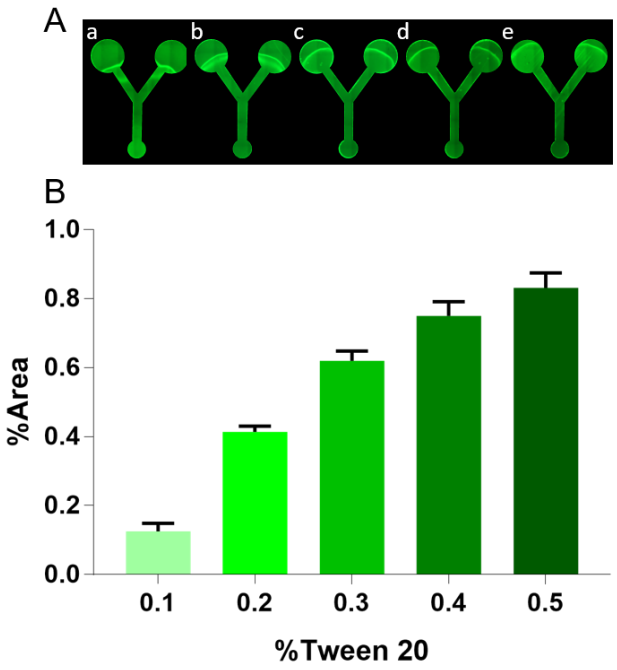

Figure 4.6. Optimization of the concentration of Tween 20 (concentration of the fluorescent probe, [FAS] = 10 ug mL^{-1}). A. Fluorescence microscope images of the µPAD using a) 0.1%, b) 0.2%, c) 0.3%, d) 0.4%, e) 0.5% of Tween 20. B. Percentage of the area covered by the sample with different concentrations of Tween 20. *Published under Creative Commons (CC by 4.0).*[75] *https://creativecommons.org/licenses/by/4.0/legalcode.*

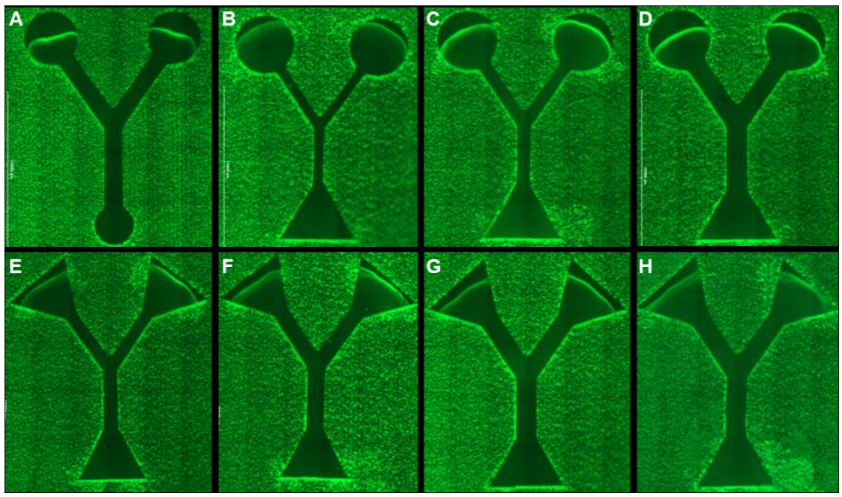

Figure 4.7. Optimization design of microfluidic circuit. See Table S1, each image corresponds to a row of such a Table S1. *Published under Creative Commons (CC by 4.0).*[75] *https://creativecommons.org/licenses/by/4.0/legalcode.*

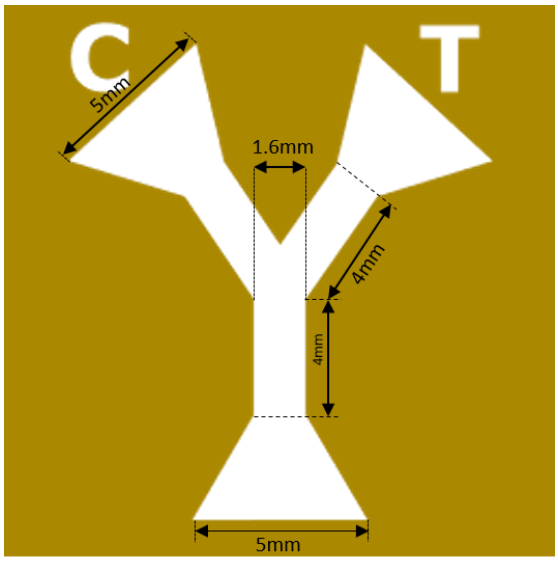

Figure 4.8. *Optimal design of the microfluidic circuit. Published under Creative Commons (CC by 4.0).*[75] *https://creativecommons.org/licenses/by/4.0/legalcode.*

Optimization of the fluorescence quenching

The quenching of fluorescence derived from the nonradiative energy transfer between the GO film (acceptor) and the FAS (donor) in the disposable device, was evaluated using several concentrations of FAS (from 40 to 100 ng mL^{-1}) in devices with one, two, and three depositions of GO concentrated at 500 µg mL^{-1} in the test area. Figure B2 in Appendix II is shown the analysis of this series of experiments, where we can observe that using 3 depositions of GO, the device reached the higher quenching ratio in the test zone, which considering Equation 1 accounts from 0.15 to 0.55. The optimal concentration of the bioprobe was [FAS] = 80 µg mL^{-1}, which exhibited a similar fluorescence intensity in the control zone when compared with the highest concentration of FAS (100 µg mL-1). Besides, in the test zone [FAS] = 80 µg mL^{-1} showed the maximum (optimal) quenching ratio (Q) using 3 depositions of GO, which is around 0.15 units.[75]

Biosensing performance

It is worth to remember that the design of the microfluidic circuit was optimized to ensure that (i) the sample reached the zones of interests (control and test zone, respectively) and (ii) the quenching of fluorescence via non-radiative energy transfer between FAS (donor) and GO film (acceptor) was optimal. After the design and optimization process, we verified that the biosensing mechanism previously developed using polystyrene microwell plates could be transferred into the proposed paper-based device. For that purpose, we drop casted samples containing the analyte at different concentrations in the microfluidic device and we successfully noted that the fluorescence intensity was proportional to the analyte concentration. With this information we built a calibration curve by analyzing standard samples of sialidase at different concentrations, particularly from 0.3 to 4.8 ng mL^{-1}, see Figure B3 in Appendix II. Figure 4.9 illustrates the analytical performance of the device, which was modeled as a two-phase exponential decay equation. The quenching ratio (Q) is inversely proportional to the analyte concentration, that is, the higher the analyte concentration the lower the Q ratio. In fact, in the test zone of each device, it can be observed that the higher the analyte concentration the higher the fluorescence intensity until reaching a saturation state, in particular at those concentrations higher than 2.4 ng mL^{-1}. The calibration curve shown in Figure 4.9B exhibited

a limit of detection of 0.2 ng mL^{-1}. The limit of detection was obtained by interpolating the mean of the blank plus three times its standard deviation in the respective equation of the calibration curve. Precision, in terms of coefficient of variation (CV), was estimated using 3 devices measuring the same analyte concentration and accounts from 4.91 to 14.69 %. The biggest rate of variability was observed in the sample concentrated at 0.6 ng mL^{-1} with a CV of 14.69% and the lower rate of variability was observed in the blank sample with 4.91% of CV. Table B-2 in Appendix II summarizes the CVs exhibited by each measured concentration.[75] It is worth mentioning that according to the literature, this precision is acceptable in immunoassays.[38,78]

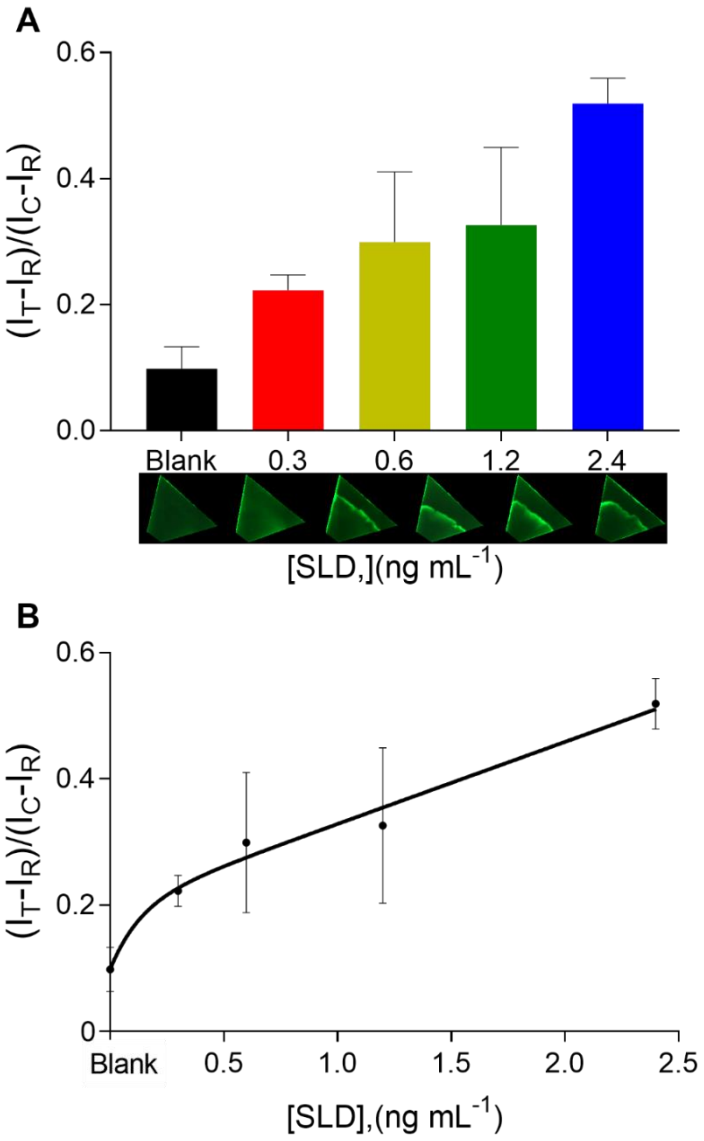

Figure 4.9. *Analytical behavior of the disposable device.* ***A****. Bar chart of the fluorescence quenching ratio, Q. Images below the x axis show the fluorescence in the test zone of the respective disposable device.* ***B****. The resulting calibration curve. Error bars represent the standard deviation of three parallel experiments. Published under Creative Commons (CC by 4.0).*[75] *https://creativecommons.org/licenses/by/4.0/legalcode.*

Vaginal swab sample analysis

To prove the proposed disposable device as a potential BV diagnosis tool, it is necessary to perform the analysis of real samples using the proposed device. To this end, we tested the behavior of our disposable device by analyzing 14 vaginal swabs previously studied and determined as BV positive or NM via Amsel and Nugent criteria. In Amsel criteria, the presence of at least 3 criteria (white or grayish vaginal discharge, vaginal pH > 3.5, amine production, and the presence of "clue cells") is considered as a BV positive case. The Nugent score is a standardized scored system, which is based on the classification of Gram-positive rods and lactobacilli (i.e., normal flora) and Gram-negative or Gram-variable morphotypes (BV flora). A score is then assigned to these observations accordingly: 0 to 3 (normal flora), 4 to 6 (intermediate or mixed flora), and 7 to 10 (BV).[22,64] Figure 4.10 shows the analytical behavior of the analyzed clinical samples.[75]

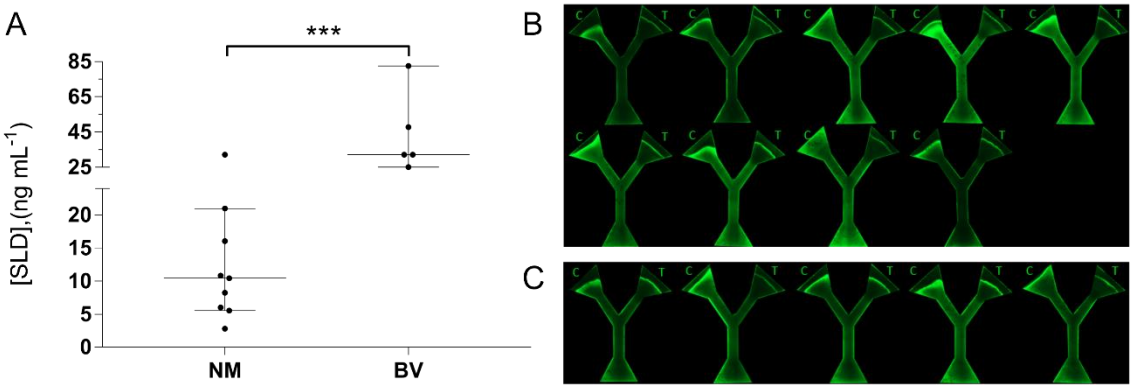

Figure 4.10. *Analysis of clinical samples (vaginal swabs), dilution factor 1:32. 9 samples of NM cases and 5 samples of BV cases were analyzed.* ***A****. Distribution of the analyzed groups.* ***B****. Fluorescence micrographs of the NM samples tested.* ***C****. Fluorescence micrographs of the BV samples tested. Published under Creative Commons (CC by 4.0).*[75] *https://creativecommons.org/licenses/by/4.0/legalcode.*

In general, the samples from NM patients exhibited a Sialidase concentration lower than 25.1 ng mL^{-1}, and the samples from BV patients displayed a concentration higher than 25.1 ng mL^{-1}, which is consistent with an immunoassay previously reported.[22] Likewise, low sialidase concentrations (< 25.1 ng mL^{-1}) are related to those samples with 0-3 Nugent score and 1-2 Amsel criteria, whereas high sialidase concentrations (>25.1 ng mL^{-1}) correspond to a 7-10 Nugent score and more than 2 Amsel criteria. Table 4-4 and Table 4-5 compare the results obtained with the proposed biosensing device and the previous results obtained through Amsel and Nugent criteria.[75]

Regarding the variability, the CV (resulting from 3 parallel assays) of those disposable devices tested with NM samples accounted from 3.14 to 14.75 %, whereas the CV of those disposable devices tested with BV samples ranged from 3.48 to 11.31%, see Table B-3 in Appendix II.[75]

Table 4-3. NM samples. Comparison of Amsel/Nugent criteria and the concentration measured though the proposed device. *MC µPAD: Concentration measured with the µPAD biosensor

Sample	**Nugent score**	**Amsel Diagnostic**	**µPAD (*Q* ratio)**	**MC µPAD (ng mL^{-1})**
NM 1	0-3	1-2	0.199 ± 0.0147	6.016
NM 2	0-3	1-2	0.283 ± 0.023	20.992
NM 3	0-3	3-4	0.194 ± 0.0248	5.548
NM 4	0-3	1-2	0.158 ± 0.0042	2.808
NM 5	0-3	1-2	0.218 ± 0.0100	8.216
NM 6	0-3	0	0.262 ± 0.0158	16.067
NM 7	0-3	0	0.329 ± 0.0486	32.116
NM 8	0-3	1-2	0.232 ± 0.0148	10.433
NM 9	0-3	0	0.235 ± 0.0257	10.823

Table 4-4. *BV samples. Comparison of Amsel/Nugent criteria and the concentration measured though the proposed device. *MC µPAD: Measured concentration with the µPAD biosensor*

Sample	Nugent score	Amsel Diagnostic	µPAD (Q ratio)	MC µPAD (ng mL^{-1})
BV 1	7-10	3 - 4	0.329 ± 0.026	32.086
BV 2	7-10	3 - 4	0.300 ± 0.0111	25.117
BV 3	7-10	1-2	0.534 ± 0.0186	82.460
BV 4	7-10	Not performed	0.393 ± 0.0351	47.742
BV 5	7-10	1 – 2	0.329 ± 0.0271	32.130

In Figure IV.6 and Table IV-2 is observable that only one NM sample is overlapping the BV group, which could be considered a false positive case within the explored samples, however, due to the limited availability of clinical samples (n = 14), a robust determination of the respective clinical sensitivity or specificity of the developed device is out of the scope of this thesis. Besides, there is a possibility that this misdiagnose may come from the conventional criteria (Amsel or Nugent) because of a human error or an asymptomatic case. Importantly, at laboratory scale, the disposable device had an estimated cost of $1.85 USD (see Table 4.5).[75]

Table 4-5. *Estimation of the cost*

	Total volume	**Concentration**		**Cost**	**Volume per device**	**Required concentration**		**Cost per device**
Nitrocellulose	100 m	N/A	$	290.00	0.025 m	N/A	$	0.0725
Wax	264000 devices	N/A	$	130.00	1 device	N/A	$	0.0005
GO	1 L	5000 µg mL^{-1}	$	210.00	1.5 µL	500 µg mL^{-1}	$	0.0003
FAS	120 µL	833.33 µg mL^{-1}	$	375.00	0.57 µL	160 µg mL^{-1}	$	1.78
PBS	100 tablets	N/A	$	130.00	6 µL	N/A	$	0.0002
Tween 20	1 L	N/A	$	100.00	0.03 µL	N/A	$	0.000003
						Total per device	**$**	**1.8548**

*****FAS: Antibody conjugated with FITC. The cost of 100µL of [Anti-sialidase] = 1 $mgmL^{-1}$ is $55.00 USD. The cost of FITC conjugation kit is $320.00 USD.

In this chapter it was detailed the process to engineer a competitive-cost disposable device with potential application at the POC taking advantage of an immunosensing technology that only requires a single antibody to capture and detect the analyte. As future work, we aim to develop a paper-based fluorescence reader designed for FITC,[79] which will allow for the employment of the disposable device at the POC. Moreover, using Amsel and Nugent criteria as conventional methods for BV diagnosis as comparison methods, the device was proven useful to analyze clinical samples and discriminate between NM and BV cases.[75]

CHAPTER 5. Conclusions

This thesis dissertation highlights a novel biosensing principle which was proven useful to determine a set of pathogen-related analytes. Such an operation principle is based on nonradiative energy transfer through dipolar interactions between a donor and an acceptor material. Taking advantage of this biosensing principle, we developed three biosensing technologies: (i) a biosensing platform targeting *E. coli* in industrial food samples, (ii) a COVID-19 serological test, proven useful for clinical serum samples analysis and (iii) a disposable biosensor for Bacterial vaginosis diagnosis, tested with clinical swab samples.

The biosensing platform targeting pathogen related analytes, used both for determination of *E. coli* in food samples and COVID-19 serological test exhibit several advantages such as real-time interrogation capabilities while avoiding time-consuming methods, single-step and wash-free process eliminating the need of cumbersome procedures, besides, it uses a single antibody eliminating the need for capture or secondary antibodies and saving expensive bioreagents. It has a standard format suitable for high-throughput applications and high sensitivity. Furthermore, the reported biosensing technology is transformative as GO can quench different fluorophores, and different analytes can be detected by simply changing the involved antibody or biorecognition element, this advantage was exploit during this research project, to determine different analytes such as *E. coli*, antibodies anti-RBD and Sialidase. The biosensing platform offers wide applicability for industrial food sample analysis as well as clinical samples. Moreover, the proposed test can be transferred to on-site applications using miniaturized technologies involving microfluidics and/or paper-based analytical devices, this device was designed, developed and evaluated for Sialidase detection.

The bacterial detection platform based on microwells coated with GO and using QDs conjugated with antibodies anti-*E.coli*, was developed, evaluated and found to have several advantages, this setup provide a fast response (within 30 minutes) and high sensitivity (up to 2 CFU mL^{-1}). Besides the bacterial detection platform was able to successfully discriminate between negative and positive industrial *E.coli* samples, this ability to analyze samples in real matrixes highlights the importance of the biosensing platform because this demonstrates a real-world application of the investigated technology.

Generally, GO-based photoluminescent biosensing systems rely on bioprobes made of oligonucleotides or antibodies complexed with fluorophores. In particular, for COVID-19 serological test reported, the platform employs fluorescence-tagged SARS-CoV-2 spike receptor-binding domain recombinant protein (F-RBD) as bioprobes which can be quenched in the absence of the analyte. The serological test is fast-response (around 42 min) and cost-effective (0.47 USD per test at laboratory scale). Besides, the serological test demonstrates to be a potential tool in a clinical scenario, because it is able to discriminate between samples containing anti-RBD and samples pre-COVID-19.

We used our innovative immunosensing technology that only requires a single antibody for both capturing and detecting the analyte to engineer a low-cost disposable device that has the potential for point-of-care (POC) application. Our disposable device was optimized for sensitive and rapid detection of Sialidase as BV biomarker within just 20 minutes and had a laboratory-scale estimated cost of $1.85 USD. As future work, we aim to develop a paper-based fluorescence reader to enable POC use of the device.[79] Comparing with conventional Amsel and Nugent criteria for BV diagnosis, the device demonstrate to be effective analyzing clinical samples and differentiating between normal microbiota and BV cases. This disposable device can be useful for timely detection and monitoring of BV therapy, as well as identifying asymptomatic cases to prevent its consequences. Additionally, this transformative device can be used for detecting other analytes by simply modifying the biorecognition element linked to a fluorophore.

FINAL REMARKS AND PERSPECTIVE

Biosensors are relevant tools for various applications. In this work, we focus on the detection of analytes related to infectious diseases. Therefore, the biosensing platforms and the biosensor device detailed in this study are relevant in the prevention of infection transmission, as well as the timely diagnosis of these diseases. In most cases, timely diagnosis of infections can prevent serious consequences and the spread of the infection, besides aid in the timely selection of treatment.

During the pandemic, the importance of diagnostic testing to avoid the spread of infectious diseases has become evident to the general community. All the tools we have relied on as a society during this context have been scientific developments, from the decoding of the SARS-CoV-2 genome, PCR diagnostic tests, to vaccines with different mechanisms of operation, among others. The presented work promotes the development of useful biosensors for the real world, and although they are efficient tools, these tools can be improved, and must be adapted to future world, for example to integrated it to artificial intelligent and modern electronic devices. Therefore, in addition to the obtained results, this work contributes to the future development of new tools and the consolidation of the existing ones, because we demonstrate that the operating principle is efficient in real applications, and this can be use as basis for de development of more devices and solutions.

The operation of the reported biosensors is based on the use of optically active nanomaterials, which means we take advantage of the radiation-matter interaction as a transduction method for the detection of chemical-biological analytes. For the characterization and reading of the developed biosensors, we used a spectrometer, an instrument that allows us to measure different properties of light, in this case, fluorescence and absorption.

The developed technology is based on the use of graphene oxide, a nanomaterial with specific optical properties. By implementing these optically active nanomaterials in biosensor development, we can improve the sensitivity and effectiveness of detection, for example, using graphene oxide we enhance the quenching of fluorescence.

The 96-well biosensing platform coated with graphene oxide is highly adaptable, as changing the biorecognition element allows the detection of different analytes for a wide range of applications. Besides, we demonstrate that the technology can be applied to a paper-based device.

In the case of the presented biosensor device, in addition to retaining the characteristics of the 96-well biosensing platform, we are talking about an advancement not only in science but also in technology. Successfully transferring the technology to a ready-to-use paper-based device represents a further step in the journey from the laboratory to the industry. We could even consider it as the development of a potentially commercial product.

In summary, the advancement of this biosensing principle utilizing optically active nanomaterials, as well as its potential as a platform and disposable device, has a noteworthy influence on various areas, including the food industry for prevention of gastrointestinal diseases, determination of COVID-19 seroconversion for clinical and health services, and the clinical diagnosis of Bacterial Vaginosis, thereby mitigating the risks associated with misdiagnosis. Moreover, the adaptable operating principle holds promise for other pertinent applications.

REFERENCES

[1] P. Bhattarai, S. Hameed, In *Nanobiosensors*, **2020**, pp. 1–22.
[2] A. Michelmore, In *Thin Film Coatings for Biomaterials and Biomedical Applications* (Ed.: Griesser, H. J.), Woodhead Publishing, **2016**, pp. 29–47.
[3] B. Jurado-Sánchez, *Biosensors* **2018**, *8*.
[4] K. J. Land, D. I. Boeras, X.-S. Chen, A. R. Ramsay, R. W. Peeling, *Nat. Microbiol.* **2019**, *4*, 46.
[5] Y. Rasmi, X. Li, J. Khan, T. Ozer, J. R. Choi, *Anal. Bioanal. Chem.* **2021**, *413*, 4137.
[6] M. Ramesh, R. Janani, C. Deepa, L. Rajeshkumar, *Biosensors* **2023**, *13*.
[7] J. W. Austin, F. J. Pagotto, In *Encyclopedia of Food Sciences and Nutrition (Second Edition)* (Ed.: Caballero, B.), Academic Press, Oxford, **2003**, pp. 3886–3892.
[8] B. O'Farrell, In *The Immunoassay Handbook (Fourth Edition)* (Ed.: Wild, D.), Elsevier, Oxford, **2013**, pp. 89–107.
[9] J. C. Blackstock, In *Guide to Biochemistry* (Ed.: Blackstock, J. C.), Butterworth-Heinemann, **1989**, pp. 78–90.
[10] M. Y. Azab, M. F. O. Hameed, S. S. A. Obayya, *Biology* **2023**, *12*.
[11] N. J. Ronkainen, H. B. Halsall, W. R. Heineman, *Chem. Soc. Rev.* **2010**, *39*, 1747.
[12] B. Bhushan, In *Springer Handbook of Nanotechnology* (Ed.: Bhushan, B.), Springer Berlin Heidelberg, Berlin, Heidelberg, **2017**, pp. 1–19.
[13] U. Laraib, S. Sargazi, A. Rahdar, M. Khatami, S. Pandey, *Int. J. Biol. Macromol.* **2022**, *195*, 356.
[14] M. Holzinger, A. Le Goff, S. Cosnier, *Front. Chem.* **2014**, *2*.
[15] A. Mokhtarzadeh, R. Eivazzadeh-Keihan, P. Pashazadeh, M. Hejazi, N. Gharaatifar, M. Hasanzadeh, B. Baradaran, M. de la Guardia, *TrAC Trends Anal. Chem.* **2017**, *97*, 445.
[16] E. Morales-Narváez, A. Merkoçi, *Adv. Mater.* **2012**, *24*, 3298.
[17] E. Morales-Narváez, A. Merkoçi, *Adv. Mater.* **2019**, *31*, 1805043.
[18] E. Morales-Narváez, B. Pérez-López, L. B. Pires, A. Merkoçi, *Carbon* **2012**, *50*, 2987.
[19] H. Chen, K. Liu, Z. Li, P. Wang, *Clin. Chim. Acta* **2019**, *493*, 138.
[20] M. L. Sin, K. E. Mach, P. K. Wong, J. C. Liao, *Expert Rev. Mol. Diagn.* **2014**, *14*, 225.
[21] L. Hamm, A. Gee, A. S. De Silva Indrasekara, *Appl. Sci.* **2019**, *9*, 1448.
[22] C. Rodríguez-Nava, K. Cortés-Sarabia, M. D. Avila-Huerta, E. J. Ortiz-Riaño, A. K. Estrada-Moreno, L. del C. Alarcón-Romero, O. Mata-Ruíz, Y. Medina-Flores, A. Vences-Velázquez, E. Morales-Narváez, *ACS Pharmacol. Transl. Sci.* **2021**, *4*, 365.
[23] C.-P. Segeritz, L. Vallier, In *Basic Science Methods for Clinical Researchers* (Eds.: Jalali, M.; Saldanha, F. Y. L.; Jalali, M.), Academic Press, Boston, **2017**, pp. 151–172.
[24] A. S. A. Shuaibu Abdullahi Hudu, *Cell Culture, Technology: Enhancing the Culture of Diagnosing Human Diseases*, March 1,2016., Vol. 10, **2016**, pp. DE01–DE05.
[25] M. Alhajj, A. Farhana, *Enzyme Linked Immunosorbent Assay*, StatPearls Publishing, **2022**.
[26] S. Yang, R. E. Rothman, *Lancet Infect. Dis.* **2004**, *4*, 337.
[27] M. D. Avila-Huerta, E. J. Ortiz-Riaño, D. L. Mancera-Zapata, E. Morales-Narváez, *Anal. Chem.* **2020**, *92*, 11511.
[28] M. D. Avila-Huerta, E. J. Ortiz-Riaño, D. L. Mancera-Zapata, K. Cortés-Sarabia, E. Morales-Narváez, *ACS Sens.* **2021**, *6*, 2136.
[29] C. Dincer, R. Bruch, E. Costa-Rama, M. T. Fernández-Abedul, A. Merkoçi, A. Manz, G. A. Urban, F. Güder, *Adv. Mater.* **2019**, *31*, 1806739.

[30] E. Noviana, T. Ozer, C. S. Carrell, J. S. Link, C. McMahon, I. Jang, C. S. Henry, *Chem. Rev.* **2021**, *121*, 11835.
[31] R. Koivunen, E. Jutila, R. Bollström, P. Gane, *Microfluid. Nanofluidics* **2016**, *20*, 83.
[32] Phosphate buffered saline, used in diagnostic assay manufacturing, .
[33] T. H. Giddings, J. B. Meehl, C. G. Pearson, M. Winey, In *Methods in Cell Biology* (Ed.: Müller-Reichert, T.), Academic Press, **2010**, pp. 117–141.
[34] 10X Immuno Wash Buffer - K005 - Diagnostic BioSystems(dbiosys) DBS, .
[35] What is the function of adding BSA as buffer in Biotin-Streptavidin system? | AAT Bioquest, .
[36] P. C. Weber, D. H. Ohlendorf, J. J. Wendoloski, F. R. Salemme, *Science* **1989**, *243*, 85.
[37] B. A. Otieno, C. E. Krause, J. F. Rusling, In *Methods in Enzymology* (Ed.: Kumar, C. V.), Academic Press, **2016**, pp. 135–150.
[38] E. C. Peláez, M. C. Estevez, A. Mongui, M.-C. Menéndez, C. Toro, O. L. Herrera-Sandoval, J. Robledo, M. J. García, P. D. Portillo, L. M. Lechuga, *ACS Infect. Dis.* **2020**, *6*, 1110.
[39] P. Vizzini, M. Braidot, J. Vidic, M. Manzano, *Micromachines* **2019**, *10*.
[40] S.-Y. Wu, J. Hulme, S. S. A. An, *BioChip J.* **2015**, *9*, 173.
[41] N. Amin, A. S. Torralba, R. Álvarez-Diduk, A. Afkhami, A. Merkoçi, *Anal. Chem.* **2020**, *92*, 4209.
[42] E. Morales-Narváez, C. Dincer, *Biosens. Bioelectron.* **2020**, *163*, 112274.
[43] M. Ciotti, M. Ciccozzi, A. Terrinoni, W.-C. Jiang, C.-B. Wang, S. Bernardini, *Crit. Rev. Clin. Lab. Sci.* **2020**, *57*, 365.
[44] J. Lan, J. Ge, J. Yu, S. Shan, H. Zhou, S. Fan, Q. Zhang, X. Shi, Q. Wang, L. Zhang, X. Wang, *Nature* **2020**, *581*, 215.
[45] J. Zhang, T. Xiao, Y. Cai, B. Chen, *Curr. Opin. Virol.* **2021**, *50*, 173.
[46] Definition of serology test - NCI Dictionary of Cancer Terms - NCI, **2011**.
[47] E. J. Ortiz-Riaño, M. D. Avila-Huerta, D. L. Mancera-Zapata, E. Morales-Narváez, *Biosens. Bioelectron.* **2020**, *165*, 112319.
[48] F. Amanat, D. Stadlbauer, S. Strohmeier, T. H. O. Nguyen, V. Chromikova, M. McMahon, K. Jiang, G. A. Arunkumar, D. Jurczyszak, J. Polanco, M. Bermudez-Gonzalez, G. Kleiner, T. Aydillo, L. Miorin, D. S. Fierer, L. A. Lugo, E. M. Kojic, J. Stoever, S. T. H. Liu, C. Cunningham-Rundles, P. L. Felgner, T. Moran, A. García-Sastre, D. Caplivski, A. C. Cheng, K. Kedzierska, O. Vapalahti, J. M. Hepojoki, V. Simon, F. Krammer, *Nat. Med.* **2020**, *26*, 1033.
[49] S. Zhang, A. Garcia-D'Angeli, J. P. Brennan, Q. Huo, *Analyst* **2014**, *139*, 439.
[50] D. J. Steiner, J. S. Cognetti, E. P. Luta, A. M. Klose, J. Bucukovski, M. R. Bryan, J. J. Schmuke, P. Nguyen-Contant, M. Y. Sangster, D. J. Topham, B. L. Miller, *Biosens. Bioelectron.* **2020**, *169*, 112643.
[51] N. C. Cady, N. Tokranova, A. Minor, N. Nikvand, K. Strle, W. T. Lee, W. Page, E. Guignon, A. Pilar, G. N. Gibson, *Biosens. Bioelectron.* **2021**, *171*, 112679.
[52] N. Psychogios, D. D. Hau, J. Peng, A. C. Guo, R. Mandal, S. Bouatra, I. Sinelnikov, R. Krishnamurthy, R. Eisner, B. Gautam, N. Young, J. Xia, C. Knox, E. Dong, P. Huang, Z. Hollander, T. L. Pedersen, S. R. Smith, F. Bamforth, R. Greiner, B. McManus, J. W. Newman, T. Goodfriend, D. S. Wishart, *PLOS ONE* **2011**, *6*, e16957.
[53] C.-T. Kung, C.-Y. Hou, Y.-N. Wang, L.-M. Fu, *Sens. Actuators B Chem.* **2019**, *301*, 126855.
[54] B. Selvakumar, A. Kathiravan, *Talanta* **2021**, *235*, 122733.

[55] T. Songjaroen, W. Dungchai, O. Chailapakul, W. Laiwattanapaisal, *Talanta* **2011**, *85*, 2587.
[56] J. F. C. Loo, A. H. P. Ho, A. P. F. Turner, W. C. Mak, *Trends Biotechnol.* **2019**, *37*, 1104.
[57] A. Reda, S. A. El-Safty, M. M. Selim, M. A. Shenashen, *Biosens. Bioelectron.* **2021**, *185*, 113237.
[58] L.-X. Feng, C. Tang, X.-X. Han, H.-C. Zhang, F.-N. Guo, T. Yang, J.-H. Wang, *Talanta* **2021**, *232*, 122499.
[59] D. Lin, B. Li, L. Fu, J. Qi, C. Xia, Y. Zhang, J. Chen, J. Choo, L. Chen, *Microsyst. Nanoeng.* **2022**, *8*, 53.
[60] A. H. C. Ng, R. Fobel, C. Fobel, J. Lamanna, D. G. Rackus, A. Summers, C. Dixon, M. D. M. Dryden, C. Lam, M. Ho, N. S. Mufti, V. Lee, M. A. M. Asri, E. A. Sykes, M. D. Chamberlain, R. Joseph, M. Ope, H. M. Scobie, A. Knipes, P. A. Rota, N. Marano, P. M. Chege, M. Njuguna, R. Nzunza, N. Kisangau, J. Kiogora, M. Karuingi, J. W. Burton, P. Borus, E. Lam, A. R. Wheeler, *Sci. Transl. Med.* **2018**, *10*, eaar6076.
[61] K. Kaarj, P. Akarapipad, J.-Y. Yoon, *Sci. Rep.* **2018**, *8*, 12438.
[62] Y. Zhao, D. Zeng, C. Yan, W. Chen, J. Ren, Y. Jiang, L. Jiang, F. Xue, D. Ji, F. Tang, M. Zhou, J. Dai, *Analyst* **2020**, *145*, 3106.
[63] G. Mahajan, E. Doherty, T. To, A. Sutherland, J. Grant, A. Junaid, A. Gulati, N. LoGrande, Z. Izadifar, S. S. Timilsina, V. Horváth, R. Plebani, M. France, I. Hood-Pishchany, S. Rakoff-Nahoum, D. S. Kwon, G. Goyal, R. Prantil-Baun, J. Ravel, D. E. Ingber, *Microbiome* **2022**, *10*, 201.
[64] Coleman Jenell S., Gaydos Charlotte A., *J. Clin. Microbiol.* **2018**, *56*, e00342.
[65] R. Amsel, P. A. Totten, C. A. Spiegel, K. C. S. Chen, D. Eschenbach, K. K. Holmes, *Am. J. Med.* **1983**, *74*, 14.
[66] Nugent R P, Krohn M A, Hillier S L, *J. Clin. Microbiol.* **1991**, *29*, 297.
[67] OSOM® BVBLUE® Test, .
[68] K. Cortés-Sarabia, C. Rodríguez-Nava, Y. Medina-Flores, O. Mata-Ruíz, J. E. López-Meza, M. D. Gómez-Cervantes, I. Parra-Rojas, B. Illades-Aguiar, E. Flores-Alfaro, A. Vences-Velázquez, *Appl. Microbiol. Biotechnol.* **2020**, *104*, 6173.
[69] M. Imani, N. Mohajeri, M. Rastegar, N. Zarghami, *Anal. Biochem.* **2021**, *630*, 114323.
[70] M. D. Avila-Huerta, E. J. Ortiz-Riaño, D. L. Mancera-Zapata, E. Morales-Narváez, *Anal. Chem.* **2020**, *92*, 11511.
[71] E. J. Ortiz-Riaño, M. D. Avila-Huerta, D. L. Mancera-Zapata, E. Morales-Narváez, *Biosens. Bioelectron.* **2020**, *165*, 112319.
[72] M. D. Avila-Huerta, E. J. Ortiz-Riaño, D. L. Mancera-Zapata, K. Cortés-Sarabia, E. Morales-Narváez, *ACS Sens.* **2021**, *6*, 2136.
[73] Y. H. Tan, M. Liu, B. Nolting, J. G. Go, J. Gervay-Hague, G. Liu, *ACS Nano* **2008**, *2*, 2374.
[74] L. S. Robinson, J. Schwebke, W. G. Lewis, A. L. Lewis, *J. Biol. Chem.* **2019**, *294*, 5230.
[75] M. D. Avila-Huerta, K. Leyva-Hidalgo, K. Cortés-Sarabia, A. K. Estrada-Moreno, A. Vences-Velázquez, E. Morales-Narváez, *ACS Meas. Sci. Au* **2023**.
[76] R. Tang, M. Y. Xie, M. Li, L. Cao, S. Feng, Z. Li, F. Xu, *Appl. Mater. Today* **2022**, *26*, 101305.
[77] J. Sui, H. Lin, Y. Xu, L. Cao, *Food Anal. Methods* **2011**, *4*, 245.
[78] P. Ramirez-Priego, M.-C. Estévez, H. J. Díaz-Luisravelo, J. J. Manclús, Á. Montoya, L. M. Lechuga, *Anal. Chim. Acta* **2021**, *1152*, 338276.
[79] L. A. Ireta-Muñoz, E. Morales-Narváez, *Biosensors* **2020**, *10*.

Appendix I

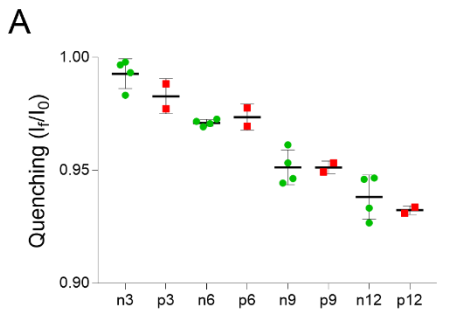

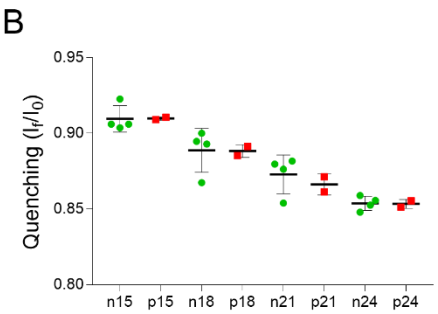

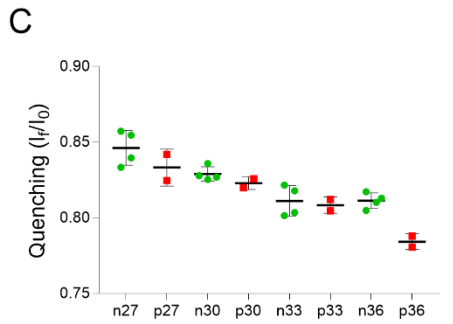

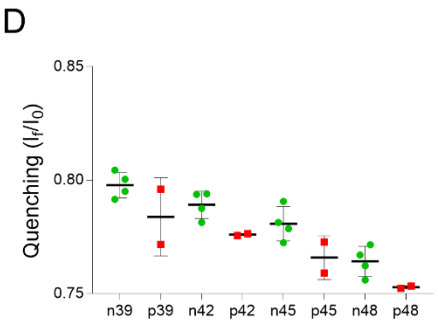

E

1/8875	
Time (min)	P
3	0.1712
6	0.4099
9	>0.9999
12	0.4751
15	0.9811
18	0.9689
21	0.5492
24	0.9249
27	0.2709
30	0.1980
33	0.7547
36	0.0038
39	0.1791
42	0.0434
45	0.1009
48	0.0845

Figure A1. *Performance of the assay with diluted sera throughout time (3 to 48 min). Dilution factor: 1/8875. 4 pre-COVID-19 samples (n) and 2 samples from COVID-19 subjects (p) were assayed.* ***A****. Analysis from 3 to 12 min, respectively.* ***B****. Analysis from 15 to 24 min, respectively.* ***C****. Analysis from 27 to 36 min, respectively.* ***D****. Analysis from 39 to 48 min, respectively. The box plots display the median and the extreme values of the respective distribution. P values were obtained by means of an unpaired T-student test. The employed confidence interval was 95 %. Adapted with permission.*[28] *Copyright 2021, ACS.*

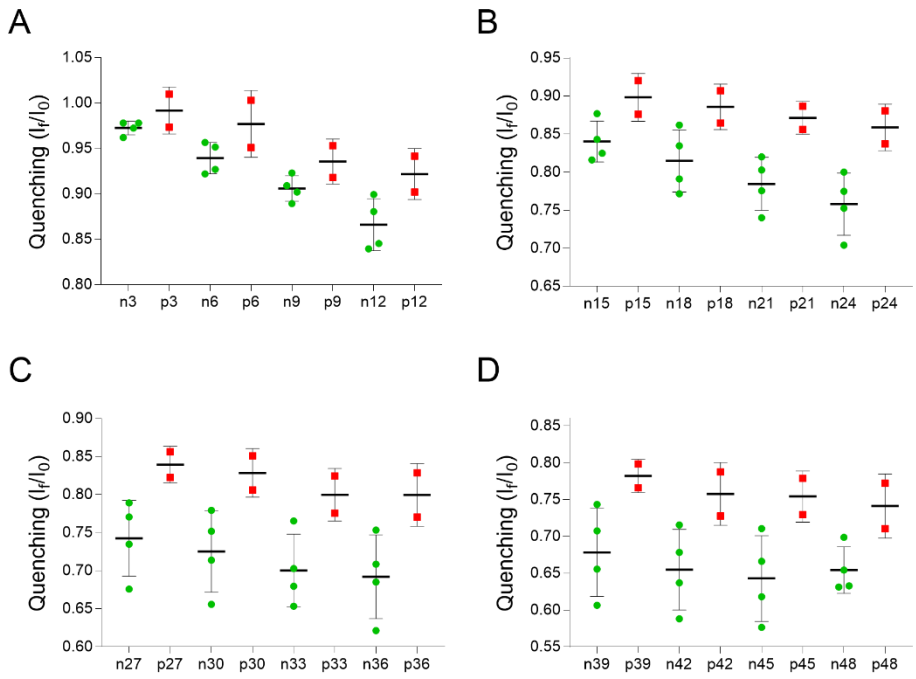

E

1/9000	
Time (min)	P
3	0.2015
6	0.1405
9	0.1196
12	0.0867
15	0.0751
18	0.1000
21	0.0355
24	0.0389
27	0.0670
30	0.0716
33	0.0624
36	0.0749
39	0.0867
42	0.0845
45	0.0735
48	0.0449

Figure A2. *Performance of the assay with diluted sera throughout time (3 to 48 min). Dilution factor: 1/9000. 4 pre-COVID-19 samples (n) and 2 samples from COVID-19 subjects (p) were assayed.* ***A****. Analysis from 3 to 12 min, respectively.* ***B****. Analysis from 15 to 24 min, respectively.* ***C****. Analysis from 27 to 36 min, respectively.* ***D****. Analysis from 39 to 48 min, respectively. The box plots display the median and the extreme values of the respective distribution. P values were obtained by means of an unpaired T-student test. The employed confidence interval was 95 %. Adapted with permission.*[28] *Copyright 2021, ACS.*

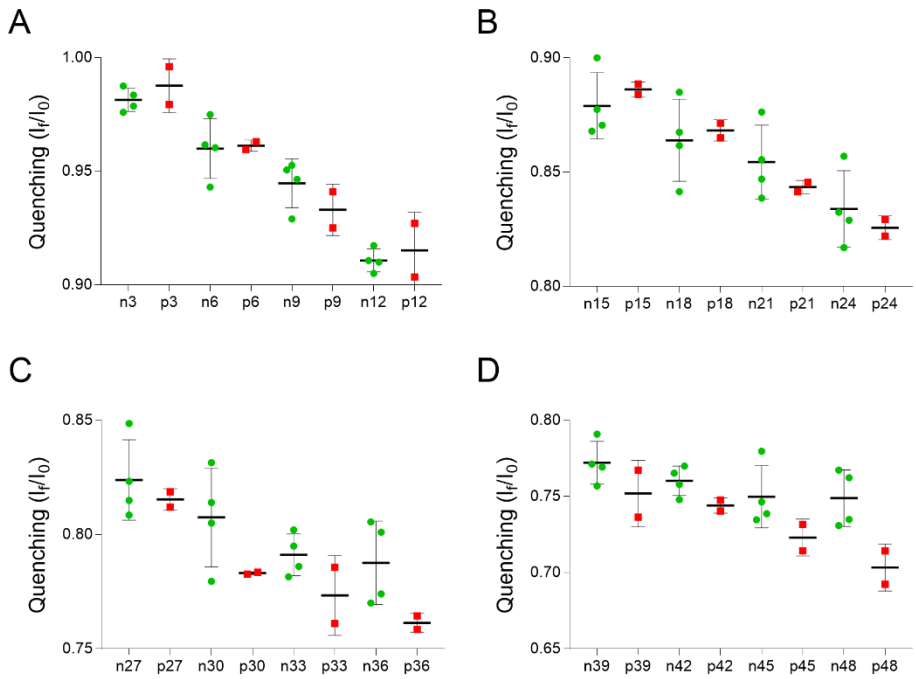

E

1/10000	
Time (min)	P
3	0.3828
6	0.9056
9	0.2833
12	0.6097
15	0.5462
18	0.7659
21	0.4197
24	0.5559
27	0.5574
30	0.2074
33	0.1565
36	0.1298
39	0.2258
42	0.0968
45	0.1739
48	0.0421

Figure A3. *Performance of the assay with diluted sera throughout time (3 to 48 min). Dilution factor: 1/10000. 4 pre-COVID-19 samples (n) and 2 samples from COVID-19 subjects (p) were assayed.* ***A****. Analysis from 3 to 12 min, respectively.* ***B****. Analysis from 15 to 24 min, respectively.* ***C****. Analysis from 27 to 36 min, respectively.* ***D****. Analysis from 39 to 48 min, respectively. The box plots display the median and the extreme values of the respective distribution. P values were obtained by means of an unpaired T-student test. The employed confidence interval was 95 %. Adapted with permission.*[28] *Copyright 2021, ACS.*

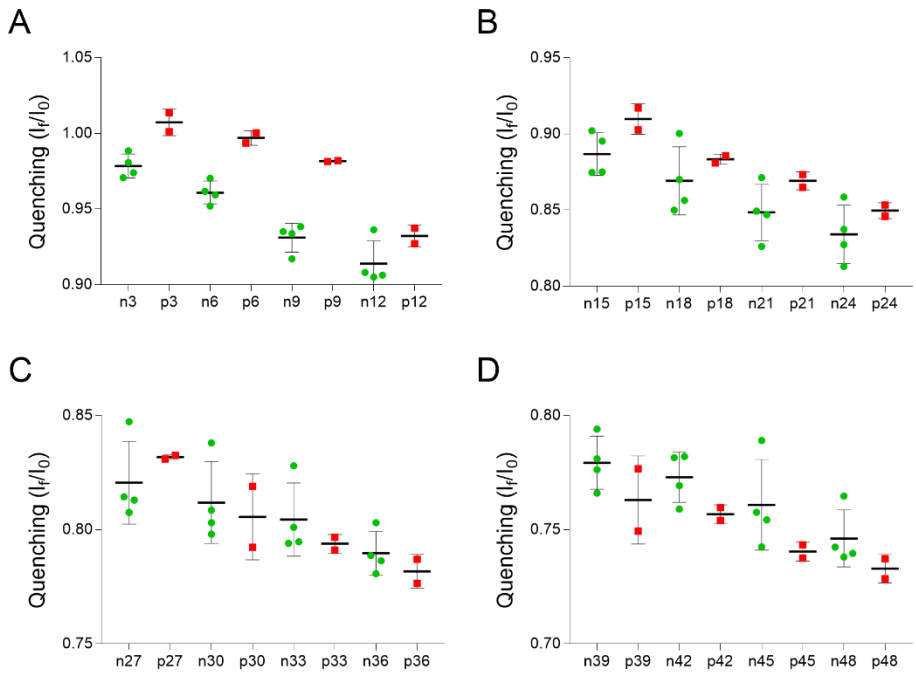

E

1/11000	
Time (min)	P
3	0.0150
6	0.0039
9	0.0021
12	0.1933
15	0.1129
18	0.4479
21	0.2160
24	0.3423
27	0.4557
30	0.7133
33	0.4329
36	0.3685
39	0.2477
42	0.1282
45	0.2441
48	0.2449

Figure A4. *Performance of the assay with diluted sera throughout time (3 to 48 min). Dilution factor: 1/11000. 4 pre-COVID-19 samples (n) and 2 samples from COVID-19 subjects (p) were assayed.* ***A****. Analysis from 3 to 12 min, respectively.* ***B****. Analysis from 15 to 24 min, respectively.* ***C****. Analysis from 27 to 36 min, respectively.* ***D****. Analysis from 39 to 48 min, respectively. The box plots display the median and the extreme values of the respective distribution. P values were obtained by means of an unpaired T-student test. The employed confidence interval was 95 %. Adapted with permission.*[28] *Copyright 2021, ACS.*

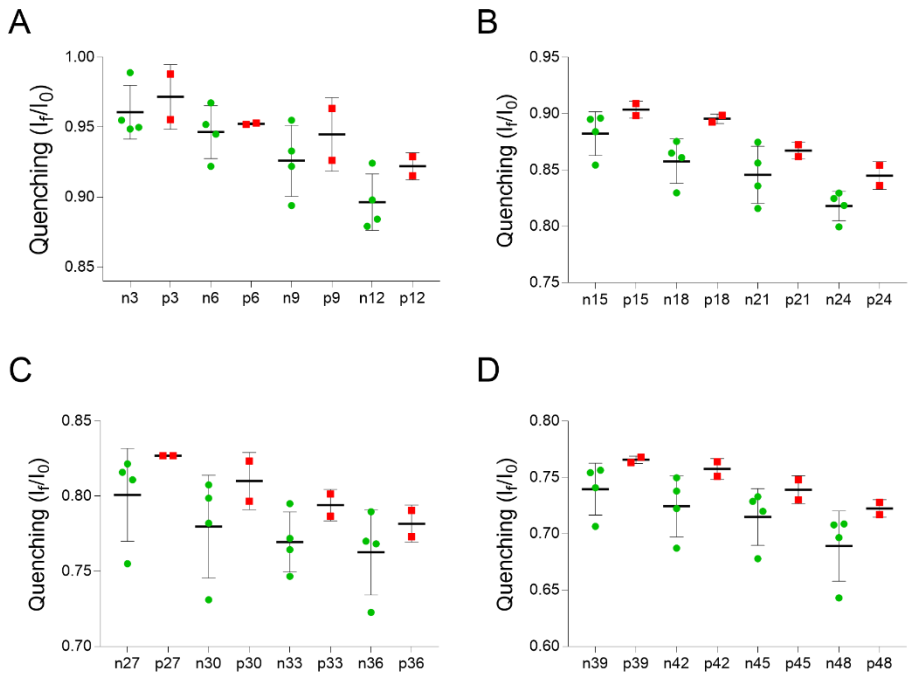

1/11250	
Time (min)	P
3	0.5629
6	0.6972
9	0.4415
12	0.1772
15	0.2266
18	0.0647
21	0.3274
24	0.0729
27	0.3224
30	0.3237
33	0.1928
36	0.4336
39	0.2059
42	0.1848
45	0.2849
48	0.2305

Figure A5. *Performance of the assay with diluted sera throughout time (3 to 48 min). Dilution factor: 1/11250. 4 pre-COVID-19 samples (n) and 2 samples from COVID-19 subjects (p) were assayed.* ***A****. Analysis from 3 to 12 min, respectively.* ***B****. Analysis from 15 to 24 min, respectively.* ***C****. Analysis from 27 to 36 min, respectively.* ***D****. Analysis from 39 to 48 min, respectively. The box plots display the median and the extreme values of the respective distribution. P values were obtained by means of an unpaired T-student test. The employed confidence interval was 95 %. Adapted with permission.*[28] *Copyright 2021, ACS.*

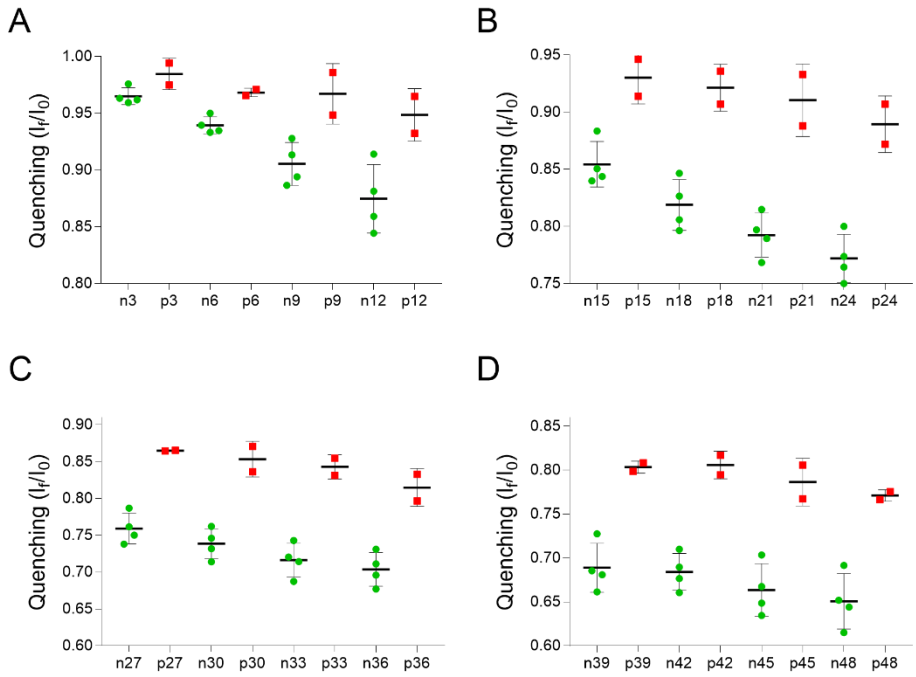

1/11500	
Time (min)	P
3	0.0742
6	0.0081
9	0.0276
12	0.0406
15	0.0135
18	0.0056
21	0.0041
24	0.0035
27	0.0025
30	0.0035
33	0.0024
36	0.0056
39	0.0055
42	0.0021
45	0.0083
48	0.0072

Figure A6. *Performance of the assay with diluted sera throughout time (3 to 48 min). Dilution factor: 1/11500. 4 pre-COVID-19 samples (n) and 2 samples from COVID-19 subjects (p) were assayed.* ***A****. Analysis from 3 to 12 min, respectively.* ***B****. Analysis from 15 to 24 min, respectively.* ***C****. Analysis from 27 to 36 min, respectively.* ***D****. Analysis from 39 to 48 min, respectively. The box plots display the median and the extreme values of the respective distribution. P values were obtained by means of an unpaired T-student test. The employed confidence interval was 95 %. Adapted with permission.*[28] *Copyright 2021, ACS.*

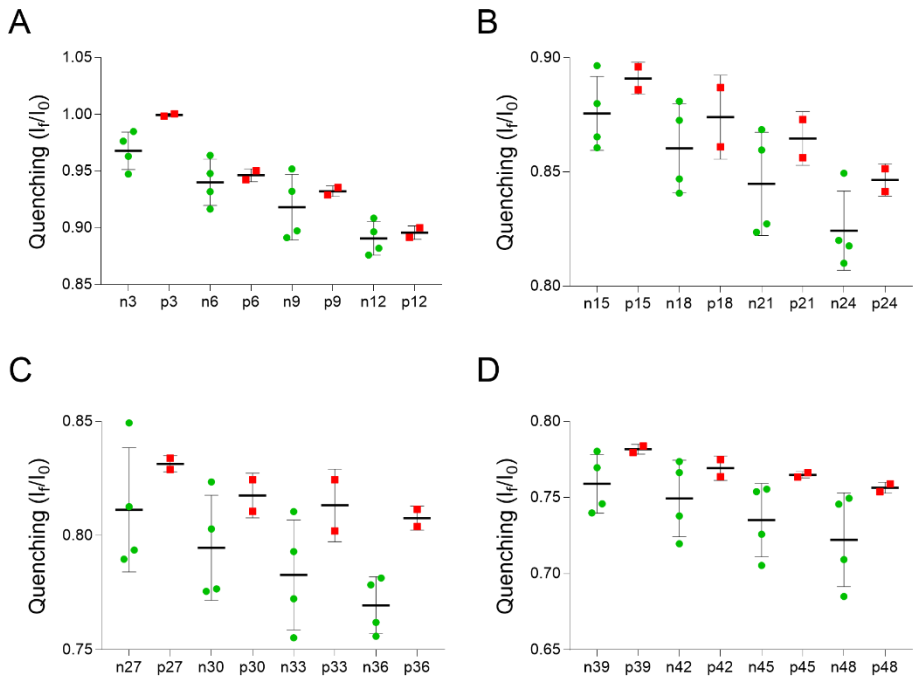

1/12500	
Time (min)	P
3	0.0627
6	0.7110
9	0.5546
12	0.6790
15	0.2864
18	0.4583
21	0.3246
24	0.1718
27	0.3808
30	0.2671
33	0.1898
36	0.0163
39	0.1916
42	0.3584
45	0.1746
48	0.2144

Figure A7. *Performance of the assay with diluted sera throughout time (3 to 48 min). Dilution factor: 1/12500. 4 pre-COVID-19 samples (n) and 2 samples from COVID-19 subjects (p) were assayed.* ***A****. Analysis from 3 to 12 min, respectively.* ***B****. Analysis from 15 to 24 min, respectively.* ***C****. Analysis from 27 to 36 min, respectively.* ***D****. Analysis from 39 to 48 min, respectively. The box plots display the median and the extreme values of the respective distribution. P values were obtained by means of an unpaired T-student test. The employed confidence interval was 95 %. Adapted with permission.*[28] *Copyright 2021, ACS.*

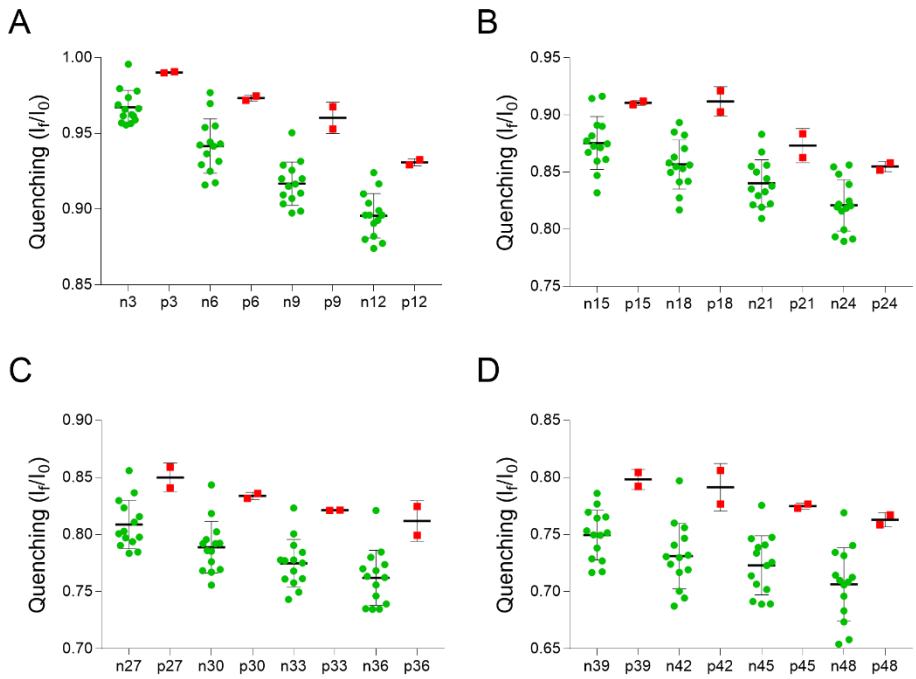

1/11875	
Time (min)	P
3	0.0136
6	0.0292
9	0.0011
12	0.0052
15	0.0560
18	0.0037
21	0.0480
24	0.0584
27	0.0197
30	0.0166
33	0.0088
36	0.0149
39	0.0086
42	0.0135
45	0.0158
48	0.0305

Figure A8. *Performance of the assay with diluted sera throughout time (3 to 48 min). Dilution factor: 1/11875. 14 pre-COVID-19 samples (n) and 2 samples from COVID-19 subjects (p) were assayed.* ***A****. Analysis from 3 to 12 min, respectively.* ***B****. Analysis from 15 to 24 min, respectively.* ***C****. Analysis from 27 to 36 min, respectively.* ***D****. Analysis from 39 to 48 min, respectively. The box plots display the median and the extreme values of the respective distribution. P values were obtained by means of an unpaired T-student test. The employed confidence interval was 95 %. Adapted with permission.*[28] *Copyright 2021, ACS.*

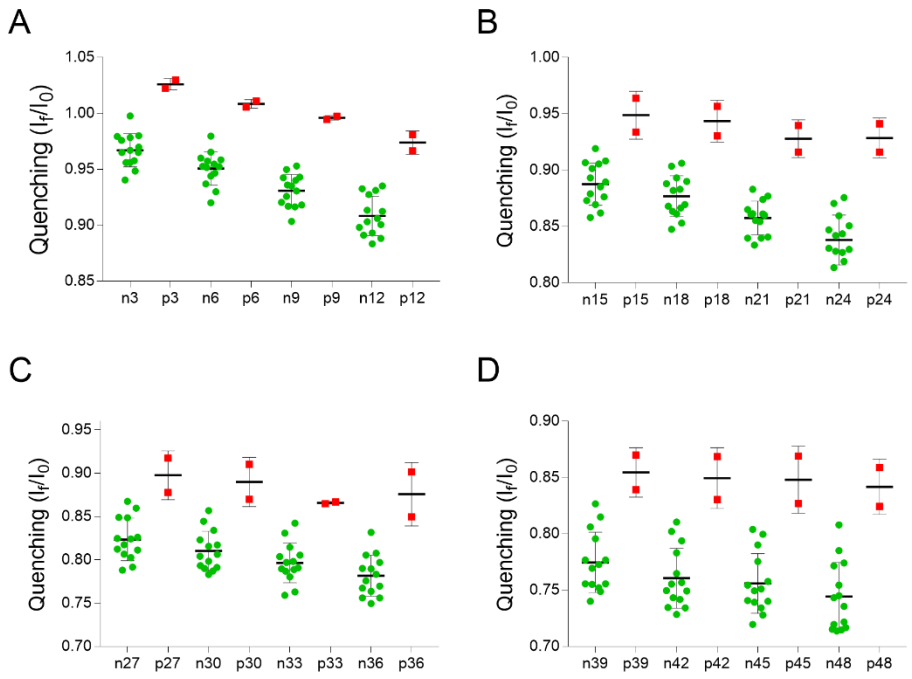

E

1/12000	
Time (min)	P
3	<0.0001
6	0.0001
9	<0.0001
12	0.0002
15	0.0008
18	0.0003
21	<0.0001
24	<0.0001
27	0.0015
30	0.0004
33	0.0009
36	0.0002
39	0.0013
42	0.0006
45	0.0005
48	0.0008

Figure A9. *Performance of the assay with diluted sera throughout time (3 to 48 min). Dilution factor: 1/12000. 14 pre-COVID-19 samples (n) and 2 samples from COVID-19 subjects (p) were assayed.* ***A****. Analysis from 3 to 12 min, respectively.* ***B****. Analysis from 15 to 24 min, respectively.* ***C****. Analysis from 27 to 36 min, respectively.* ***D****. Analysis from 39 to 48 min, respectively. The box plots display the median and the extreme values of the respective distribution. P values were obtained by means of an unpaired T-student test. The employed confidence interval was 95 %. Adapted with permission.*[28] *Copyright 2021, ACS.*

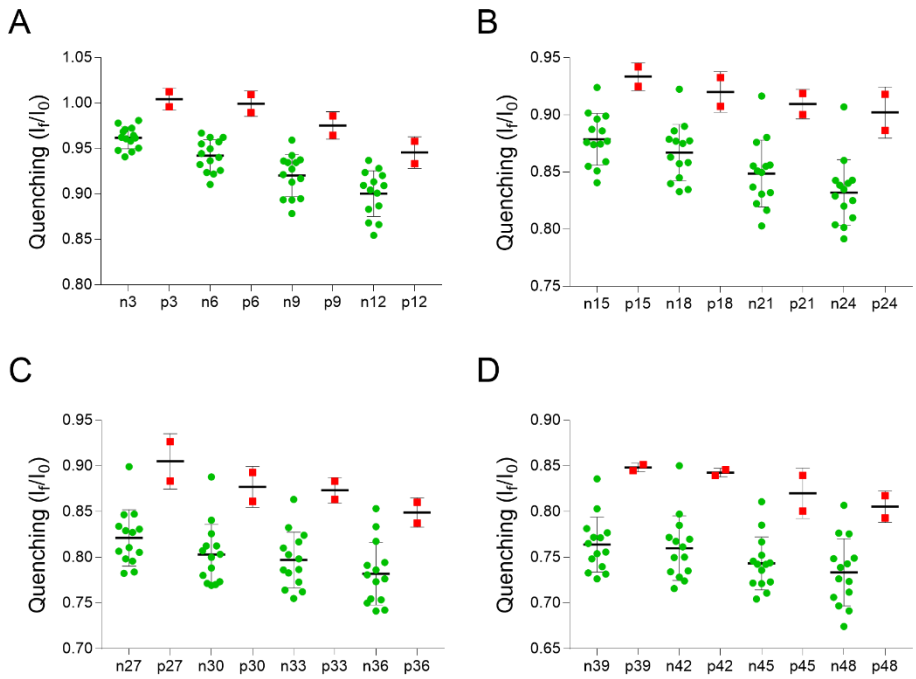

1/12125	
Time (min)	P
3	0.0004
6	0.0007
9	0.0061
12	0.0291
15	0.0053
18	0.0119
21	0.0131
24	0.0057
27	0.0029
30	0.0091
33	0.0042
36	0.0185
39	0.0018
42	0.0063
45	0.0035
48	0.0186

Figure A10. *Performance of the assay with diluted sera throughout time (3 to 48 min). Dilution factor: 1/12125. 14 pre-COVID-19 samples (n) and 2 samples from COVID-19 subjects (p) were assayed.* ***A****. Analysis from 3 to 12 min, respectively.* ***B****. Analysis from 15 to 24 min, respectively.* ***C****. Analysis from 27 to 36 min, respectively.* ***D****. Analysis from 39 to 48 min, respectively. The box plots display the median and the extreme values of the respective distribution. P values were obtained by means of an unpaired T-student test. The employed confidence interval was 95 %. Adapted with permission.*[28] *Copyright 2021, ACS.*

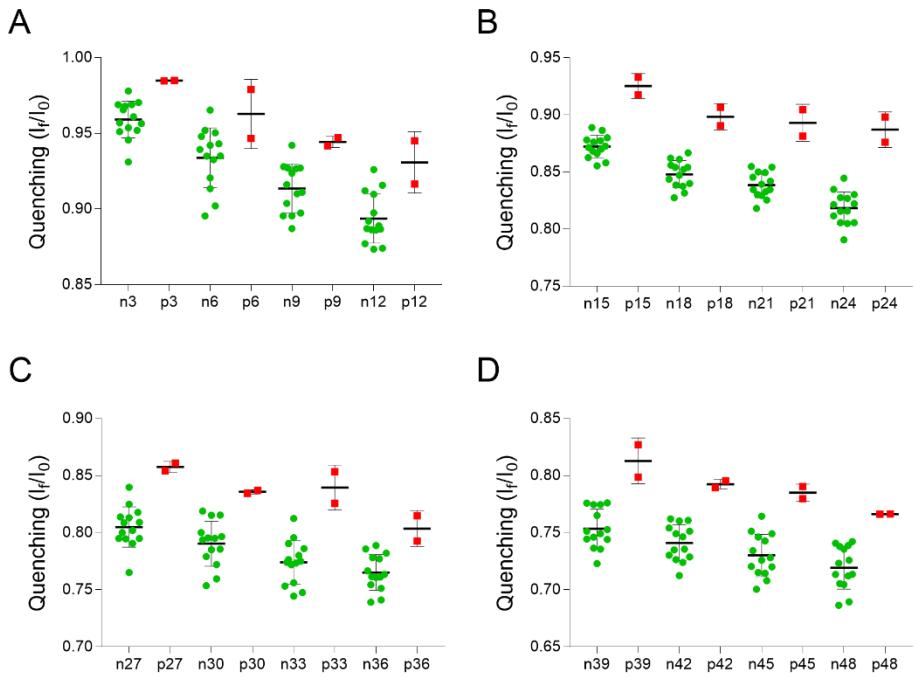

1/12200	
Time (min)	P
3	0.0118
6	0.0754
9	0.0208
12	0.0104
15	<0.0001
18	<0.0001
21	<0.0001
24	<0.0001
27	0.0011
30	0.0071
33	0.0005
36	0.0057
39	0.0005
42	0.0005
45	0.0012
48	0.0039

Figure A11. *Performance of the assay with diluted sera throughout time (3 to 48 min). Dilution factor: 1/12200. 14 pre-COVID-19 samples (n) and 2 samples from COVID-19 subjects (p) were assayed.* ***A****. Analysis from 3 to 12 min, respectively.* ***B****. Analysis from 15 to 24 min, respectively.* ***C****. Analysis from 27 to 36 min, respectively.* ***D****. Analysis from 39 to 48 min, respectively. The box plots display the median and the extreme values of the respective distribution. P values were obtained by means of an unpaired T-student test. The employed confidence interval was 95 %. Adapted with permission.*[28] *Copyright 2021, ACS.*

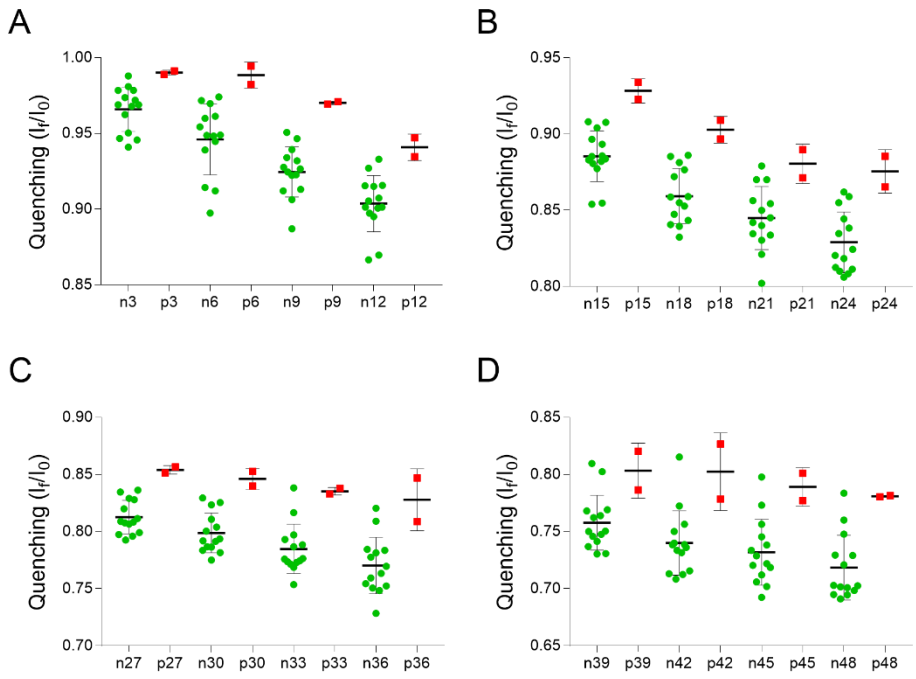

E

1/12250	
Time (min)	P
3	0.0405
6	0.0265
9	0.0021
12	0.0166
15	0.0034
18	0.0055
21	0.0353
24	0.0071
27	0.0017
30	0.0025
33	0.0063
36	0.0083
39	0.0249
42	0.0121
45	0.0177
48	0.0090

Figure A12. *Performance of the assay with diluted sera throughout time (3 to 48 min). Dilution factor: 1/12250. 14 pre-COVID-19 samples (n) and 2 samples from COVID-19 subjects (p) were assayed.* ***A****. Analysis from 3 to 12 min, respectively.* ***B****. Analysis from 15 to 24 min, respectively.* ***C****. Analysis from 27 to 36 min, respectively.* ***D****. Analysis from 39 to 48 min, respectively. The box plots display the median and the extreme values of the respective distribution. P values were obtained by means of an unpaired T-student test. The employed confidence interval was 95 %. Adapted with permission.*[28] *Copyright 2021, ACS.*

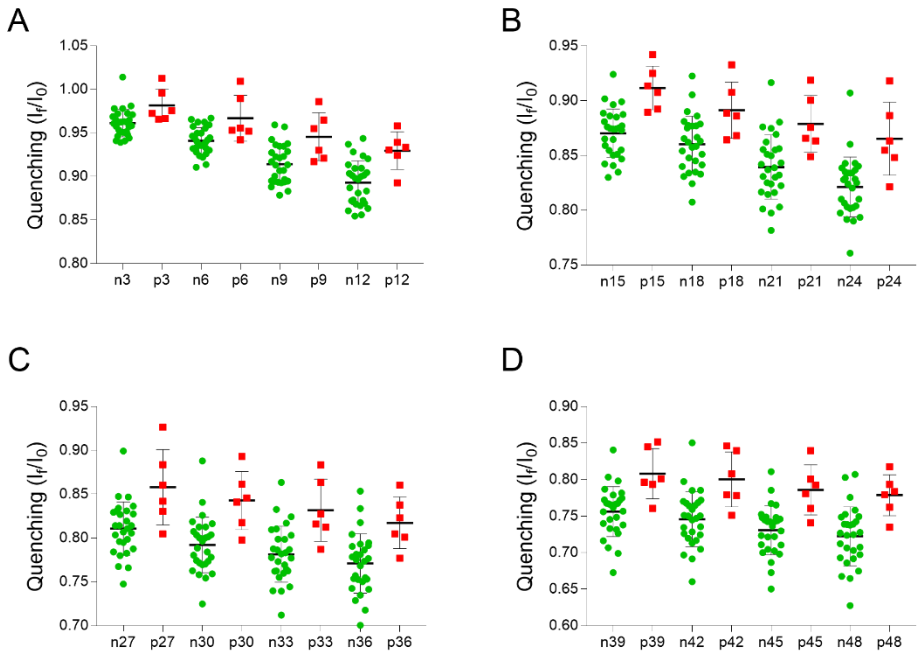

1/12125	
Time (min)	P
3	0.0087
6	0.0024
9	0.0045
12	0.0022
15	0.0002
18	0.0112
21	0.0047
24	0.0016
27	0.0031
30	0.0013
33	0.0017
36	0.0039
39	0.0020
42	0.0029
45	0.0010
48	0.0029

Figure A13. *Performance of the assay with diluted sera throughout time (3 to 48 min). Dilution factor: 1/12125. 28 pre-COVID-19 samples (n) and 6 samples from COVID-19 subjects (p) were assayed.* ***A****. Analysis from 3 to 12 min, respectively.* ***B****. Analysis from 15 to 24 min, respectively.* ***C****. Analysis from 27 to 36 min, respectively.* ***D****. Analysis from 39 to 48 min, respectively. The box plots display the median and the extreme values of the respective distribution. P values were obtained by means of an unpaired T-student test. The employed confidence interval was 95 %. Adapted with permission.*[28] *Copyright 2021, ACS.*

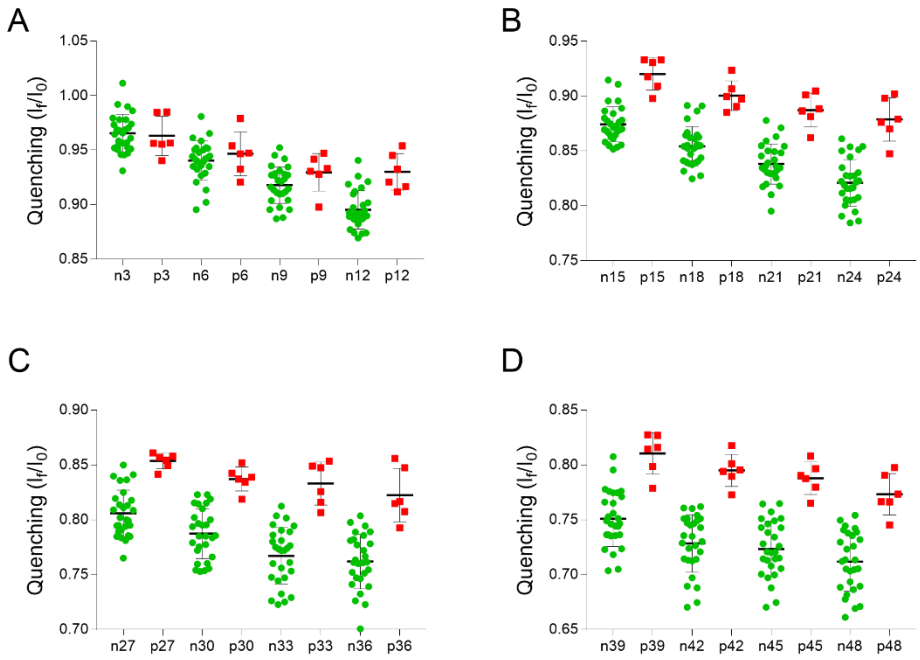

E

1/12200	
Time (min)	P
3	0.7646
6	0.448
9	0.1345
12	<0.0001
15	<0.0001
18	<0.0001
21	<0.0001
24	<0.0001
27	<0.0001
30	<0.0001
33	<0.0001
36	<0.0001
39	<0.0001
42	<0.0001
45	<0.0001
48	<0.0001

Figure A14. *Performance of the assay with diluted sera throughout time (3 to 48 min). Dilution factor: 1/12200. 28 pre-COVID-19 samples (n) and 6 samples from COVID-19 subjects (p) were assayed.* ***A****. Analysis from 3 to 12 min, respectively.* ***B****. Analysis from 15 to 24 min, respectively.* ***C****. Analysis from 27 to 36 min, respectively.* ***D****. Analysis from 39 to 48 min, respectively. The box plots display the median and the extreme values of the respective distribution. P values were obtained by means of an unpaired T-student test. The employed confidence interval was 95 %. Adapted with permission.*[28] *Copyright 2021, ACS.*

Table A-1. *Performance of the assay with diluted sera throughout time (3 to 48 min). Dilution factor: 1/12125. 28 pre-COVID-19 samples (n) and 6 samples from COVID-19 subjects (p) were assayed. Adapted with permission.*[28] *Copyright 2021, ACS.*

1/12125			
Time	**Mean**	***P***	**Mean of group *n* – Mean of group *p***
3n	0.961	0.0087	0.0203 ± 0.00727
3p	0.981		
6n	0.941	0.0024	0.026 ± 0.00788
6p	0.967		
9n	0.914	0.0045	0.0316 ± 0.0103
9p	0.946		
12n	0.893	0.0022	0.0368 ± 0.0111
12p	0.93		
15n	0.87	0.0002	0.0414 ± 0.00983
15p	0.912		
18n	0.86	0.0112	0.031 ± 0.0115
18p	0.891		
21n	0.839	0.0047	0.0394 ± 0.013
21p	0.879		
24n	0.821	0.0016	0.044 ± 0.0128
24p	0.865		
27n	0.811	0.0031	0.0472 ± 0.0147
27p	0.858		
30n	0.792	0.0013	0.0507 ± 0.0144
30p	0.843		
33n	0.781	0.0017	0.0502 ± 0.0147
33p	0.832		
36n	0.771	0.0039	0.0464 ± 0.0149
36p	0.817		
39n	0.756	0.002	0.0519 ± 0.0154
39p	0.808		
42n	0.746	0.0029	0.0546 ± 0.0169
42p	0.8		
45n	0.731	0.001	0.0553 ± 0.0152
45p	0.786		
48n	0.722	0.0029	0.0562 ± 0.0174
48p	0.779		

Table A-2. *Performance of the assay with diluted sera throughout time (3 to 48 min). Dilution factor: 1/12200. 28 pre-COVID-19 samples (n) and 6 samples from COVID-19 subjects (p) were assayed. Adapted with permission.*[28] *Copyright 2021, ACS.*

1/12200			
Time	**Mean**	***P***	**Mean of group *n* – Mean of group *p***
3n	0.965	0.7646	-0.00235 ± 0.00779
3p	0.963		
6n	0.94	0.448	0.00634 ± 0.00826
6p	0.947		
9n	0.918	0.1345	0.0117 ± 0.00763
9p	0.93		
12n	0.895	<0.0001	0.0348 ± 0.00781
12p	0.93		
15n	0.874	<0.0001	0.0459 ± 0.00712
15p	0.92		
18n	0.854	<0.0001	0.0461 ± 0.00774
18p	0.9		
21n	0.838	<0.0001	0.0492 ± 0.00803
21p	0.887		
24n	0.821	<0.0001	0.0579 ± 0.00946
24p	0.879		
27n	0.806	<0.0001	0.0477 ± 0.00889
27p	0.854		
30n	0.787	<0.0001	0.0498 ± 0.0096
30p	0.837		
33n	0.767	<0.0001	0.0659 ± 0.0112
33p	0.833		
36n	0.762	<0.0001	0.0605 ± 0.0111
36p	0.822		
39n	0.751	<0.0001	0.0594 ± 0.011
39p	0.81		
42n	0.728	<0.0001	0.0666 ± 0.0111
42p	0.795		
45n	0.724	<0.0001	0.0643 ± 0.0109
45p	0.788		
48n	0.712	<0.0001	0.0615 ± 0.0116
48p	0.773		

Appendix II

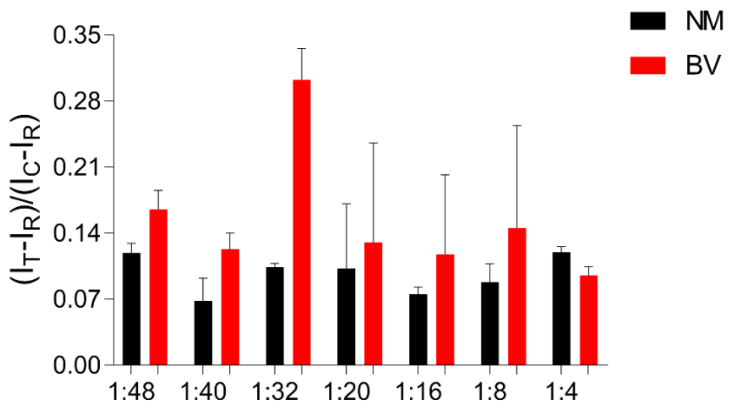

Figure B1. *Evaluation of different dilution factors of the clinical samples. NM, normal microbiota sample. BV, bacterial vaginosis sample.*

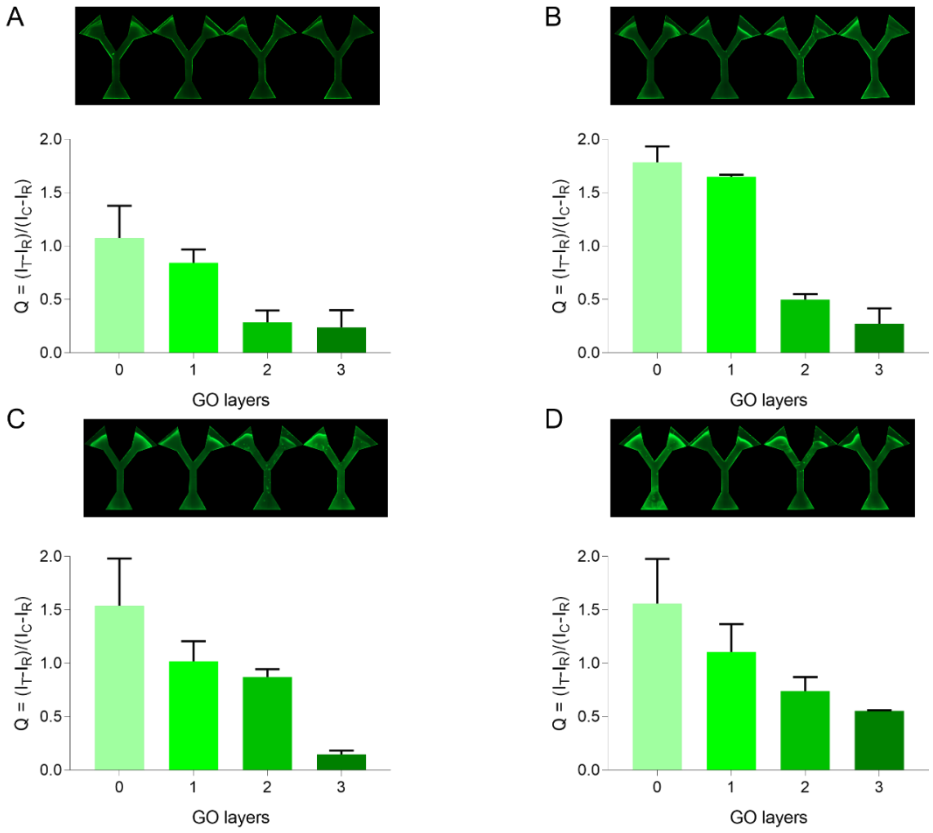

Figure B2. *FAS and GO optimization. 0, 1, 2 and 3 layers of 5µL of GO concentrated at 500 µg mL^{-1} were used for each FAS concentration explored.* ***A****. Evaluation of the fluorescence quenching in terms of the Q ratio (see Eq. 1) in those devices tested with [FAS] = 40 µg mL^{-1}.* ***B****. Q ratio in those devices tested with [FAS] = 60µg mL^{-1}.* ***C****. Q ratio in the devices tested with [FAS] = 80µg mL^{-1}.* ***D****. Q ratio in those devices tested with [FAS] = 100µg mL^{-1}.*

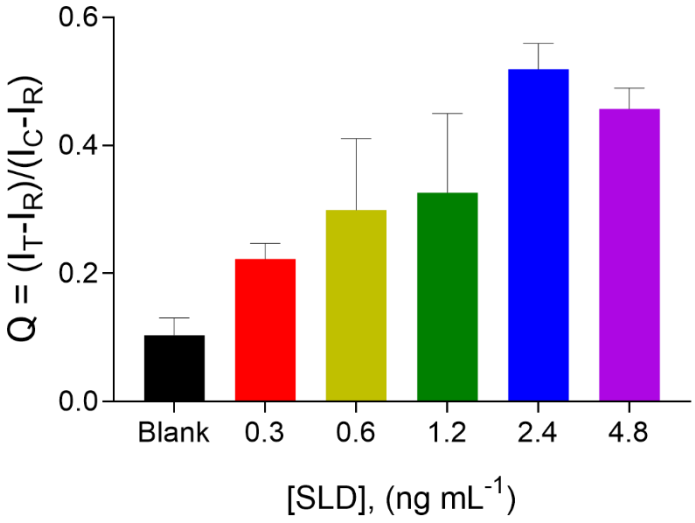

Figure B3. *Quantitative performance of the proposed disposable device. FAS was employed at 80 µg mL^{-1} and 3 layers of GO concentrated at 500 µg mL^{-1} were deposited in the corresponding device. Dynamic range from 0.3 to 4.8 ng mL^{-1}.*

Table B-1. *The resulting P values (corresponding to a t-test) to determine the optimal dilution factor of the vaginal swab samples.*

Dilution	p
1:4	0.0311
1:8	0.4196
1:16	0.4370
1:20	0.7697
1:32	**0.0141**
1:40	0.0724
1:48	0.0246

Table B-2. *CVs of the disposable biosensor testing standard samples.*

[Sialidase], (ng mL^{-1})	CV
0	4.91%
0.3	11.05%
0.6	14.69%
1.2	7.31%
2.4	7.69%
4.8	7.12%

Table B-3. *CVs of the disposable biosensor testing clinical samples.*

Sample	CV
NM 1	11.33%
NM 2	8.13%
NM 3	13.59%
NM 4	3.14%
NM 5	4.82%
NM 6	6.02%
NM 7	14.75%
NM 8	4.59%
NM 9	9.78%
BV 1	10.90%
BV 2	11.31%
BV 3	3.48%

BV 4	9.99%
BV 5	7.49%

Appendix III

2/5/23, 11:16 Rightslink® by Copyright Clearance Center

RightsLink

Home | Help | Live Chat | Sign in | Create Account

ACS Publications
Most Trusted. Most Cited. Most Read.

Real-Time Photoluminescent Biosensing Based on Graphene Oxide-Coated Microplates: A Rapid Pathogen Detection Platform

Author: Mariana D. Avila-Huerta, Edwin J. Ortiz-Riaño, Diana L. Mancera-Zapata, et al
Publication: Analytical Chemistry
Publisher: American Chemical Society
Date: Sep 1, 2020

Copyright © 2020, American Chemical Society

PERMISSION/LICENSE IS GRANTED FOR YOUR ORDER AT NO CHARGE

This type of permission/license, instead of the standard Terms and Conditions, is sent to you because no fee is being charged for your order. Please note the following:

- Permission is granted for your request in both print and electronic formats, and translations.
- If figures and/or tables were requested, they may be adapted or used in part.
- Please print this page for your records and send a copy of it to your publisher/graduate school.
- Appropriate credit for the requested material should be given as follows: "Reprinted (adapted) with permission from {COMPLETE REFERENCE CITATION}. Copyright {YEAR} American Chemical Society." Insert appropriate information in place of the capitalized words.
- One-time permission is granted only for the use specified in your RightsLink request. No additional uses are granted (such as derivative works or other editions). For any uses, please submit a new request.

If credit is given to another source for the material you requested from RightsLink, permission must be obtained from that source.

BACK CLOSE WINDOW

ACS Publications
Most Trusted. Most Cited. Most Read.

Facile Determination of COVID-19 Seroconversion via Nonradiative Energy Transfer

Author: Mariana D. Avila-Huerta, Edwin J. Ortiz-Riaño, Diana L. Mancera-Zapata, et al
Publication: ACS Sensors
Publisher: American Chemical Society
Date: Jun 1, 2021

PERMISSION/LICENSE IS GRANTED FOR YOUR ORDER AT NO CHARGE

This type of permission/license, instead of the standard Terms and Conditions, is sent to you because no fee is being charged for your order. Please note the following:

- Permission is granted for your request in both print and electronic formats, and translations.
- If figures and/or tables were requested, they may be adapted or used in part.
- Please print this page for your records and send a copy of it to your publisher/graduate school.
- Appropriate credit for the requested material should be given as follows: "Reprinted (adapted) with permission from {COMPLETE REFERENCE CITATION}. Copyright {YEAR} American Chemical Society." Insert appropriate information in place of the capitalized words.
- One-time permission is granted only for the use specified in your RightsLink request. No additional uses are granted (such as derivative works or other editions). For any uses, please submit a new request.

If credit is given to another source for the material you requested from RightsLink, permission must be obtained from that source.

BACK CLOSE WINDOW